DYNAMIC MOTIONS AND STRUCTURAL ANALYSES OF DEEP WATER FREE STANDING HYBRID RISER FOR FPSO

A Thesis

by

JAEHUN JUNG

Submitted to the Office of Graduate and Professional Studies of
Texas A&M University
in partial fulfillment of the requirements for the degree of

MASTER OF SCIENCE

Chair of Committee,	Moo-Hyun Kim
Committee Members,	Robert Randall
	Jerome Schubert
Head of Department,	Robin Autenrieth

August 2015

Major Subject: Ocean Engineering

ABSTRACT

In deep water with severe environmental conditions, the Free Standing Hybrid Riser (FSHR) is suitable for high motion vessels like FPSOs (Floating Production Storage and Offloading). As the FSHR is capable of decoupling from vessel induced motion, the riser exhibits exceptional motional and structural performances. In this study, the motional and structural characteristics of the FSHR were investigated under 100- and 500-yr hurricane conditions in time domain by using a coupled hull/mooring/riser dynamic analysis program, CHARMD3D. Then, the estimated short-term fatigue damage was compared with SCRs and LWSCRs. In addition, fixed-fairlead analysis of the FPSO uncoupled FSHR was conducted separately, and the results were used to compare with those of the moving-fairlead analysis to check the effects of the environmental loads against the riser system.

In the moving-fairlead analysis, the FPSO coupled FSHR was investigated for 100- and 500-yr hurricane conditions with parallel winds, waves and currents. Firstly, the motion analysis was conducted with respect to the submerged structures and the flexible jumper. Regarding to the behavioral characteristics of the flexible jumper, the FPSO-induced motions were dissipated along the jumper due to the decoupling effect. Secondly, structural strength analysis was conducted for the grades X65/X70/X80 using normalized von Mises stress, Method 1 and Design Membrane Loading Utilization (DMLU). The grade X65 was shown to be near failure limitation in DMLU considering ultimate limit state in both 100 and 500-yr hurricane conditions. Finally, the short-term

fatigue damage was estimated for the given material. The grade X65 with the high class safety factor did not meet the targeted product service life of 25 years in 500-yr hurricane conditions. In comparison with SCRs and LWSCRs, the FSHR had outstanding lower maximum fatigue damage of 4.78E-08 in such extreme conditions.

In conclusion, for the riser system the difference of both the motion responses and the stress evaluation results were minor, regardless of the environmental conditions. The results definitely indicate that the flexible jumper decouples the overall riser system from FPSO induced motions. Therefore, the variations of the flexible jumper length or the underwater-location of the submerged structures is carefully analyzed. In addition, with respect to the structural analysis results, the maximum value of X65 in DMLU approached limit state, and the estimated fatigue service life was below the targeted level. These results prove that using low strength material X65 for the vertical riser material is completely hazardous considering survival condition. Therefore, the grade X70 or the high strength material X80 should be considered in order to prevent structural and fatigue failures in advance.

DEDICATION

To my wife, Dujin, and my son, Sunwoo with love.

ACKNOWLEDGEMENTS

I would like to offer special thanks to my advisor, Dr. M.H. Kim, for his encouragement and guidance during my graduate studies. Special thanks are extended to my committee members, Dr. Randall and Dr. Schubert, for their guidance and excellent teaching, and also thanks to Dr. S.J. Kim and Dr. H.Y. Kang for their friendship and mentorship. Last but not least, thanks to my parents for their continuous encouragement and to my wife, Dujin for her patience and love, and I would like to express my love to my son, Sunwoo.

TABLE OF CONTENTS

Page

ABSTRACT ii

DEDICATION iv

ACKNOWLEDGEMENTS v

TABLE OF CONTENTS vi

LIST OF FIGURES viii

LIST OF TABLES xii

CHAPTER I INTRODUCTION 1

1.1 General 1
1.2 Literature Review 4
1.3 Research Objective 6

CHAPTER II THEORETICAL BACKGROUND 7

2.1 Motions of Submerged Body and Risers 7
2.1.1 Linear Wave Theory 7
2.1.1.1 Governing Equations 7
2.1.1.2 Boundary Conditions 9
2.1.1.3 Incident Wave 11
2.1.1.4 Wave Body Interaction 13
2.1.2 Morison's Equation 15
2.1.2.1 Morison's Equation for Fixed Body 15
2.1.2.2 Morison's Equation for Moving Body 16
2.1.2.3 Hydrodynamic Coefficients 16
2.1.2.4 Mass and Hydrostatic Stiffness Matrices 17
2.1.3 Mooring Dynamics 21
2.1.4 Governing Equation in Time-Domain 22
2.2 Structural Analysis of Risers 23
2.2.1 Design Specification Criteria 24
2.2.1.1 Bursting Criterion 24
2.2.1.2 Hoop Buckling Criterion 25
2.2.1.3 Yield Criterion 27

2.2.1.4 Fatigue Criterion 28
2.2.2 Stress Analysis 29
2.2.2.1 Axial and Bending Normal Stresses 29
2.2.2.2 Radial and Hoop Stresses 31
2.2.3 Short-term Fatigue Analysis 32

CHAPTER III DESIGN BASE LINES 36

3.1 FPSO Numerical Model 36
3.2 Free Standing Hybrid Riser Numerical Model 39
3.3 Submerged Structures Numerical Model 42
3.4 Environmental Conditions 44

CHAPTER IV CASE STUDIES 49

4.1 Fixed-Fairlead Analysis 49
4.1.1 Dynamic Response of Submerged Structures 50
4.1.2 Inertial and Viscous Forces on Submerged Structures 54
4.1.3 Dynamic Response of Flexible Jumper 59
4.1.4 Stress Evaluation on Riser 60
4.2 Moving-Fairlead Analysis 63
4.2.1 Dynamic Response of Submerged Structures 64
4.2.2 Inertial and Viscous Forces on Submerged Structures 70
4.2.3 Dynamic Response of Flexible Jumper 74
4.2.4 Stress Evaluation on Riser 79
4.2.5 von-Mises Stress Evaluation on Riser 86
4.2.6 Combined Load Evaluation on Riser 91
4.2.7 Short-term Fatigue Damage Analysis 94

CHAPTER V SUMMARY AND CONCLUSION 101

REFERENCES 104

LIST OF FIGURES

Page

Fig. 1.1 Various types of offshore structures *(Image source: www.modec.com)*.....1

Fig. 1.2 Various types of risers *(Image source*: DNV-OS-F201*)*……2

Fig. 1.3 Schematic of FSHR ……4

Fig. 1.4 Buoyancy Supported *(Image source: www.subsea7.com)* ……..…….4

Fig. 2.1 Wave Characteristic……...…….14

Fig. 2.2 Direction of axial force……30

Fig. 2.3 Bending normal stress *(Image source*: *POSCO_RIST_2nd Final)*…….31

Fig. 2.4 Radial and Hoop stresses *(Image source: www.engrapps.com)*….....31

Fig. 3.1 General arrangement of mooring (a) and riser (b) systems *(Image source: Taha and Kim 2003)*……..……..37

Fig. 3.2 Configuration of Free Standing Hybrid Riser (FSHR)……...41

Fig. 3.3 Direction of environmental loads, 180^{o} from east to west……44

Fig. 3.4 JONSWAP Wave Spectrum……45

Fig. 3.5 API Wind Spectrum……..47

Fig. 4.1 Slope of vertical riser (fixed-fairlead condition)……49

Fig. 4.2 6DOF motions of BC & URA under 100-yr hurricane condition (fixed-fairlead analysis)……...…….50

Fig. 4.3 6DOF motions of BC & URA under 500-yr hurricane condition (fixed-fairlead analysis)……51

Fig. 4.4 Motion response spectra of BC & URA (fixed-fairlead analysis)……53

Fig. 4.5 Inertial & viscous forces acting on BC&URA under 100-yr hurricane condition (fixed-fairlead analysis)……55

Fig. 4.6 Inertial & viscous Forces acting on BC&URA under 500-yr hurricane condition (fixed-fairlead analysis)……56

Fig. 4.7 Inertial & viscous forces response spectra of BC&URA……....57

Fig. 4.8 Vertical velocity and acceleration under 100 and 500-yr hurricane Conditions……..……59

Fig. 4.9 Axial and bending normal stress distributions of the flexible jumper under 100 and 500-yr hurricane conditions (fixed-fairlead analysis)……..…..…60

Fig. 4.10 Axial and bending normal stress distributions of the vertical riser under 100 and 500-yr hurricane conditions (fixed-fairlead analysis)……61

Fig. 4.11 Slope of vertical riser (moving-fairlead condition)……...……63

Fig. 4.12 6DOF motions of BC & URA in 100-yr hurricane condition……...64

Fig. 4.13 6DOF motions of BC & URA in 500-yr hurricane condition……...65

Fig. 4.14 Response spectra of the surge, heave and pitch of BC & URA……66

Fig. 4.15 Motion tracking of the submerged structures (Top) and FPSO (Down) for 3hr under 100 and 500-yr hurricane conditions…..……..67

Fig. 4.16 Inertial and viscous forces acting on BC& URA under 100-yr hurricane condition……..……...70

Fig. 4.17 Inertial and viscous forces acting on BC&URA under 500-yr hurricane condition……...71

Fig. 4.18 Inertial and viscous response spectra under 100 and 500-yr hurricane conditions……..…72

Fig. 4.19 Vertical velocity and acceleration under 100 and 500-yr hurricane conditions of the flexible jumper……...……....75

Fig. 4.20 Vertical velocity response spectra of the flexible jumper under 100 and 500-yr hurricane conditions……..…76

Fig. 4.21 Minimum Bend Radius (MBR) of flexible riser *(Image source: User's Guide of Coflexip Flexible Steel Pipes for Drilling and Service Application of Technip)* ……..77

Fig. 4.22 Minimum radius of curvature of the flexible jumper under 100 and 500-yr hurricane conditions……..……..…78

Fig. 4.23 MBR occurrence time of the flexible jumper under 100 and 500-yr hurricane conditions…….……79

Fig. 4.24 Axial stress distributions of the flexible jumper and vertical riser under 100 and 500-yr hurricane conditions……..80

Fig. 4.25 Bending normal stress distributions of the flexible jumper and the vertical riser under 100 and 500-yr hurricane conditions ……....81

Fig. 4.26 Horizontal curvature of the flexible jumper under 100 and 500-yr hurricane conditions……...……..…82

Fig. 4.27 Nearest and farthest horizontal offsets between FPSO and the submerged structures……..……83

Fig. 4.28 Configuration of the flexible jumper at nearest and farthest offsets under 100 and 500-yr hurricane conditions……...83

Fig. 4.29 Axial stress distribution of the flexible jumper at nearest and farthest offsets under 100 and 500-yr hurricane conditions…….……84

Fig. 4.30 Bending normal stress distributions of the flexible jumper at nearest and farthest offsets under 100 and 500-yr hurricane conditions……85

Fig. 4.31 Internal/External pressures and Radial/Hoop stresses of the vertical riser….86

Fig. 4.32 Normalized von-Mises Stress of the Vertical Riser……88

Fig. 4.33 Normalized von-Mises Stress of X60, X70 and X80 Vertical Riser……89

Fig. 4.34 Combined membrane loads of X65, X70 and X80……...92

Fig. 4.35 Design Membrane Load Utilization of X65, X70 and X80 under 100 and 500-yr hurricane conditions……93

Fig. 4.36 Fatigue service life of the X65, X70 and X80 under 100-yr and 500-yr…..…94

Fig. 4.37 Comparison of the fatigue service life between 100 and 500-yr hurricane conditions with respect to X65, X70 and X80……..96

Fig. 4.38 Fatigue service life of X65 under 100 and 500-yr hurricane conditions…….97

Fig. 4.39 Short-term fatigue damages of LWSCRs (left) and SCRs (right)…….99

Fig. 4.40 Short-term fatigue damage distribution of free standing hybrid riser…… 100

LIST OF TABLES

Page

Table 2.1 Safety class & Material resistance factors……26

Table 2.2 Design Fatigue Factor (DFF) Safety Class……..28

Table 3.1 Main particulars of the vessel (Tahar and Kim 2003)……..36

Table 3.2 Main particular of FPSO mooring system (Tahar and Kim 2003)……..38

Table 3.3 Main particular of risers (Tahar and Kim 2003)……..39

Table 3.4 Main particular of FSHR……39

Table 3.5 Length Information of FSHR……40

Table 3.6 Yield strength of the vertical riser ……..…41

Table 3.7 Main particulars of the submerged structures……...42

Table 3.8 Hydrodynamic coefficients of the submerged structures……...42

Table 3.9 Wave conditions……46

Table 3.10 Current profiles……..46

Table 3.11 1-hour Mean Wind Speed (10 m Elevation)……..48

Table 4.1 Statistics of the submerged structures (fixed-fairlead analysis)……54

Table 4.2 Statistics of the inertial and viscous forces acting on BC&URA ……..58

Table 4.3 Summary table of axial and bending normal stresses of the FSHR under 100 and 500-yr hurricane conditions (fixed-fairlead analysis)……62

Table 4.4 Statistics of the submerged structures……...68

Table 4.5 Statistics of the FPSO……...69

Table 4.6 Statistics of the inertial and viscous forces……74

Table 4.7 Three points' vertical velocities of the flexible jumper……....76

Table 4.8 MBR Occurrence time ……..78

Table 4.9 Axial stresses of the flexible jumper and the vertical riser……..…80

Table 4.10 Bending normal stresses of flexible jumper and the vertical riser……82

Table 4.11 Horizontal offsets between the FPSO and the Submerged Structures……..84

Table 4.12 Axial stress of the flexible jumper at farthest offset of FPSO……...86

Table 4.13 Bursting confirmation with respect to the vertical riser ……..…87

Table 4.14 Hoop buckling confirmation with respect to the vertical riser……..87

Table 4.15 Normalized VMS of the vertical riser under 100 and 500-yr hurricane conditions……90

Table 4.16 Combined membrane loads of the X60, X70 and X80……..92

Table 4.17 Design Membrane Load Utilization of the X65, X70 and X80……....94

Table 4.18 Fatigue service life under 100 and 500-yr hurricanes……95

Table 4.19 Fatigue service life with applied DFF of the vertical riser……98

Table 4.20 Comparison of short-term fatigue damage without applying DFF……...99

CHAPTER I

INTRODUCTION

1.1 General

As the demand for oil and gas gradually increases through the rapid growth of newly industrialized counties-China, India, Brazil etc.-the exploration and production of oil and gas fields has steadily shifted from near shore to deep water (over 4,000 ft) and ultra-deep water (over 7,000 ft). Accordingly, the acceleration in offshore development to deepwater requires developments in technology; for example, in deep-sea drilling and production, various types of FPUs (Floating Production Units) (such as Tension Leg Platforms (TLPs), Spar, Semi-submersible and Floating Production Storage Offloading (FPSOs)) are replacing with jacket type fixed platforms. FPSO is the most preferred by

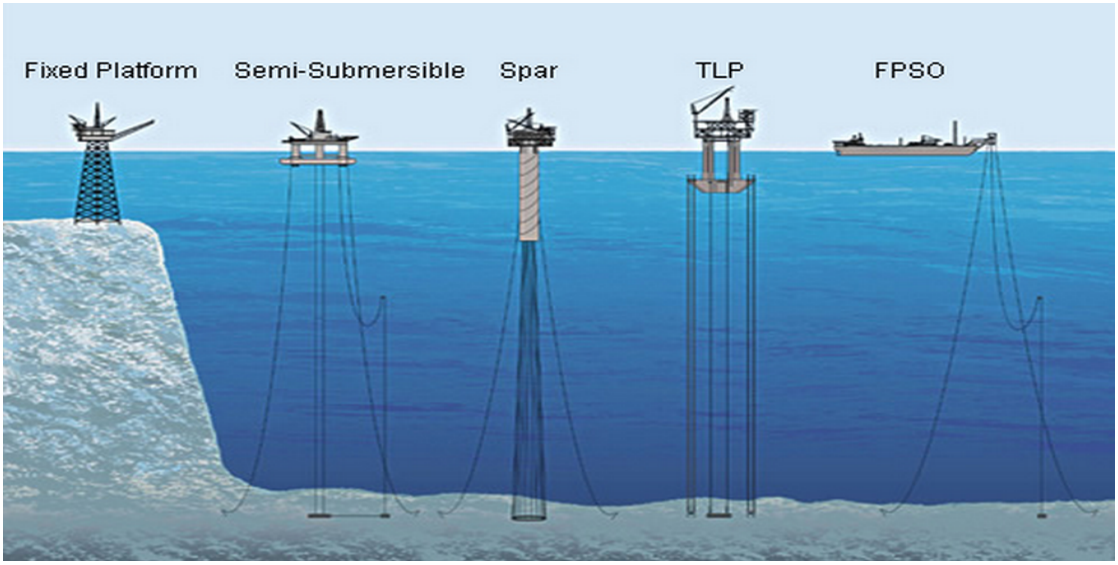

Fig. 1.1 Various types of offshore structures *(Image source: www.modec.com)*

operators for deepwater development because of wide topsides space that facilitates flexible equipment layout, vast storage volume for oil and gas, and outstanding mobility compared with other floaters. Nevertheless, the choice of riser types in deep water and ultra-deep water in the case of FPSOs is constrained, because they are basically high motion vessels. In this regards, Steel Catenary Risers (SCRs) and Lazy-Wave Steel Catenary Risers (LWSCRs) are unsuitable for deep water or ultra-deep water high motion vessels due to the structural limitations such as local buckling and short-term fatigue failure at touch-downzone , and significant payload on vessels.

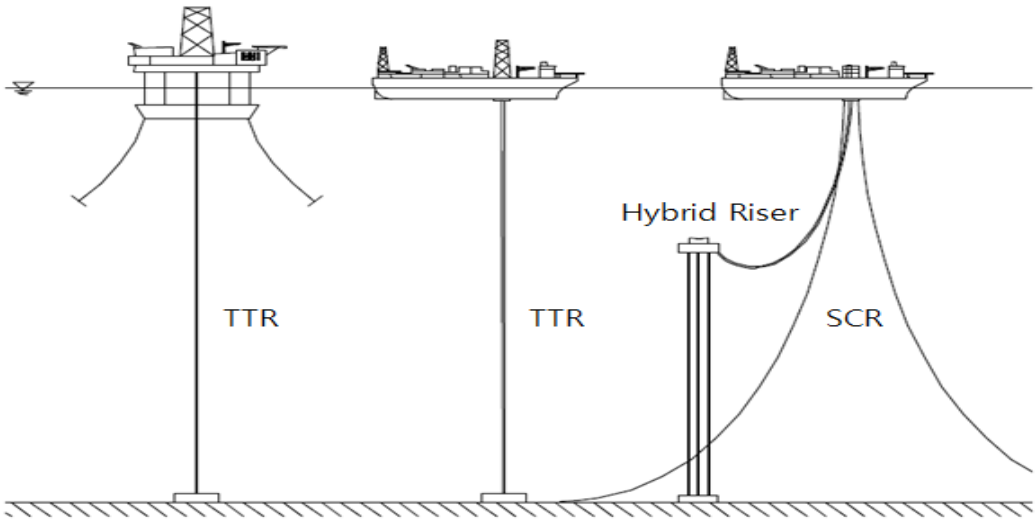

Fig. 1.2 Various types of risers *(Image source*: DNV-OS-F201*)*

For these problems with SCRs and LWSCRs, hybrid risers have been considered an alternative solution for deep water or ultra-deep water development in harsh

environmental conditions. Basically, the hybrid riser is one in which the riser system is composed of two different risers connecting with each other through subsurface buoyancy, e.g. a combination of a flexible jumper with SCR or with a vertical riser.

The hybrid riser systems are categorized into two types (Bob-Manuel, 2013). The first type is Free Standing Hybrid Risers (FSHRs) which include both single and bundled types. The other type is Buoyancy Supported Risers (BSRs). FSHRs consist of the following three main parts: flexible jumper, Buoyancy Can (BC) with Upper Riser Assembly (URA), and vertical riser. Unlike FSHRs, BSRs are composed of the following three main parts: SCRs, H-shaped buoy and flexible jumper. These two hybrid riser systems are represented schematically in Fig. 1.3 below. The world's first hybrid riser, the bundled type, was installed on a semi-submersible at Green Canyon 29 field in Gulf of Mexico in 1988, and in 2011 single line FSHRs were installed on a FPSO in the Gulf of Mexico 2011 at Cascade and Chinook field.

The FSHR is a robust solution compared with SCR and has the following several advantages (Song *et al.*, 2010):

- Low payload on Floating Production Unit (FPU)
- Decoupling of riser from FPU
- Pre-installation before arrival of FPU on site

However, the hybrid riser system has a few limitations, as shown below.

- High capital expenditure (CAPEX)
- Clashing with adjacent structures
- Required long lead components

1.2 Literature Review

There have been numerous studies with respect to various hybrid riser systems. Fisher and Berner (1988) introduced the world's first installed hybrid riser developed by Cameron Offshore Engineering in Green Canyon Block 29. Chaudhuri et al (1987) addressed the analysis results of the dynamic behaviors of hybrid riser by employing a non linear finite element analysis tool, FLEXCOM. However, the assumed environmental condition was an operational extreme condition with significant wave height 7m which did not fully reflect the extreme environment, 100 year return period

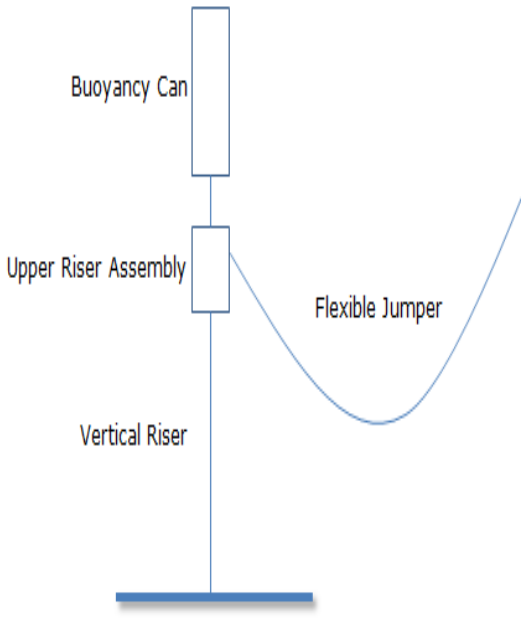

Fig. 1.3 Schematic of FSHR

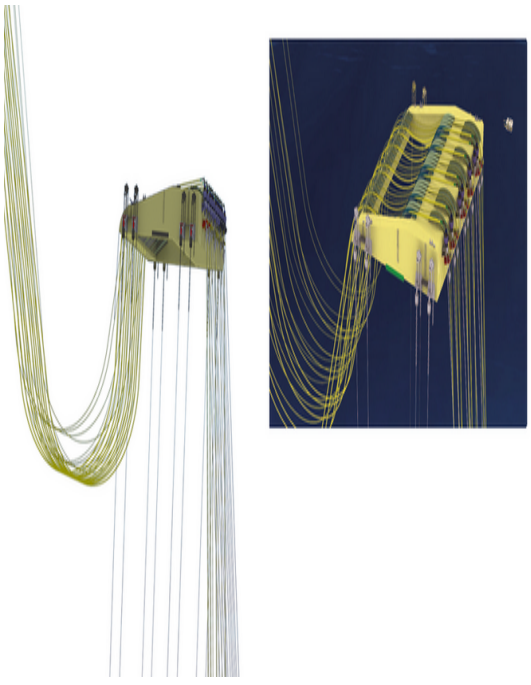

Fig. 1.4 Buoyancy Supported Riser
(Image source: www.subsea7.com)

hurricane. Hatton and Lim (1999) presented pipe-in-pipe arrangement Concentric Offset Riser (COR) which is regarded as third generation hybrid riser developed by 2H Offshore, and the numerical analysis of the COR was performed under the assumption of 100 year return period hurricane in West of Africa. As the paper only presented the maximum tension values of 3" and 10" jumpers, it was difficult to figure out the overall tension variations along the jumper. Sertã et al (2000) presented following three hybrid riser systems: The first one is the Cameron concept same as the first installed hybrid riser developed in 1980's which installed in Green Canyon Block 29 field. The second hybrid riser type is the steel catenary riser is connected with flexible jumper via submerged buoy moored by means of four tendons. The last one is vertical riser is connected from sea bottom to flexible jumper through buoyancy can that has alike FSHR configuration. Andueza and Stefen (2001) described steel hybrid riser concept that consists of steel catenary jumper and self-standing vertical riser. Petruska et al (2002) analyzed and compared among the following three riser systems; Steel Lazy Wave Riser, Single Line Hybrid Riser and Tension Leg Riser in terms of moving-fairlead analysis by employing commercial program OrcaFlex. Roveri et al (2008) presented the FSHR installed in Campos Basin, offshore Brazil in 2007. The paper explained that the fatigue caused by first and second order motions is negligible due to the fatigue service life exceeding 9999 years. Francesco lob et al (2014) addressed the fatigue service life of hybrid risers with respect to first order motion and VIV. The paper explained that the fatigue caused by first order motion is negligible due to the decoupling effect of a flexible jumper.

1.3 Research Objective

The main aim of this study is to confirm the outstanding motion decoupling between Free Standing Hybrid Riser and surface floater even in extreme and semi-survival environmental conditions. To prove the decoupling effect, following points are confirmed.

- Dissipation of FPSO induced dynamic motions via flexible jumper
- Lower axial and bending normal stresses distribution along jumper
- Stable movements of vertical riser with lower stress level
- Stable movements of submerged structures
- Extremely long fatigue service life of the vertical riser compared with different types of risers

In this study, the FPSO coupled Free Standing Hybrid Riser is investigated under 100 and 500-yr hurricane conditions of deep-water Gulf of Mexico in the time-domain using 6-DOF coupled hull/riser/mooring dynamic simulation program CHARM3D. The commercial software CHARM3D has been proved over the past decade with numerous experimental results and field data, and the program is useful to analyze coupled floater and riser/mooring systems (Kim et al, 2001)

CHAPTER II

THEORETICAL BACKGROUND

2.1 Motions of Submerged Body and Risers

The sequence of this chapter is that firstly the background of first order wave theory is discussed, secondly calculation of wave load against a submerged body by employing Morison's equation is dealt, thirdly the slender rod theory used in commercial code CHARM3D is briefly reviewed, and finally the governing equation of motion in time-domain program CHARM3D is addressed.

2.1.1 Linear Wave Theory

As the first-order wave is only considered in this study, the governing equations of fluid, boundary conditions, incident wave formula and two length scale ratios related with wave-body interaction for linear wave theory are discussed as follows.

2.1.1.1 Governing Equations

It is assumed that the fluid is ideal fluid: incompressible, inviscid and irrotational, and the first two conditions satisfy below conservation of mass equation (2.1), conservation of momentum equation (2.2), and Laplace equation (2.3).

$$\vec{\nabla} \bullet \vec{V} = 0 \tag{2.1}$$

$$\rho\left[\frac{\partial \vec{V}}{\partial t} + (\vec{V} \bullet \vec{\nabla})\vec{V}\right] = -\vec{\nabla}p + \rho\vec{g} + \mu\nabla^2\vec{V} \tag{2.2}$$

where viscous term ($\mu\nabla^2\vec{V}$) is negligible, and then it turns to Euler's equation.

$$\nabla^2\phi = 0 \tag{2.3}$$

where, $\vec{\nabla}\phi = \vec{V}$, and ϕ is velocity potential

The irrotational fluid comes from inviscid fluid assumption, and the irrotational fluid satisfies the below equation.

$$\vec{\nabla} \times \vec{V} = 0 \tag{2.4}$$

From conservation of momentum, we can derive the Bernoulli equation as below, and the pressure in fluid can be obtained from the below formula.

$$p = -\rho\frac{\partial\phi}{\partial t} - \frac{\rho}{2}(\vec{\nabla}\phi)^2 - \rho gz + C(\mathrm{t}) \tag{2.5}$$

where the term $C(\mathrm{t})$ is arbitrary constant and usually set as zero.

The velocity potential (ϕ) can be solved from Laplace equation (2.3) with the following two boundary conditions, Kinematic Free Surface Boundary Condition and

Dynamic Free Surface Condition, which are dealt with the next chapter.

2.1.1.2 Boundary Conditions

To find velocity potential (ϕ) from Laplace equation, Kinematic Free Surface Boundary Condition and Dynamic Free Surface Condition should be considered. From these boundary conditions, we can derive further two boundary conditions: Bottom Boundary Condition and Combined Free Surface Boundary Condition.

- Kinematic Free Surface Boundary Condition (KFSBC)

  The mathmatical expression of a surface is

$$S(\mathrm{x},\mathrm{y},\mathrm{z},\mathrm{t}) = 0 \tag{2.6}$$

Since the fluid particles always should stay on boundary surface.

$$S(\mathrm{x}_p,\mathrm{y}_p,\mathrm{z}_p,\mathrm{t}) = 0 \tag{2.7}$$

Required by KFSBC, material derivative of a surface is always zero.

$$\frac{DS}{Dt} = \frac{\partial S}{\partial t} + \vec{V} \bullet \nabla S \tag{2.8}$$

where $S(\mathrm{x},\mathrm{y},\mathrm{z},\mathrm{t}) = \eta(\mathrm{x},\mathrm{y},\mathrm{t}) - \mathrm{z} = 0$

Therefore, Kinematic Free Surface Boundary Condition is

$$\frac{\partial \eta}{\partial t} + \frac{\partial \phi}{\partial x}\frac{\partial \eta}{\partial x} + \frac{\partial \phi}{\partial y}\frac{\partial \eta}{\partial y} - \frac{\partial \phi}{\partial z} = 0 \qquad \text{on } z = \eta \tag{2.9}$$

Let set flow velocity as $\vec{\nabla}\phi$, then the normal velocity on the wetted surface is

$$\vec{\nabla}\phi \bullet \vec{n} = \frac{\partial \phi}{\partial n} \tag{2.10}$$

- Dynamic Free Surface Boundary Condition (DFSBC)

From the Kinematic Free Surface Boundary Condition, the new unknown variable η is added. The Bernoulli equation (2.5) is employed to specify the new variable.

$$\frac{\partial \phi}{\partial t} + \frac{1}{2}(\vec{\nabla}\phi)^2 + g\eta = 0 \qquad \text{on } z = \eta \tag{2.11}$$

- Bottom Boundary Condition (BBC)

According to the Kinematic Free Surface Boundary Condition, the normal velocity of fluid particles should be the same as the velocity of seafloor boundary. Since

the seafloor is always stationary, the normal velocity of fluid particles is zero as below.

$$\frac{\partial \phi}{\partial z} = 0 \qquad \text{on} \qquad z = -h \tag{2.12}$$

- Combined Free Surface Boundary Condition

From Taylor expansion, the non-linearity in KFSBC and DFSBC can be removed, and the free surface condition is moved from free surface ($z = \eta$) to mean water level ($z = 0$).

$$\frac{\partial \eta}{\partial t} - \frac{\partial \phi}{\partial z} = 0 \quad \& \quad \eta = -\frac{1}{g}\frac{\partial \phi}{\partial t} \quad \text{on } z = 0 \tag{2.13}$$

These above two equations are combined into one equation as below.

$$\frac{\partial^2 \phi}{\partial t^2} + g\frac{\partial \phi}{\partial z} = 0 \qquad \text{on } z = 0 \tag{2.14}$$

2.1.1.3 Incident Wave

From Stokes series, the velocity potential and the wave free surface can be expanded as below.

$$\phi = \varepsilon\tilde{\phi}^{(1)} + \varepsilon^2\tilde{\phi}^{(2)} + \varepsilon^3\tilde{\phi}^{(3)} + ... \tag{2.15}$$

$$\eta = \varepsilon\tilde{\eta}^{(1)} + \varepsilon^2\tilde{\eta}^{(2)} + \varepsilon^3\tilde{\eta}^{(3)} + ... \tag{2.16}$$

where wave steepness (ε) in deepwater is far small ($\varepsilon = \frac{H}{2\pi\lambda} \ll 1$).

The expanded series are substituted into the governing equations in the previous chapter, and then they are sorted into several terms based on orders. For the free surface of KFSBC and DFSBC, the nonlinearity should be removed by expanding Taylor series with respect to $z = 0$. Therefore, the governing equations of the first order are summarized as below.

$$\nabla^2\phi^{(1)} = 0 \qquad \text{in fluid} \tag{2.17}$$

$$\frac{\partial\phi^{(1)}}{\partial z} = 0 \qquad \text{on } z = -h \tag{2.18}$$

$$\frac{\partial\eta^{(1)}}{\partial t} - \frac{\partial\phi^{(1)}}{\partial z} = 0 \qquad \text{on } z = 0 \tag{2.19}$$

$$\frac{\partial\phi^{(1)}}{\partial t} + g\eta^{(1)} = 0 \qquad \text{on } z = 0 \tag{2.20}$$

where $\phi^{(1)} = \varepsilon\tilde{\phi}^{(1)}$ and $\eta^{(1)} = \varepsilon\tilde{\eta}^{(1)}$.

From the first order of KFSBC and DFSBC, we can derive the first order combined boundary condition as below

$$\frac{\partial^2 \phi^{(1)}}{\partial t^2} + g\frac{\partial \phi^{(1)}}{\partial z} = 0 \qquad \text{on } z = 0 \tag{2.21}$$

The first order velocity potential, $\phi^{(1)} = \frac{gh}{2\omega}\frac{\cosh(\mathrm{k(z+h)})}{\cosh(\mathrm{kh})}\sin(\mathrm{kx}-\omega\mathrm{t})$, can be derived from by employing separation variable method with Laplace equation, bottom boundary condition and dynamic free surface boundary condition. In deep water, the first order velocity potential is converted into $\phi^{(1)} = \frac{gh}{2\omega}\sin(kx-\omega t)e^{kz}$. The dispersion relationship ($\omega^2 = gk\tanh(kh)$) is induced by after substituting first order velocity potential into the combined free surface boundary condition.

2.1.1.4 Wave Body Interaction

In order to predict wave diffraction effect and dominant force between inertia and viscous forces, the below two length scale ratios are employed.

scatter parameter (ka) (2.22)

Keulegan-Carpenter number (H/a) (2.23)

where in scatter parameter, "k" is wave number and "a" is characteristic body dimension.

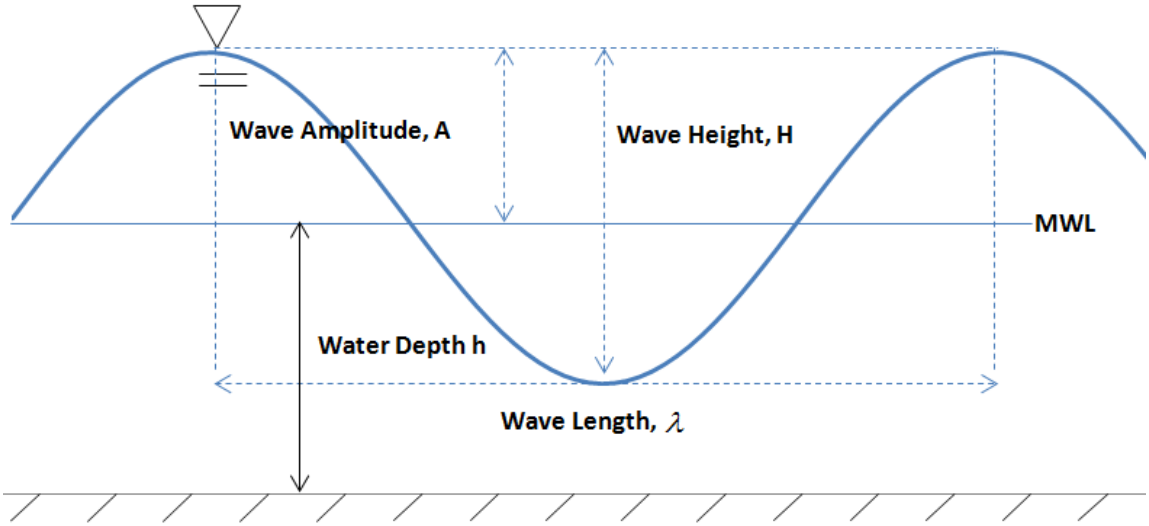

Fig. 2.1 Wave Characteristic

If the characteristic body dimension is far smaller than wave length ($ka \ll 1$), the incident wave will not be significantly scattered off against the body. In this case, Morison's equation is employed to calculate the wave force on body. For $ka \geq \vartheta(1)$, however, the wave diffraction effect will happen to significant degree.

In KC (Keulegan-Carpenter) number, "H"is wave height. From the KC number, dominant force between inertia and drag forces can be predicted. If the wave motion is far smaller than body size ($H / a \ll 1$), wave inertia force is dominant in fluid domain. For $H / a \geq \vartheta(1)$, however, wave drag force is dominant due to the occurrence of fluid separation on body surface.

There are two methods to calculate wave loads on floater. The first one is diffraction theory based on velocity potentials. The other method is Morison's equation (semi-empirical method). In this research, we focus on wave forces against Buoyancy

Can (BC) and Upper Riser Assembly (URA) rather than FPSO. It is assumed that the dimensions of the BC and URA are far smaller than wave length ($ka \ll 1$), so Morison's equation is employed. The Morison's equation will be discussed in a later chapter.

2.1.2 Morison's Equation

The semi-empirical formula, Morison's equation, is simply composed of inertial and drags terms and the method is useful to calculate fluid loading on circular structures in unsteady viscous flow. As discussed in previous chapters, also, the scatter parameter (ka) is far smaller than wave length (λ), then Morison's equation is employed to calculate wave force on the offshore floater. Before applying the equation, firstly it is important to confirm whether the body is moving or not and then set inertial and drag coefficients based on several factors such as Reynolds number, Roughness number, KC number (H / a), etc.

2.1.2.1 Morison's Equation for Fixed Body

When the body is fixed case and the wave loading can be calculated as below.

$$F = \rho C_M \forall \ddot{\eta} + \frac{1}{2}\rho C_D A \dot{\eta}\left|\dot{\eta}\right| \tag{2.24}$$

where ρ : seawater density, C_M : inertia coefficient, $\forall$: volume of body,

A : cross sectional area perpendicular to wave propagation, $\dot{\eta}$: wave velocity.

2.1.2.2 Morison's Equation for Moving Body

When the body is moving, then the above formula should be modified as below.

$$F_m = \rho\forall\ddot{\eta} + \rho C_a\forall(\ddot{\eta} - \ddot{X}) + \frac{1}{2}\rho C_D A(\dot{\eta} - \dot{X})\left|\dot{\eta} - \dot{X}\right| \tag{2.25}$$

where C_a : added mass coefficient, $\dot{X}$: body velocity.

From the Morison's equation for moving the body, it can be confirmed that the Froude-Krylov force ($\rho\forall\ddot{\eta}$) is independent of body motion.

2.1.2.3 Hydrodynamic Coefficients

From the previous chapter, it should be noted that hydrodynamic coefficients of C_D and C_a are playing an important role in calculation of wave load against the fixed or moving body. However, these coefficients are not certain fixed constant, so the values can be obtained through experiments.

- ***Drag Coefficient,*** $C_D = \dfrac{F_d}{\frac{1}{2}\rho(\dot{\eta} - \dot{X})\left|\dot{\eta} - \dot{X}\right| A}$

Drag coefficient is the function of Reynolds number, $\frac{\rho\left|\dot{\eta}-\dot{X}\right|L}{\mu}$

where, μ : Dynamic viscosity of wave ($Pa\cdot s$), L :characteristic linear dimension

The coefficient can be obtained by employing following the drag force formula, $F_d=\frac{1}{2}\rho(\dot{\eta}-\dot{X})\left|\dot{\eta}-\dot{X}\right|C_D A$ In this study, the drag coefficient for submerged structures, 1.0 is employed.

- ***Inertia Coefficient,*** $C_m=C_a+1=\frac{F_i}{\rho\forall\ddot{\eta}}$

$C_a=C_m-1$ is added mass coefficient or called virtual mass coefficient. Same as the above mentioned drag coefficient, the value of inertia coefficient is not fixed constant. The coefficient can be varied based on the body shape. In this study, the inertia coefficient for submerged structures, 1.0 is employed.

2.1.2.4 Mass and Hydrostatic Stiffness Matrices

The mass and hydrostatic stiffness matrices are employed in this study to derive the equation of motions of submerged structures, upper riser assembly and buoyancy can, and these matrices are summarized as follow.

· ***Mass Matrix***

$$\begin{bmatrix} m & 0 & 0 & 0 & mz_{B,\mathrm{g}} & -my_{B,\mathrm{g}} \\ 0 & m & 0 & -mz_{B,\mathrm{g}} & 0 & mx_{B,\mathrm{g}} \\ 0 & 0 & m & my_{B,\mathrm{g}} & -mx_{B,\mathrm{g}} & 0 \\ 0 & -mz_{B,\mathrm{g}} & my_{B,\mathrm{g}} & (I_{YY}^{B}+I_{ZZ}^{B}) & -I_{YX}^{B} & -I_{YX}^{B} \\ mz_{B,\mathrm{g}} & 0 & -mx_{B,\mathrm{g}} & -I_{XY}^{B} & (I_{ZZ}^{B}+I_{XX}^{B}) & -I_{ZY}^{B} \\ -my_{B,\mathrm{g}} & mx_{B,\mathrm{g}} & 0 & -I_{XZ}^{B} & -I_{YZ}^{B} & (I_{XX}^{B}+I_{YY}^{B}) \end{bmatrix} \tag{2.26}$$

where,

a) m : body mass

b) $I_X^B = mx_{B,g}$, $I_Y^B = my_{B,g}$, $I_Z^B = mz_{B,g}$

c) $(x_{B,g} y_{B,g} z_{B,g})$: Center of gravity in body-fixed coordinate

d) Products of inertia $I_{XX}^B, I_{YY}^B, I_{ZZ}^B, I_{XY}^B = I_{YX}^B, I_{XZ}^B = I_{ZX}^B, I_{YZ}^B = I_{ZY}^B$

· ***Hydrostatic Stiffness Matrix***

$$\begin{bmatrix} 0 & 0 & 0 & 0 & 0 & 0 \\ 0 & 0 & 0 & 0 & 0 & 0 \\ 0 & 0 & \rho g A^{(0)} & \rho g I_Y^A & -\rho g I_X^A & 0 \\ 0 & 0 & \rho g I_Y^A & \rho g[I_{YY}^A + V^{(0)} z_{B,b}] - mgz_{B,\mathrm{g}} & -\rho g I_{YX}^A & -\rho g V^{(0)} x_{B,b} + mgx_{B,\mathrm{g}} \\ 0 & 0 & -\rho g I_X^A & -\rho g I_{YX}^A & \rho g[I_{XX}^A + V^{(0)} z_{B,b}] - mgz_{B,\mathrm{g}} & -\rho g V^{(0)} y_{B,b} + mgy_{B,\mathrm{g}} \\ 0 & 0 & 0 & 0 & 0 & 0 \end{bmatrix} \tag{2.27}$$

where,

a) $A^{(0)}$ = water-plane area, $V^{(0)}$ = submerged volume

b) Center of buoyancy in body-fixed coordinate is $(x_{B,\mathrm{b}} y_{B,\mathrm{b}} z_{B,\mathrm{b}})$

c) $I_X^V = V^{(0)} x_{B,\mathrm{b}}, I_Y^V = V^{(0)} y_{B,\mathrm{b}}, I_Z^V = V^{(0)} z_{B,\mathrm{b}}$

d) Moments of water-plane area is $I_X^A, I_Y^A, I_{XX}^A, I_{YY}^A, I_{XY}^A = I_{YX}^A$

The above two matrices are derived from the following two principles: conservation of linear momentum and conservation of angular momentum.

Firstly conservation of linear-momentum ($\vec{P} = m\vec{v}$) means the total linear momentum of rigid body is always constant without net external force. In other words, the summation of external forces is the same as the product of the moored floater mass and its acceleration as below.

$$m \frac{d^2 \vec{x}_g}{dt^2} = \iint_{S_B} p\vec{n}\, dS - mg\vec{k} + \vec{F} \tag{2.28}$$

From the above formula, the equations of linear momentum in x, y, z axes can be induced, respectively as below.

$$m\left[\frac{d^2 X^{(1)}}{dt^2} + \frac{d^2 \beta}{dt^2} z_{B,g} - \frac{d^2 \gamma}{dt^2} y_{B,g} \right] = -\rho \iint_{S_B^{(0)}} \frac{\partial \phi^{(1)}}{dt} n_1\, dS + F_X^{(1)} \tag{2.29}$$

$$m\left[\frac{d^2 Y^{(1)}}{dt^2} + \frac{d^2 \gamma}{dt^2} x_{B,g} - \frac{d^2 \alpha}{dt^2} z_{B,g} \right] = -\rho \iint_{S_B^{(0)}} \frac{\partial \phi^{(1)}}{dt} n_2\, dS + F_Y^{(1)} \tag{2.30}$$

$$m\left[\frac{d^2Z^{(1)}}{dt^2}+\frac{d^2\alpha}{dt^2}y_{B,g}-\frac{d^2\beta}{dt^2}x_{B,g}\right]=-\rho\iint_{S_B^{(0)}}\frac{\partial\phi^{(1)}}{dt}n_3\,dS+F_Z^{(1)} \tag{2.31}$$

Conservation of angular-momentum ($\vec{L}=I\vec{\omega}$) means the total angular momentum of rigid body is always constant without net external moment (or called torque). In other words, the summation of external net torque is same as the cross product of instantaneous position of a point and the force at the instantaneous position in the rigid body over to the entire submerged volume of moored floater as below.

$$\frac{d}{dt}\iiint_{V_B}\vec{x}\times\frac{d\vec{x}}{dt}dm=\iiint_{V_B}\vec{x}\times\frac{d^2\vec{x}}{dt^2}dm=\iiint_{V_B}\vec{x}\times p\vec{n}\,dS+\vec{x}_g\times(-mg\vec{k})+\vec{T} \tag{2.32}$$

From the above formula, we can derive equations of angular momentums as below.

$$\text{In } x\text{-axis, } I_Y^B\frac{d^2Z^{(1)}}{dt^2}-I_Y^B\frac{d^2Y^{(1)}}{dt^2}+(I_{YY}^B+I_{ZZ}^B)\frac{d^2\alpha}{dt^2}-I_{YX}^B\frac{d^2\beta}{dt^2}-I_{ZX}^B\frac{d^2\gamma}{dt^2} \tag{2.33}$$

$$=-\rho\iint_{S_B^{(0)}}\frac{\partial\phi^{(1)}}{\partial t}n_4\,dS-\rho g\left[Z^{(1)}I_Y^A+\alpha I_{YY}^A-\beta I_{XY}^A-\gamma_X^V+\alpha_Z^V\right]+mg\left[\alpha z_{B,\mathrm{g}}-\gamma x_{B,\mathrm{g}}\right]+\mathrm{T}_X^{(1)}$$

$$\text{In } y\text{-axis, } I_Z^B\frac{d^2X^{(1)}}{dt^2}-I_X^B\frac{d^2Z^{(1)}}{dt^2}+(I_{ZZ}^B+I_{XX}^B)\frac{d^2\beta}{dt^2}-I_{YX}^B\frac{d^2\gamma}{dt^2}-I_{ZX}^B\frac{d^2\alpha}{dt^2} \tag{2.34}$$

$$=-\rho\iint_{S_B^{(0)}}\frac{\partial\phi^{(1)}}{\partial t}n_5\,dS-\rho g\left[-Z^{(1)}I_X^A-\alpha I_{YX}^A+\beta I_{XX}^A+\beta_Z^V-\gamma_Y^V\right]+mg\left[\beta z_{B,\mathrm{g}}-\gamma y_{B,\mathrm{g}}\right]+\mathrm{T}_Y^{(1)}$$

$$\text{In } z\text{-axis, } I_X^B \frac{d^2Y^{(1)}}{dt^2} - I_Y^B \frac{d^2X^{(1)}}{dt^2} + (I_{XX}^B + I_{YY}^B)\frac{d^2\gamma}{dt^2} - I_{XZ}^B \frac{d^2\alpha}{dt^2} - I_{YZ}^B \frac{d^2\beta}{dt^2} \tag{2.35}$$

$$= -\rho \iint_{S_B^{(0)}} \frac{\partial \phi^{(1)}}{\partial t} n_6 \, dS + \mathrm{T}_Z^{(1)}$$

2.1.3 Mooring Dynamics

In order to analyze mooring and riser lines in terms of static or dynamic condition, extensible slender rod theory (Garrett, 1982) was employed in commercial code CHARM3D. (Ran and Kim, 1997) The below linear momentum conservation equation assumes that there is no torque.

$$-(B\vec{r}'')'' + (\lambda \vec{r}')' + \vec{q} = m\ddot{\vec{r}} \tag{2.36}$$

where B is the bending stiffness, $\vec{r}(s,t)$ is the position vector with respect to space and time, $\lambda = T - Bk^2$, m is the mass per unit length, and $\vec{q}$ is the distributed force on the rod per unit length.

In λ called Lagrange multiplier, T is the local effective tension, and k is the local curvature. It is assumed that the rod is elastic and extensible that is able to the below formula.

$$\frac{1}{2}(\vec{r}\cdot\vec{r}-1)=\frac{T}{A_tE}\approx\frac{\lambda}{A_tE} \tag{2.37}$$

where A_t is effective sectional area, i.e., cross sectional area of riser, and E is Young's modulus.

2.1.4 Governing Equation in Time-Domain

Morison's equation is essential equation in this study to derive governing equation of the time-domain program, CHARM3D. In this chapter, derivation of the governing equation of the time-domain program is addressed.

If there is no external force against submerged body, the equation of motion of the body is expressed as $M\ddot{X}+KX=0$. In this study, however, waves, currents, and riser system are interacting with the body. So the equation of motion can be modified as below.

$$M\ddot{X}+KX=F_m+F_r \tag{2.38}$$

where M=mass matrix, K=hydrostatic stiffness matrix, X=body displacement,

F_m = environmental loads ($\rho\forall\ddot{\eta}+\rho C_a\forall(\ddot{\eta}-\ddot{X})+\frac{1}{2}\rho C_D A(\dot{\eta}-\dot{X})\left|\dot{\eta}-\dot{X}\right|$),

F_r = force from risers

So the equation of motion can be reformed as

$M\ddot{X} + KX = \left(\rho\forall \ddot{\eta} + \rho C_a \forall (\ddot{\eta} - \ddot{X}) + \frac{1}{2}\rho C_D A(\dot{\eta} - \dot{X})\left|\dot{\eta} - \dot{X}\right| \right) + F_r$, and the added mass term, $\rho C_a \forall \ddot{X}$, is moved to LHS of the equation. Then the equation can be revised as the following form.

$$(M + \rho C_a \forall)\ddot{X} + KX = \left(\rho\forall \ddot{\eta} + \rho C_a \forall \ddot{\eta} + \frac{1}{2}\rho C_D A(\dot{\eta} - \dot{X})\left|\dot{\eta} - \dot{X}\right| \right) + F_r \qquad (2.39)$$

where $M_a = \rho C_a \forall$ (added mass), $F_{FK} = \rho\forall \ddot{\eta}$ (Froude Krylov force),

$F_M = \rho C_a \forall \ddot{\eta}$ (hydrodynamic mass force), and $F_D = \frac{1}{2}\rho C_D A(\dot{\eta} - \dot{X})\left|\dot{\eta} - \dot{X}\right|$ (drag force).

Therefore, the final governing equation in the time-domain program can be summarized as below form.

$$(M + M_a)\ddot{X} + KX = F_{FK} + F_M + F_D + F_r \qquad (2.40)$$

where $M_a = \rho C_a \forall$, $F_{FK} = \rho C_a \forall \ddot{\eta}$, $F_M = \rho C_a \forall \ddot{\eta}$, $F_D = \frac{1}{2}\rho C_D A(\dot{\eta} - \dot{X})\left|\dot{\eta} - \dot{X}\right|$,

and F_r = external force from risers

2.2 Structural Analysis of Risers

In the previous chapters, the theoretical background of hydrodynamics to calculate wave loads and body motions are reviewed. From this chapter, fundamental

background knowledge for structural analysis is discussed. The sequence is firstly the criteria in API and DNV codes for structural strength are dealt, secondly the required stress types of the mentioned codes are dealt, and finally the procedure of short-term fatigue analysis is discussed.

2.2.1 Design Specification Criteria

In this design specification criteria chapter, the criteria of bursting, hoop buckling, von-Mises yield, and short-term fatigue are discussed. The criteria are generally based on API and DNV codes, and its details can be confirmed in later chapters.

2.2.1.1 Bursting Criterion

If the internal pressure exceeds the strength of riser wall, then the rupture of the riser wall called bursting can occur. Therefore the below formula is employed for the bursting check required to conduct before engineering stage (DNV-OS-F201, Dynamic Risers).

$$(p_{li} - p_e) \le \frac{p_b(t_1)}{\gamma_m \cdot \gamma_{SC}} \tag{2.41}$$

where P_{li}, P_e: Local incidental pressure, External pressure, $P_b(t)$: Burst Resistance, and it can be calculated as below.

$$p_b(t) = \frac{2}{\sqrt{3}} \cdot \frac{2 \cdot t}{D - t} \cdot \min\left(f_y ; \frac{f_u}{1.15} \right) \tag{2.42}$$

2.2.1.2 Hoop Buckling Criterion

If riser is subjected to overpressure in deepwater, the riser cross section can collapse or called hoop buckling phenomenon. Therefore, the confirmation to the mentioned buckling is also required prior to engineering stage, and the below formulas are from DNV-OS-F201 (Dynamic Risers).

In deep water, riser should be designed to the below condition.

$$(\mathrm{p}_e - \mathrm{p}_{\min}) \le \frac{\mathrm{p}_c(\mathrm{t}_1)}{\gamma_{SC} \cdot \gamma_m} \tag{2.43}$$

where $\mathrm{p}_{\min}$: minimum internal pressure, p_c : resistance for hoop buckling (external pressure), and it is expressed as below.

$$(\mathrm{p}_c(\mathrm{t}) - \mathrm{p}_{el}(\mathrm{t})) \cdot (\mathrm{p}^2{}_c(\mathrm{t}) - \mathrm{p}^2{}_p(\mathrm{t})) = \mathrm{p}_c(\mathrm{t}) \cdot \mathrm{p}_{el}(\mathrm{t}) \cdot \mathrm{p}_p(\mathrm{t}) \cdot \mathrm{f}_0 \cdot \frac{D}{t} \tag{2.44}$$

where $p_{el}(t) = \frac{2 \cdot E\left(\frac{t}{D}\right)^3}{1-v^2}$: The elastic collapse pressure, poisson's ratio(v) for pipe wall material is 0.3, $p_p(t) = 2\frac{t}{D} \cdot f_y \cdot \alpha_{fab}$: The plastic collapse pressure, fabrication factor(α_{fab}) for UOE pipe is 0.85, $f_0 = \frac{D_{max} - D_{min}}{D}$: initial ovality ≥ 0.005, assumed 0.005 in this study.

Table 2.1 Safety class & Material resistance factors

Safety class resistance factor γ_{sc}		
Low	*Normal*	*High*
1.04	1.14	1.26
Safety class resistance factor γ_m		
ULS & ALS	*SLS & FLS*	
1.15	1.0	

2.2.1.3 Yield Criterion

Generally von-Mises stress can be used to check whether the riser will withstand under the extreme environmental loadings and other forces. As for plain round pipe, generally the transverse shear and torsion are negligible. So the three principal stress components of primary membrane stress are radial, hoop, and normal (axial + bending normal) stresses referred to 5.2.4.1 of API RP 2ND. Therefore von-Mises stress can be calculated by employing normal, hoop and radial stresses based on the below formula in API RP 2RD.

$$\sigma_v = \frac{1}{\sqrt{2}}\sqrt{(\sigma_n - \sigma_h)^2 + (\sigma_h - \sigma_r)^2 + (\sigma_r - \sigma_n)^2} \tag{2.45}$$

where $\sigma_{v,}\sigma_n$: von-Mises equivalent stress, and total normal stress (axial + bending normal), $\sigma_{r,}\sigma_h$: radial stress, and hoop stress

API RP 2RD describes the below formula that von-Mises equivalent stress should be less than allowable stress in extreme or survival conditions.

$$\sigma_v \le C_f \sigma_a = C_f C_a \sigma_y \tag{2.46}$$

where C_f : design case factor, e.g., extreme environmental condition, 1.2, σ_a : basic allowable combined stress= $C_a \cdot \sigma_y$, C_a, σ_y : allowable stress factor (C_a=2/3), min. yield strength of riser material.

The normalized von-Mises stress can be expressed as below and the value should be less than 1.0, otherwise it means the riser is structural fail.

2.2.1.4 Fatigue Criterion

In clause 2.2 and 6.2 of DNV-RP-F204 (Riser Fatigue), the fatigue criterion by employing S-N curve and standard DFF (Design Fatigue Factors) are presented for steel risers as below.

$$Fatigue\ Criterion: D \cdot DFF \leq 1.0 \tag{2.47}$$

where D: Damage Index, DFF: Design Fatigue Factors (Please see below Table)

Table 2.2 Design Fatigue Factor (DFF) Safety Class

DFF Safety Class		
Low	*Normal*	*High*
3.0	6.0	10.0

The fatigue service life of the riser can be calculated by using the time applying to the riser under environmental loadings and damage index as below.

$$\text{Calculation of Fatigue Service Life} = \text{Force Applied Time} \times \frac{1}{D} \tag{2.48}$$

2.2.2 Stress Analysis

In previous chapters, design specific criteria based on API and DNV codes are discussed. From this chapter, the essential stresses such as axial, bending normal, radial and hoop stresses required in design specific criteria are addressed.

2.2.2.1 Axial and Bending Normal Stresses

In this study, axial stress and bending normal stress are assumed as main fluctuating stress in Free Standing Hybrid Riser system. Total normal stress in riser comes from axial stress and bending normal stress, and their definitions are described as below.

- ***Axial Stress***

If riser is subjected to axial forces, F, along its axis, then the axial stress can be calculated as below.

$$\sigma_{axial} = F / A \tag{2.49}$$

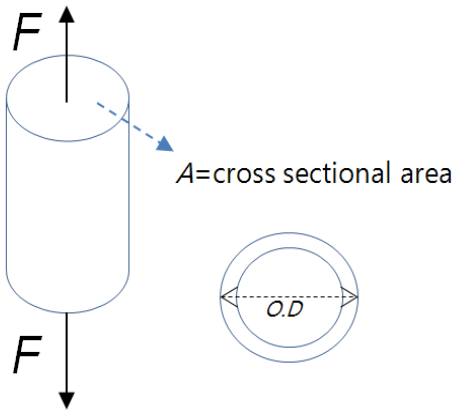

Fig. 2.2 Direction of axial force

In vertical riser, the main stress in normal direction is axial stress caused by buoyancy force comes from the Buoyancy Can because the riser attached to submerged structures is located at far below from free surface, it doesn't have significant movement by environmental loadings.

- ***Bending Normal Stress***

If the riser is subjected to bending, then the bending normal stress can be calculated as below.

$$\sigma_{b,normal} = \left(\frac{M_y}{\mathrm{I}_y}\right) z - \left(\frac{M_z}{\mathrm{I}_z}\right) \mathrm{y} \tag{2.50}$$

where M_y, M_z : moment about x and y-axis,

I_y, I_z : 2nd moment of area about x and y-axis

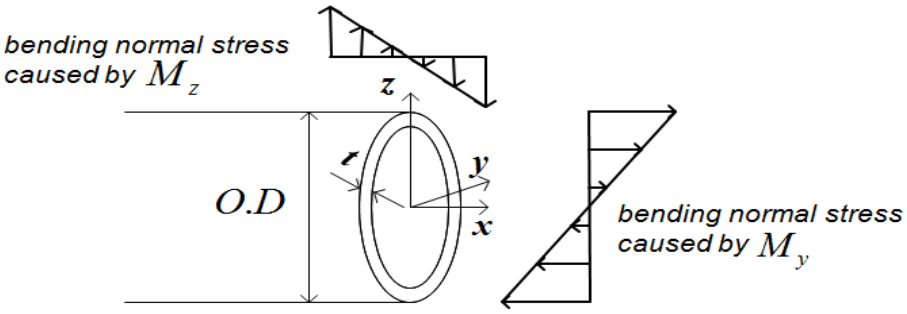

Fig. 2.3 Bending normal stress *(Image source*: *POSCO_RIST_2nd Final)*

Therefore the total normal stress can be calculated by the following formula:

$$\sigma_n = \frac{F_x}{A} + \left(\frac{M_y}{\mathrm{I}_y}\right) z - \left(\frac{M_z}{\mathrm{I}_z}\right) \mathrm{y} \tag{2.51}$$

2.2.2.2 Radial and Hoop Stresses

Principal components of radial and hoop stresses in the riser are internal and external pressures, and the stress directions are described in below the figure.

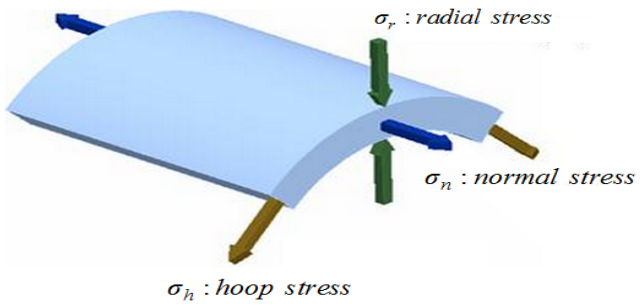

Fig. 2.4 Radial and Hoop stresses *(Image source: www.engrapps.com)*

The radial and hoop stresses can be calculated by employing below formulas in accordance with API RP 2RD.

$$\sigma_r = -\frac{\left(p_e D_o + p_i D_i\right)}{D_o + D_i} \tag{2.52}$$

$$\sigma_h = (p_i - p_e)\frac{D_o}{2t} - p_i \tag{2.53}$$

where σ_r, σ_h : radial stress, hoop stress, p_e, p_i : external stress, internal stress

In this study, the assumed maximum internal pressure set as *55.16 MPa* in the vertical riser at sea floor, and the external pressure is calculated based on the hydrostatic theory ($p_e = \rho g h$). In order to check structural strength of the overall riser system, Von-Mises yield criterion is generally employed. However, structural safety confirmation with respect to bursting and hoop buckling should be confirmed in advance.

2.2.3 Short-term Fatigue Analysis

The riser system can fail by repeatedly given environmental loadings, i.e. fluctuating stress in extreme and survival conditions. For this reason, fatigue damage analysis is important prior to starting engineering stage. In this study, the Short-term fatigue damage is calculated by employing the Palmgren-Miner linear damage hypothesis or called Miner's rule. The summarized steps to calculate Short-term fatigue

damage is as below.

1. Extract fluctuating stresses from time-series stress result .
2. Calculate effective alternating stress at failure for a lifetime of N cycles by employing appropriate mean stress correction model.
3. Divide ranges of the fluctuating amplitudes, and count stress cycles in each ranges by using rainflow counting method.
4. Select appropriate S-N curve type, and find the fatigue damage by employing Miner's rule.
5. Calculate the Short-term fatigue life from given loading time and obtained fatigue damage index.

The first step is extracting only fluctuating stress from times series stress result. As the hoop and radial stresses are calculated from internal and external pressures of the riser, they are considered to have constant values so the stresses are ruled out. Therefore, the fluctuating stress can be obtained from normal stress that composed of axial stress and bending normal stress, and they can be calculated by using the below formula.

$$\sigma_n = \frac{F_x}{A} \pm \left(\frac{M_y}{\mathrm{I}_y} \right) z \mp \left(\frac{M_z}{\mathrm{I}_z} \right) \mathrm{y} \qquad (2.51,\ 2.54)$$

The second step is applying mean stress effect to the normal stress obtained from the time-series. For instance, the vertical riser in FSHR system is tensioning by buoyancy can with considerable upthrust force, so its normal stress is always

maintaining non-zero positive value. Therefore, mean stress correction is required to accurately estimate fatigue damage. The following three models are generally used to obtain effective alternating stress at failure for a lifetime of N cycles.

$$1.\ Soderberg\ Model: \frac{\sigma_a}{\sigma_e} + \frac{\sigma_m}{\sigma_y} = 1 \tag{2.55}$$

$$2.\ Goodman\ Model: \frac{\sigma_a}{\sigma_e} + \frac{\sigma_m}{\sigma_u} = 1 \tag{2.56}$$

$$3.\ Gerber\ Model: \frac{\sigma_a}{\sigma_e} + \left(\frac{\sigma_m}{\sigma_u}\right)^2 = 1 \tag{2.57}$$

where σ_e : *effectivess alternating stress at failure for a lifetime of N cycles*,

σ_a : *stress amplitude*, σ_y, σ_u : yield stress, ultimate tensile stress

As the vertical riser is made of steel, Gerber model is selected in this study.

The third step is dividing the obtained stress into several blocks based on amplitude size and counting the stress cycles in each divided block by employing the rainflow counting method.

The fourth step is selecting appropriate S-N curve to find fatigue damage. In this study, the F1 S-N curve of DNV-RP-F204 is selected to find the ultimate number of cycles to fatigue failure.

$$\log N = \log \bar{a} - m \log \Delta\sigma \tag{2.58}$$

where N : *predicted number of cycles to failure for stress range* $\Delta\sigma$,

$\Delta\sigma$: *stress range with unit MPa*, m : *negative inverse slope of* $S-N$ *curve*,

$\log \bar{a}$: *intercept of* $\log N$ *– axis by* $S-N$ *curve*

Then fatigue damage can be calculating by using below Miner's rule.

$$\textit{Damage Index} \quad D = \sum_{i=1}^{k} \frac{n_i}{N_i} \tag{2.59}$$

where n_i = *number of effective stress cycles*

N_i = *ultimate number of cycles to fatigue failure in* $S-N$ *curve*

CHAPTER III

DESIGN BASELINES

3.1 FPSO Numerical Model

In order to extract the displacement information of the floater, the 200,000 DWT tanker turret-moored FPSO is used in this study, and the vessel is located in 1,829 m (6,000-ft) water depth. The FPSO was used in previous study performed by Tahar and Kim (2003), and its main particulars are summarized in the below Table 3.1.

Table 3.1 Main particulars of the vessel (Tahar and Kim 2003)

Designation	***Symbol***	***Unit***	***Value***
Production level		*bpd*	120,000
Storage		*bbls*	1,440,000
Vessel size		*kDWT*	200.0
Length between perpendicular	L_{pp}	*m*	310.00
Breadth	B	*m*	47.17
Depth	H	*m*	28.04
Draft	T	*m*	18.9
Displacement		*MT*	240,869
Length-beam ratio	L/B		6.57
Beam-draft ratio	B/T		2.5
Block coefficient	C_b		0.85
Center of buoyancy Forward section10	FB	*m*	6.6
Center of gravity above Base	KG	*m*	13.3
Water plane area	A	m^2	13,400
Frontal wind area	A_f	m^2	1011.7
Transverse wind area	A_b	m^2	3771.9
Roll radius of gyration at CG	R_{xx}	*m*	14.77

Designation	*Symbol*	*Unit*	*Value*
Pitch radius of gyration at CG	R_{yy}	*m*	77.47
Yaw radius of gyration CG	R_{zz}	*m*	79.30
Turret in center line behind Fpp (20.5% Lpp)	X_{tur}	*m*	63.55
Turret elevation below tanker base	Z_{tur}	*m*	1.52
Turret Diameter		*m*	15.85

Table. 3.1 Continued

General arrangement of chain-polyester-chain mooring and riser systems is shown in Fig. 3.1. Total 12 mooring lines are arranged in four groups, and each group is 90-degree apart. In the same mooring group, each mooring are 5-degree apart. Also, there are total 13 risers including the Free Standing Hybrid Riser (FSHR) located at positive x – axis (0^o). The main particulars of mooring system and risers are shown in following Tables 3.2 and 3.3, respectively.

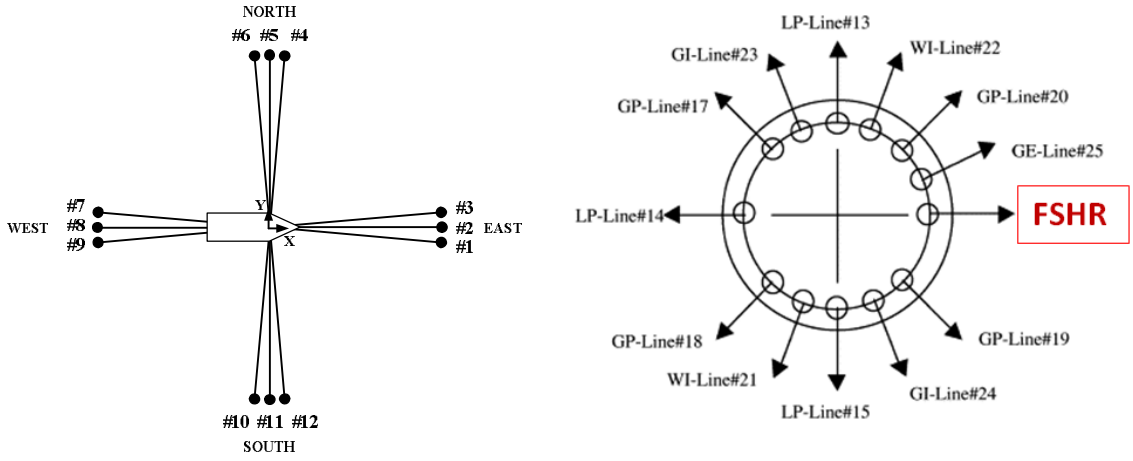

(a) mooring system (b) riser system

Fig. 3.1 General arrangement of mooring (a) and riser (b) systems
(Image source: Tahar and Kim 2003)

Table 3.2 Main particular of FPSO mooring system (Tahar and Kim 2003)

Designation	***Unit***	***Value***
Water depth	m	1829
Pre-tension	*kN*	1424
Number of lines		4 × 3
Degree between the 3 lines	*deg.*	5
Length of mooring line	*m*	2652
Radius of location of chain stoppers on turn table	*m*	7.0
Segment 1(ground section): Chain		
Length at anchor point	*m*	121.9
Diameter	*cm*	9.52
Dry weight	*N/m*	1856
Weight in water	*N/m*	1615
Stiffness AE	*kN*	912081
Mean breaking load (MBL)	*kN*	7553
Segment 2: Polyester Rope		
Length	*m*	2438
Diameter	*cm*	16.0
Dry weight	*N/m*	168.7
Weight in water	*N/m*	44.1
Stiffness AE	*kN*	186825
Mean breaking load (MBL)	*kN*	7429
Segment 3(ground section): Chain		
Length at anchor point	*m*	91.4

Table 3.3 Main particular of risers (Tahar and Kim 2003)

Designation	*OD*	*T*	*EA*	*EI*	*Weight*		C_{dn}
					dry	*wet*	
	(m)	*(m)*	*(kN)*	*(kN·m²)*	*(kg/m)*		
Liquid Production	0.254	0.023	3.34E+06	2.25E+04	133.6	98.6	1
Gas Production	0.386	0.018	4.16E+06	7.06E+04	166.5	46.6	1
Water Injection	0.531	0.018	5.80E+06	1.91E+05	232.1	197.6	1.414
Gas Injection	0.287	0.020	3.36E+06	3.01E+04	134.2	67.9	1.414
Gas Export	0.343	0.017	3.48E+06	4.64E+04	139.3	44.6	1

3.2 Free Standing Hybrid Riser Numerical Model

As mentioned in the introduction chapter, the basic concept of hybrid riser is the combination of a flexible riser with a rigid riser such as a vertical riser or a steel catenary riser. In this study, the combination of the vertical riser with the flexible jumper is used, and their main particulars are presented in the below table.

Table 3.4 Main particular of FSHR

Designation	*OD*	*T*	*EA*	*EI*	*Weight*		C_{dn}
					dry	*wet*	
	(m)	*(m)*	*(kN)*	*(kN·m²)*	*(kg/m)*		
Vertical Riser	0.457	0.025	6.89E+09	1.61E+08	270.4	102.2	1.2
Flexible Jumper	0.536	0.065	7.50E+08	1.33E+05	305.0	93.0	1.2

Along with the normal drag coefficient of 1.2, the added mass hydrodynamic coefficient of 2.0 is employed in this study for both the two risers.

Table 3.5 Length Information of FSHR

Designation	***Total Length (m)***	***Total No. of Elements***	***AVG Length per element (m)***
Vertical Riser	1670.801	42	39.78
Flexible Jumper	385	38	10.1

* The horizontal offset distance between the FPSO and the Buoyancy Can is 300 m.

** Targeted riser design life is 25 years.

With respect to boundary condition, the upper end of flexible jumper is connected with the FPSO fairlead via generalized elastic springs and damper, and the lower end of the jumper is connected with the upper riser assembly through the hinged connection. In case of vertical riser, the upper and the lower end points are connected to the seafloor and the bottom of upper riser assembly by same hinged connection conditions. The overall configuration of FSHR is shown in the following figure.

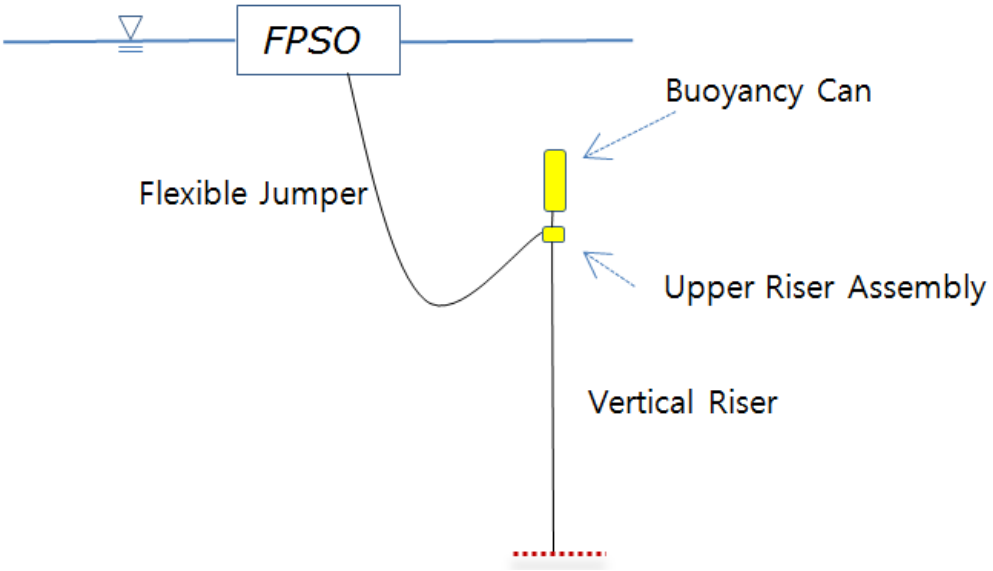

Fig. 3.2 Configuration of Free Standing Hybrid Riser (FSHR)

In this research, it is assumed that the material of the vertical riser meet the requirements of API 5L Line Pipe specification, and the minimum yield strength of material is employed to determine the structure strength by using von-Mises yield criteria in API RP 2RD as mentioned previous chapter. The minimum yield strengths of the X65, X70 and X80 are summarized in Table 3.6. The values are used in the structure strength part.

Table 3.6 Yield strength of the vertical riser

Minimum Yield Strength (MPa)			
API 5L Grade	***X65***	***X70***	***X80***
Value	448	483	552

3.3 Submerged Structures Numerical Model

The characteristic dimensions of the buoyancy can and the upper riser assembly are summarized in Table 3.7.

Table 3.7 Main particulars of the submerged structures

Buoyancy Can			***Upper Riser Assembly***		
Designation	***Value***	***Unit***	***Designation***	***Value***	***Unit***
O.D.	5.45	m	Horizontal Length	3.0	m
Vertical length	34	m	Vertical length	14	m
Net weight	277	MT	Net weight	70	MT
Volume	793	m^3	Volume	43	m^3
Upthrurst Force	5258160	N	-		

In order to calculate the added mass, inertial and drag forces in CHARM3D, the hydrodynamic coefficients should be determined in advance, and these coefficients are summarized as below Table 3.8.

Table 3.8 Hydrodynamic coefficients of the submerged structures

Structure Type	***Hydrodynamic Coefficients***		
	Added Mass	***Inertia***	***Drag***
Buoyancy Can	1.0	2.0	1.0
Upper Riser Assembly	1.0	2.0	1.0

From the Morison's equation, the environmental loads can be obtained, so the environmental forces are employed to calculate the movement of the submerged structures. In order to obtain the movements of the structures, the mass and the hydrostatic stiffness matrices of the subsurface structures are required as below.

- ***Mass Matrix***

$$\begin{bmatrix} 346991 & 0 & 0 & 0 & 1783890 & 0 \\ 0 & 346991 & 0 & -1783890 & 0 & 0 \\ 0 & 0 & 346991 & 0 & 0 & 0 \\ 0 & -1783890 & 0 & 28436077 & 0 & 0 \\ 1783890 & 0 & 0 & 0 & 28436077 & 0 \\ 0 & 0 & 0 & 0 & 0 & 54605323 \end{bmatrix} \quad (3.1)$$

- ***Hydrostatic Stiffness Matrix***

$$\begin{bmatrix} 0 & 0 & 0 & 0 & 0 & 0 \\ 0 & 0 & 0 & 0 & 0 & 0 \\ 0 & 0 & 0 & 0 & 0 & 0 \\ 0 & 0 & 0 & 68683083 & 0 & 0 \\ 0 & 0 & 0 & 0 & 68683083 & 0 \\ 0 & 0 & 0 & 0 & 0 & 0 \end{bmatrix} \quad (3.2)$$

3.4 Environmental Conditions

- Direction of environmental loads

In this study, wave, current and wind are concurrently heading from east to west (180°) shown in the Fig 3.3, and the Free Standing Hybrid Riser is placed on X – axis.

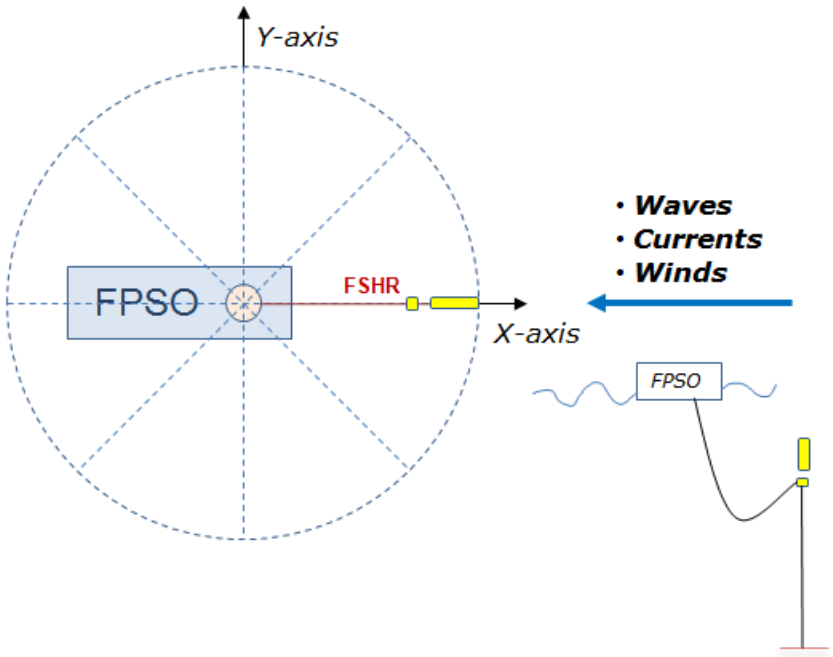

Fig. 3.3 Direction of environmental loads, 180° from east to west

In fixed-fairlead analysis, the wave and current are employed to calculate the motions and stress responses of the FPSO uncoupled Free Standing Hybrid Riser. On the other hand, in moving-fairlead analysis, the FPSO coupled FSHR is investigated under a parallel wave- current-wind conditions.

- Wave and Current Conditions

In this research JONSWAP (Joint North Sea Wave Project) wave spectrum (Fig. 3.4) is employed with peak enhancement factor $\gamma = 2.4$, and the formula is

$$S(\omega) = 155\left(\frac{H_{1/3}^2}{T_1^4\omega^5}\right)\exp\left(\frac{-944}{T_1^4\omega^4}\right)(2.4)^{\alpha}, \quad \alpha = \exp\left(-\left(\frac{0.191\omega T_1 - 1}{2^{0.5}\sigma}\right)^2\right) \qquad (3.3)$$

where, $\sigma = 0.07$ for $\omega \le 5.24/\mathrm{T}_1$ and $\sigma = 0.09$ for $\omega > 5.24/\mathrm{T}_1$, $T_1 = 0.834T_0 = 1.073T_2$.

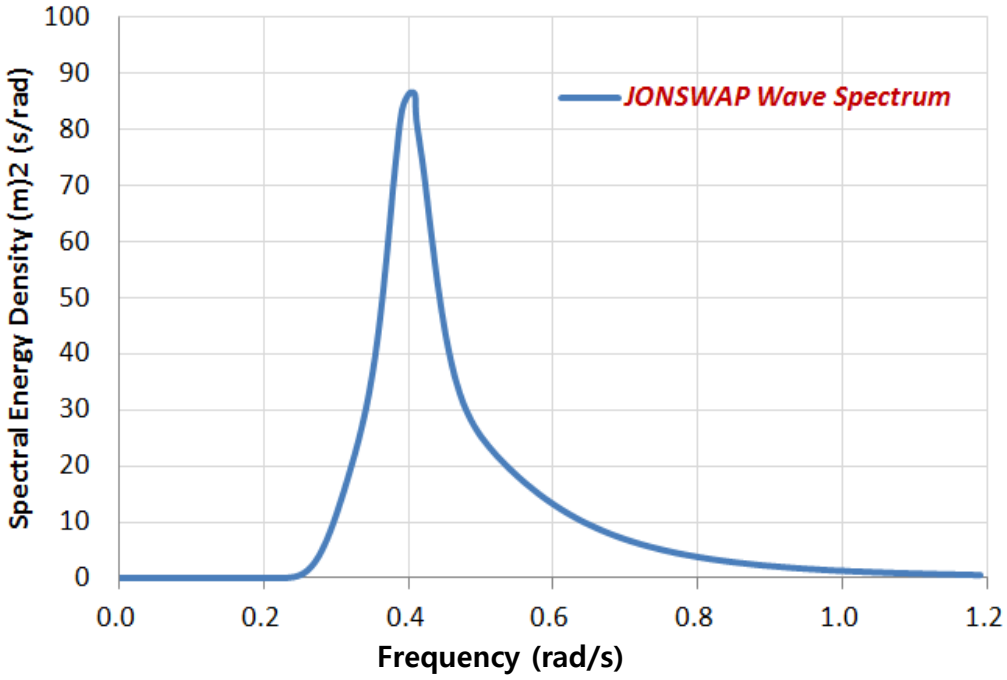

Fig. 3.4 JONSWAP Wave Spectrum

The Table 3.9 and 3.10 present the wave and current conditions of Central Gulf of Mexico (89.5°W to 86.5°W) with 100 and 500-yr return period of hurricane conditions. With respect to the 500-yr hurricane condition, the main parameters of the 500-yr significant wave height, peak period, current profiles and wind speed are generated based on the hurricanes information (10y, 25y, 50y, 100-yr, 200y, 1000y, 2000y and 10000y) in API BULLETIN 2INT-MET (2007) by curve-fitting method.

Table 3.9 Wave conditions

Designation	***Unit***	***100 yr***	***500 yr***
H_s	m	15.79	19.00
T_p	sec.	15.40	16.50
Spectrum	JONSWAP($\gamma = 2.4$)		
Direction	deg.	180°	

Table 3.10 Current profiles

100 yr		***500 yr***	
Depth (m)	*Speed (m/s)*	***Depth (m)***	*Speed (m/s)*
0	2.40	0	2.91
50.40	1.80	59.50	2.05
100.80	0	119.00	0

· Wind Condition

The wind spectrum is generated corresponding to API Bulletin 2INT-MET, and the formula for energy density spectrum is

$$S(f) = \frac{320\left(\frac{U_0}{10}\right)^2\left(\frac{z}{10}\right)^{0.45}}{(1+\tilde{f}^n)^{(5/3n)}} \tag{3.4}$$

where, $\tilde{f} = 172 f\left(\frac{z}{10}\right)^{2/3}\left(\frac{U_0}{10}\right)^{-0.75}$

$n = 0.468$, $z = the\ measured\ height\ above\ sea-surface\,(10\text{m})$

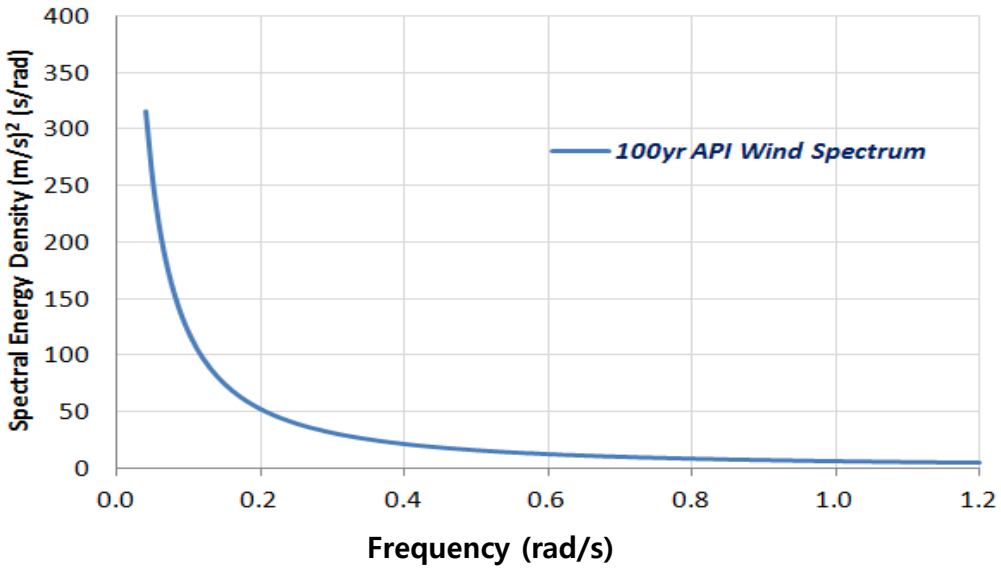

Fig. 3.5 API Wind Spectrum

The mean wind speeds at 10 m above MWL for an hour are presented in the Table 3.11.

Table 3.11 1-hour Mean Wind Speed (10 m Elevation)

Designation	***Unit***	***100 yr***	***500 yr***
Wind Speed	m/s	48.0	56.0

CHAPTER IV

CASE STUDIES

In this chapter, the Free Standing Hybrid Riser is analyzed into two tracks: the fixed-fairlead analysis and the moving-fairlead analysis. In the fixed-fairlead analysis, the FPSO uncoupled FSHR is investigated under parallel waves and currents in 100 and 500-yr hurricane conditions for 3 hours. The results are used for confirming the effects of the environmental loads on the riser system. On the other hand, in the moving-fairlead analysis, the FPSO coupled Free Standing Hybrid Riser is investigated under parallel winds, waves, currents in 100 and 500-yr hurricane conditions for 3 hours.

4.1 Fixed-Fairlead Analysis

In this analysis, the global motion analysis and stress evaluation are conducted for the submerged structures, flexible jumper and vertical riser.

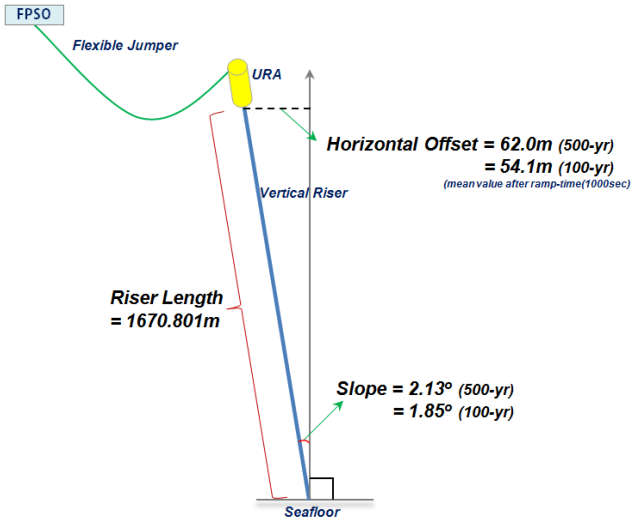

Fig. 4.1 Slope of vertical riser (fixed-fairlead condition)

Fig.4.1 shows that the mean value slopes of the vertical riser for 100- and 500-yr hurricane conditions for 3hous in fixed-fairlead condition. The occurrence of the riser slope is caused by the flexible jumper's tension force.

4.1.1 Dynamic Response of Submerged Structures

In this chapter, the dynamic motion responses of the buoyancy can and upper riser assembly are presented. From this time-series analysis results, the responses of the structures can be compared between 100 and 500-yr hurricane conditions, respectively.

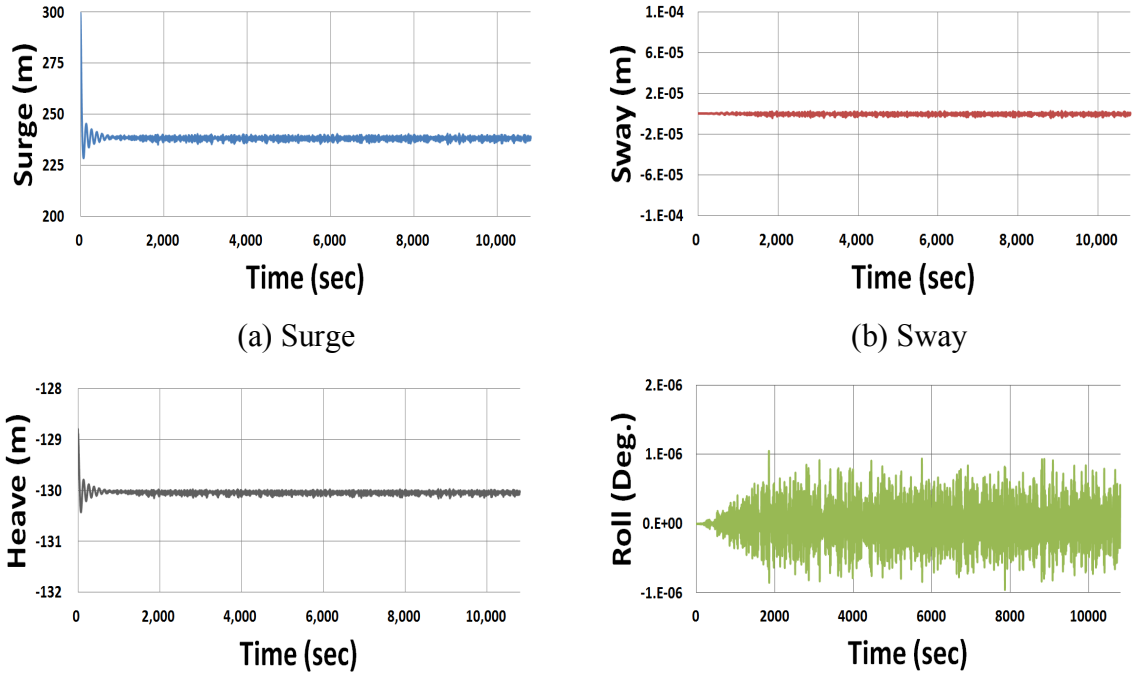

(a) Surge (b) Sway

(c) Heave (d) Roll

Fig. 4.2 6DOF motions of BC & URA under 100-yr hurricane condition (fixed-fairlead analysis)

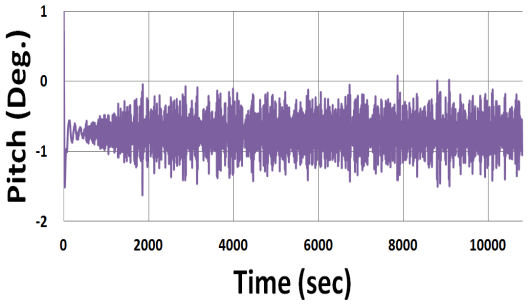

(e) Pitch

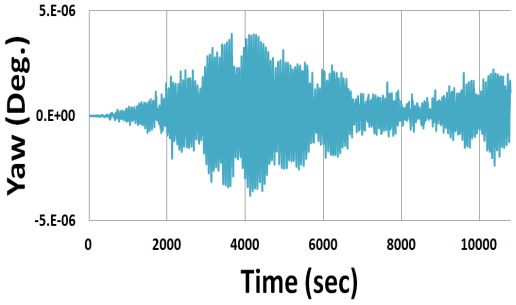

(f) Yaw

Fig. 4.2 Continued

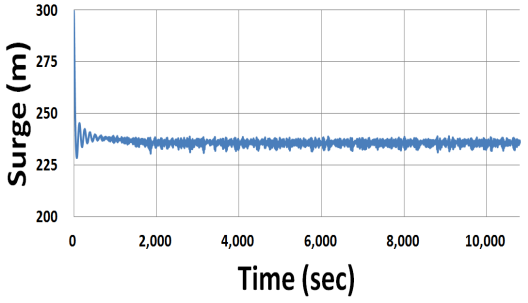

(a) Surge

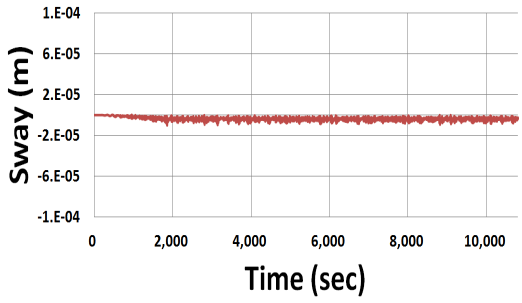

(b) Sway

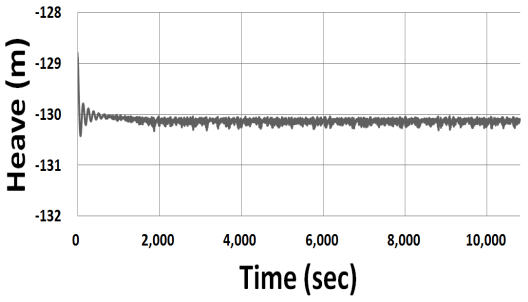

(c) Heave

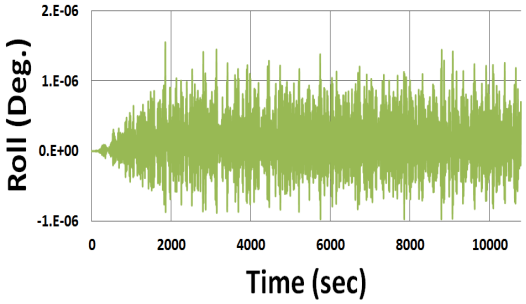

(d) Roll

Fig. 4.3 6DOF motions of BC & URA under 500-yr hurricane condition (fixed-fairlead analysis)

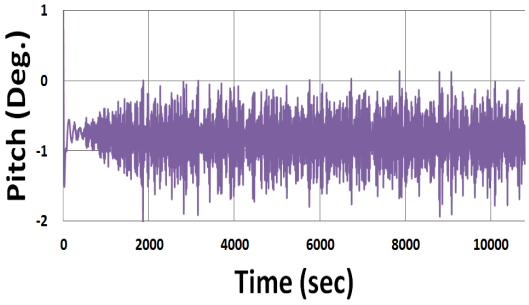

(e) Pitch

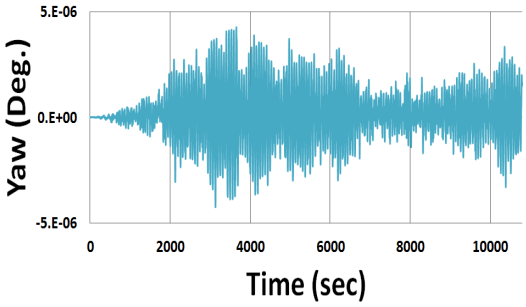

(f) Yaw

Fig. 4.3 Continued.

Figs.4.2 and 4.3 show the 6 DOF motions of the buoyancy can and the upper riser assembly under 100- and 500-yr hurricanes conditions. Overall motions of the structures are not significant compared with the moving-fairlead analysis results described in later chapter. From the fixed-fairlead analysis results, it can be determined that the affects of the environmental loads on the submerged structures are insignificant. In order to directly compare the motion responses in 100- and 500-yr hurricane conditions, the motion response spectra are employed with respect to the surge, heave and pitch.

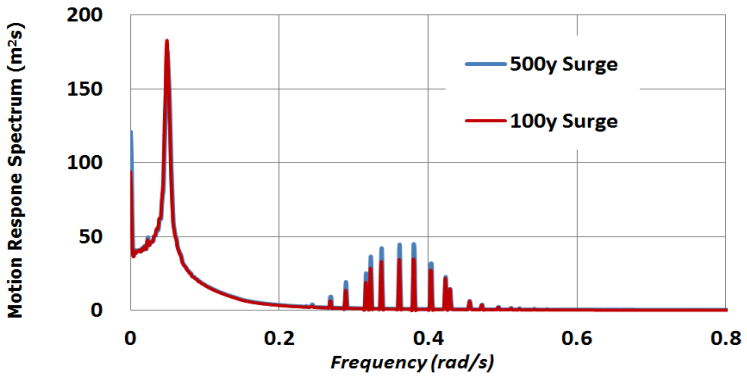

(a) Surge

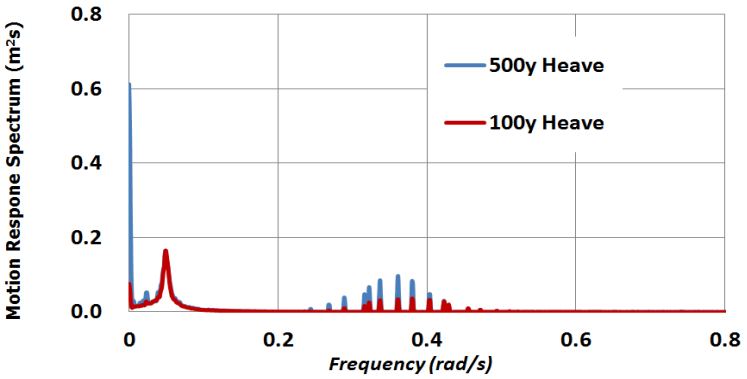

(b) Heave

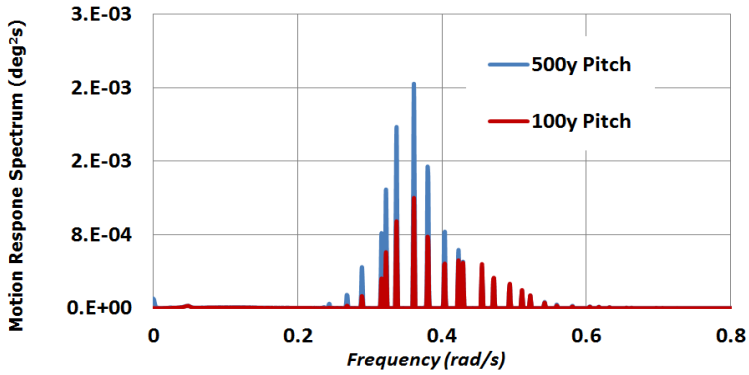

(c) Pitch

Fig. 4.4 Motion response spectra of BC & URA (fixed-fairlead analysis)

Fig. 4.4 shows the motion response spectra with respect to the surge, heave and pitch, and the response differences between 100 and 500-yr hurricanes are insignificant.

Table 4.1 Statistics of the submerged structures (fixed-fairlead analysis)

Motion	***Surge (m)*** (Horizontal Offset from FPSO Turret)		***Sway (m)***		***Heave (m)***	
	100-yr	***500-yr***	***100-yr***	***500-yr***	***100-yr***	***500-yr***
Max.	240.61	239.09	2.38E-06	4.57E-08	-129.98	-130.02
Mean	238.30	235.88	-5.37E-07	-4.02E-06	-130.04	-130.14
Min.	235.37	230.78	-4.25E-06	-1.05E-05	-130.15	-130.33
STD Dev.	0.78	1.21	9.92E-07	1.55E-06	0.03	0.04
Motion	***Roll (deg.)***		***Pitch (deg.)***		***Yaw (deg.)***	
	100-yr	***500-yr***	***100-yr***	***500-yr***	***100-yr***	***500-yr***
Max.	1.05E-06	1.55E-06	0.08	0.13	3.91E-06	4.27E-06
Mean	1.14E-08	1.52E-07	-0.74	-0.84	1.34E-07	1.44E-07
Min.	-9.55E-07	-9.68E-07	-1.62	-2.04	-3.79E-06	-4.26E-06
STD Dev.	2.96E-07	3.84E-07	0.24	0.31	1.23E-06	1.40E-06

4.1.2 Inertial and Viscous Forces on Submerged Structures

As described in the theoretical background chapter, the assumption in this study is the wave length is far longer than the characteristic dimension of the subsurface bodies. Then the environmental loads against the submerged structures can be calculated by using Morison's equation. As the Morison's equation is composed of inertial and drag terms, the calculated forces are sorted into an inertial force and the

viscous force. The below graphs show the two types of surge, heave and pitch forces of the buoyancy can and the upper riser assembly under the 100- and 500-yr hurricane conditions.

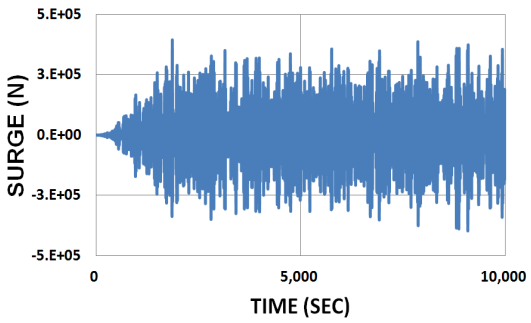

(a) Inertial Force – Surge

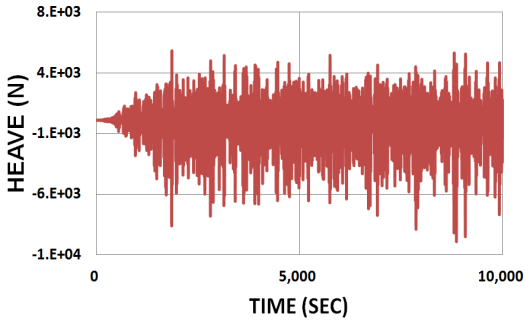

(b) Inertial Force - Heave

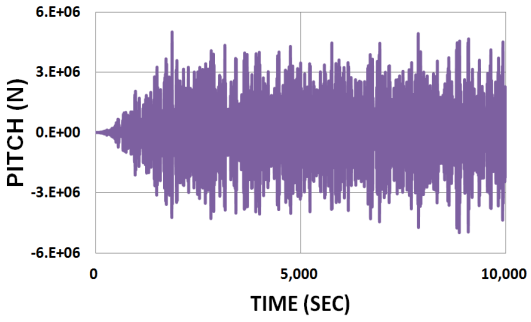

(c) Inertial Force – Pitch

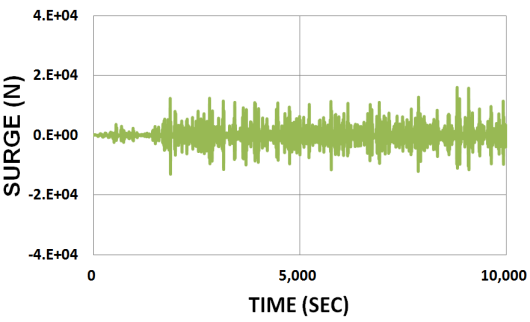

(d) Viscous Force - Surge

Fig. 4.5 Inertial & viscous forces acting on BC&URA under 100-yr hurricane condition (fixed-fairlead analysis)

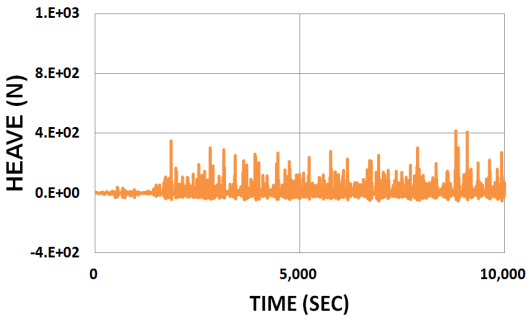

(e) Viscous Force – Heave

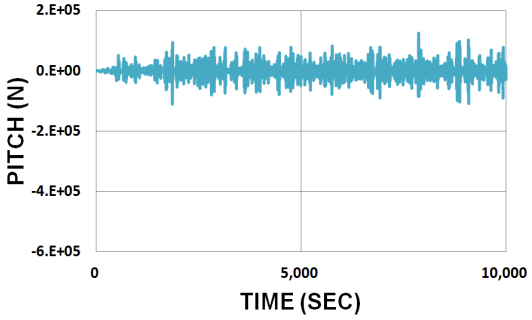

(f) Viscous Force – Pitch

Fig. 4.5 Continued.

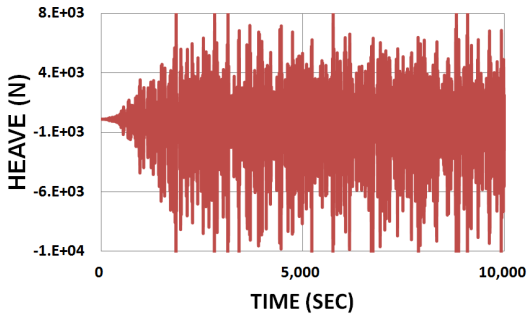

(a) Inertial Force – Surge

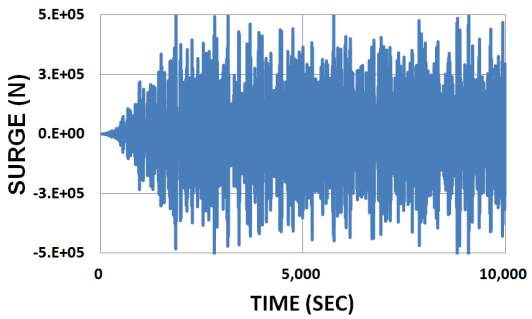

(b) Inertial Force - Heave

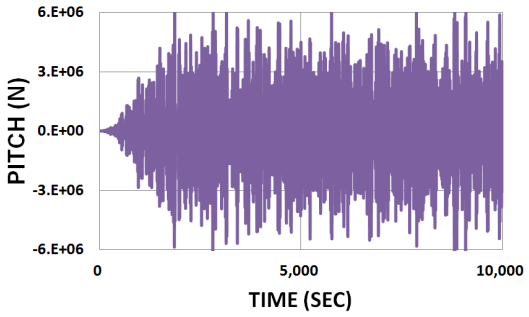

(c) Inertial Force – Pitch

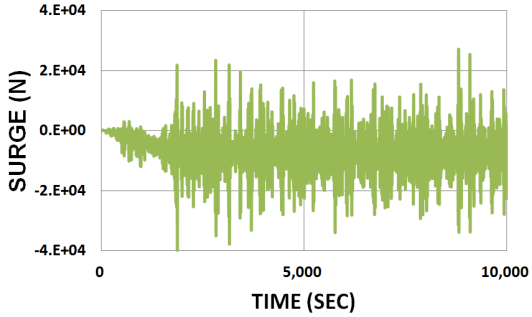

(d) Viscous Force – Surge

Fig. 4.6 Inertial & viscous Forces acting on BC&URA under 500-yr hurricane condition (fixed-fairlead analysis)

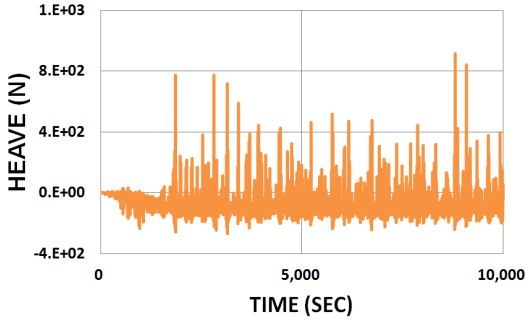

(e) Viscous Force – Heave

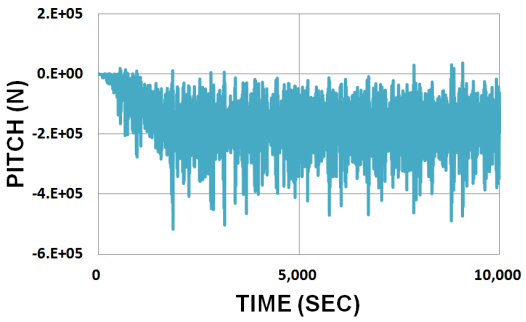

(f) Viscous Force – Pitch

Fig. 4.6 Continued.

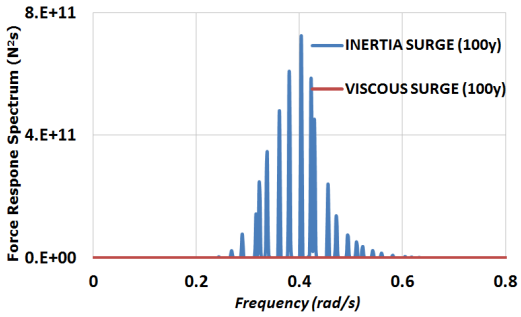

(a) Surge – 100-yr

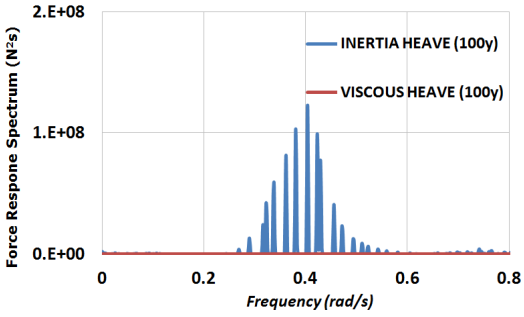

(b) Heave – 100-yr

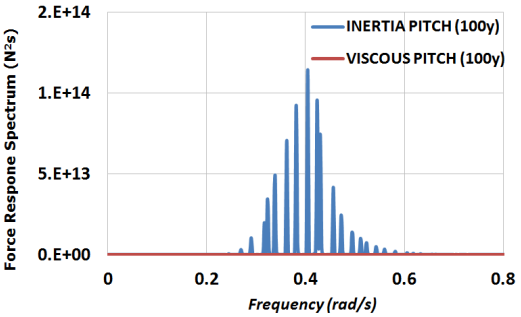

(c) Pitch – 100-yr

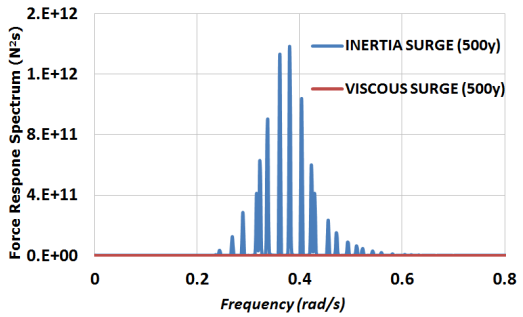

(d) Surge – 500-yr

Fig. 4.7 Inertial & viscous forces response spectra of BC&URA

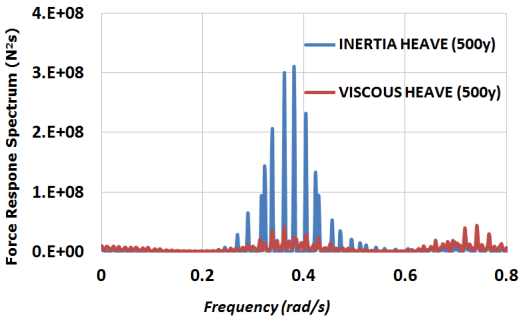

(e) Heave – 500-yr

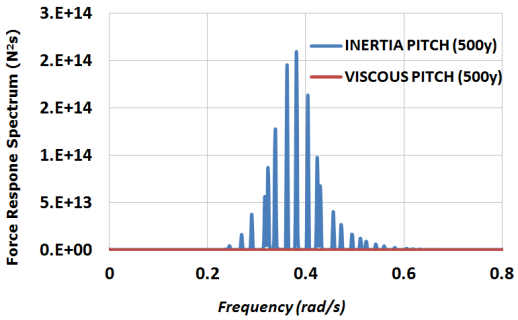

(f) Pitch – 500-yr

Fig. 4.7 Continued.

Fig. 4.7 shows that the inertial forces are dominant in 6DOF motions under 100 and 500-yr hurricane conditions..

Table 4.2 Statistics of the inertial and viscous forces acting on BC&URA

Motion	***Inertial Surge (N)***		***Inertial Heave (N)***		***Inertial Pitch (N)***	
	100-yr	***500-yr***	***100-yr***	***500-yr***	***100-yr***	***500-yr***
Max.	3.95E+05	5.49E+05	5.12E+03	9.49E+03	5.00E+06	6.82E+06
Mean	-3.40E+02	-1.45E+03	-6.09E+00	-1.97E+01	-4.06E+03	-8.15E+03
Min.	-3.97E+05	-5.39E+05	-9.01E+03	-1.40E+04	-4.97E+06	-6.64E+06
STD Dev.	1.24E+05	1.67E+05	1.70E+03	2.67E+03	1.55E+06	2.05E+06
Motion	***Viscous Surge (N)***		***Viscous Heave (N)***		***Viscous Pitch (N)***	
	100-yr	***500-yr***	***100-yr***	***500-yr***	***100-yr***	***500-yr***
Max.	1.60E+04	2.70E+04	4.20E+02	9.13E+02	1.24E+05	3.79E+04
Mean	-1.17E+01	-6.69E+03	-1.40E-01	-8.91E+01	-1.16E+02	-1.65E+05
Min.	-1.31E+04	-3.99E+04	-5.37E+01	-2.66E+02	-1.10E+05	-5.15E+05
STD Dev.	2.40E+03	6.41E+03	3.75E+01	8.40E+01	1.87E+04	7.54E+04

4.1.3 Dynamic Response of Flexible Jumper

Regarding the boundary condition of the flexible jumper, the fairlead point is modeled as fixed point in this fixed-fairlead analysis, on the other hand in the moving-fairlead analysis, the fairlead point is modeled as moving fairlead with having 3 hour FPSO displacement information.

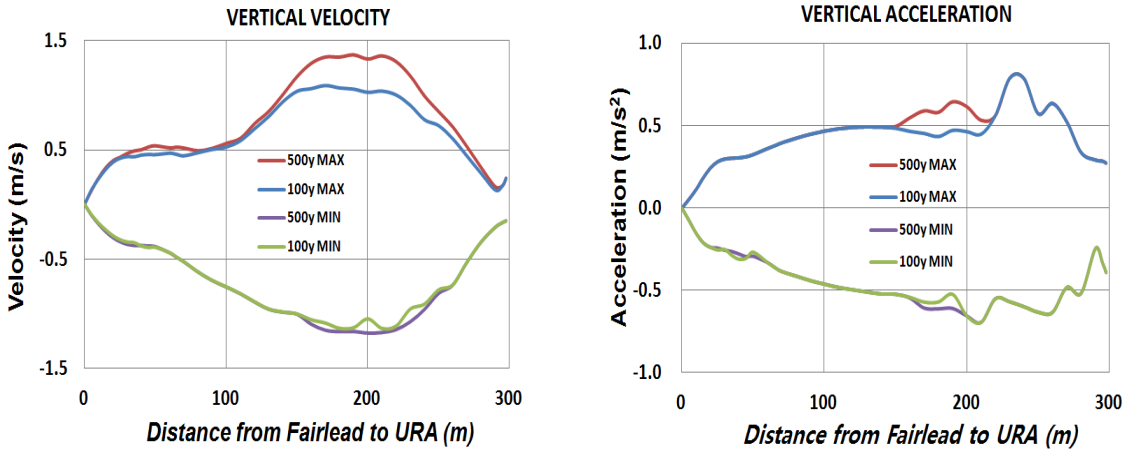

(a) Vertical velocity (b) Vertical acceleration

Fig. 4.8 Vertical velocity and acceleration under 100 and 500-yr hurricane conditions

Fig. 4.8 shows that both the vertical velocity and vertical acceleration have zero values at fairlead point. The velocity and acceleration are increased along the flexible jumper up to the sag area, and started to decrease until the upper riser assembly. However, the magnitude difference between 100- and 500-yr hurricanes are insignificant. In this regard, the effects of the environmental loads on the flexible jumper

are insignificant.

4.1.4 Stress Evaluation on Riser

The stress evaluation on the flexible jumper and vertical riser is conducted in 100- and 500-yr hurricane conditions.

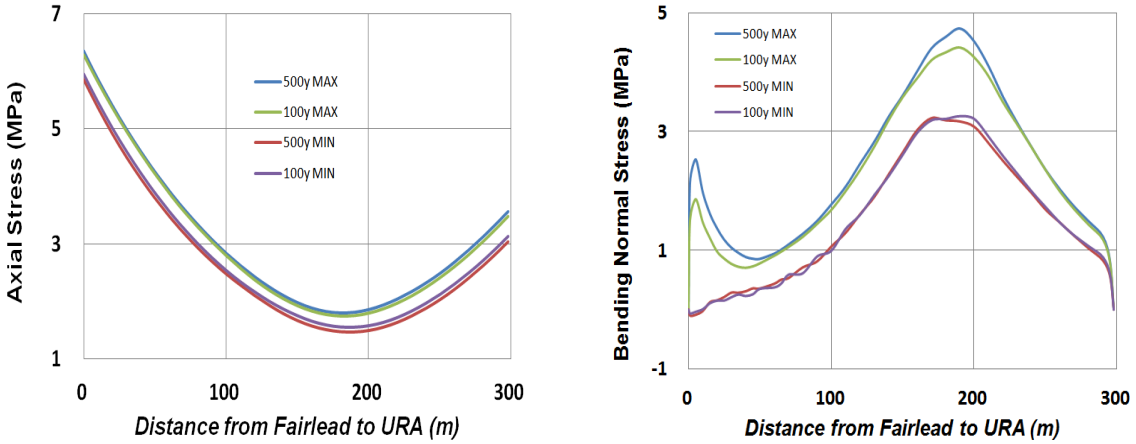

(a) Axial stress (b) Bending normal stress

Fig. 4.9 Axial and bending normal stress distributions of the flexible jumper under 100 and 500-yr hurricane conditions (fixed-fairlead analysis)

Fig. 4.9 shows the distributions of the axial and bending normal stresses of the flexible jumper. The dead load is a large part of forcing on the riser section than the environmental loads induced by waves and currents. Therefore the axial stress is changed along with the slope of the flexible jumper. Also, the bending normal stress is changed proportional to the curvature of the initial shape of the flexible jumper. It can be explained as the flexible jumper is not affected by the environmental loads both in

100 and 500-yr hurricane conditions.

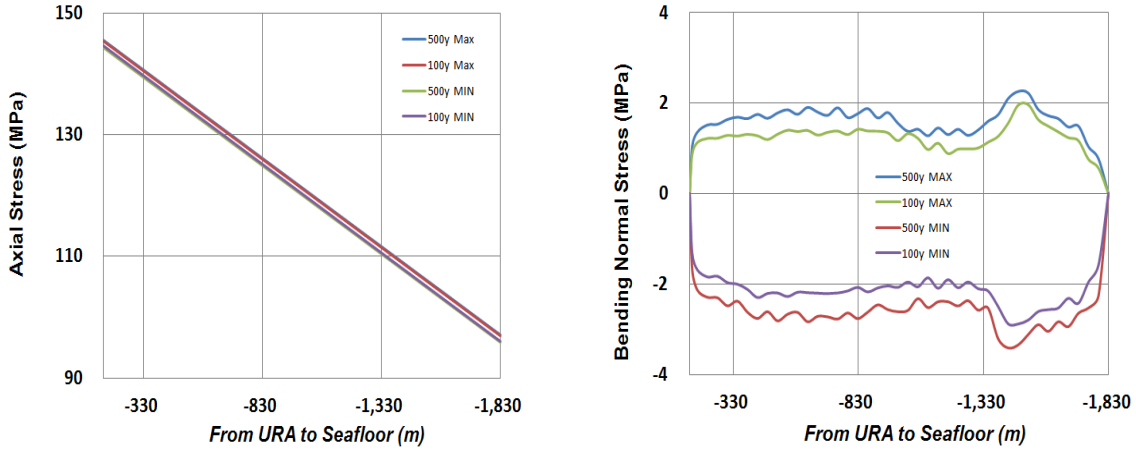

(a) Axial stress (b) Bending normal stress

Fig. 4.10 Axial and bending normal stress distributions of the vertical riser under 100 and 500-yr hurricane conditions (fixed-fairlead analysis)

Fig. 4.10 shows the axial and bending normal stress distributions of the vertical riser. Firstly, the variations of the axial stress are insignificant both in 100 and 500-yr hurricane conditions. As the heave amplitude of the subsurface structures is less than 1m given environmental conditions. Also, the magnitude difference of the bending normal stress is insignificant both in 100 and 500-yr hurricane conditions. Although, the current profile range covers the top depth of the buoyancy can in 500-yr hurricane, the effect to the bending normal stress is insignificant. From the results of the global motion and stress evaluation, it is determined that the waves and currents do not significantly affect riser system. Therefore, the analyses for the structure strength and fatigue estimation are not necessary in the fixed-fairlead analysis.

Table 4.3 Summary table of axial and bending normal stresses of the FSHR under 100 and 500-yr hurricane conditions (fixed-fairlead analysis)

Designation	***Flexible Jumper***			
	AXIAL STRESS (MPa)		***BENDING N. STRESS (MPa)***	
	100-yr	***500-yr***	***100-yr***	***500-yr***
Max.	6.208	6.354	4.415	4.737
Mean	2.895	2.880	1.239	1.238
Min.	1.551	1.469	-0.064	-0.105
Designation	***Vertical Riser***			
	AXIAL STRESS (MPa)		***BENDING N. STRESS (MPa)***	
	100-yr	***500-yr***	***100-yr***	***500-yr***
Max.	145.410	145.548	1.961	2.260
Mean	121.509	121.497	-0.387	-0.401
Min.	95.999	95.8001	-2.886	-3.406

4.2 Moving-Fairlead Analysis

The moving-fairlead analysis proceeded in the same steps of the fixed-fairlead analysis up to the stresses evaluation. In addition, the structure strength and short-term fatigue estimation analyses are added in the moving-fairlead analysis.

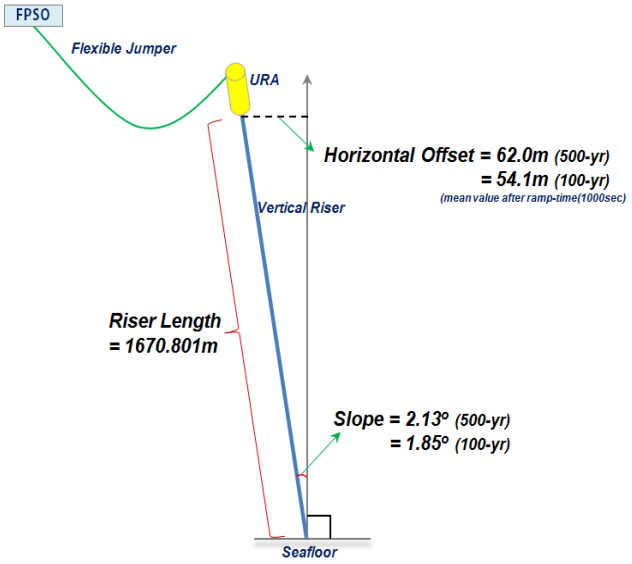

Fig. 4.11 Slope of vertical riser (moving-fairlead condition)

Fig.4.11 shows that the median slopes of vertical riser for 100- and 500-yr hurricane conditions for 3hous in moving-fairlead condition. The occurrence of the riser slope is caused by the flexible jumper's tension force. The inclination values in moving-fairlead condition are smaller than those of in fixed-fairlead condition due to the positive surge motion of FPSO.

4.2.1 Dynamic Response of Submerged Structures

In this chapter, the dynamic motion responses of the submerged structures are exhibited. The effect of the FPSO motions to the submerged structures can be confirmed in comparison with the results of the fixed-fairlead analysis.

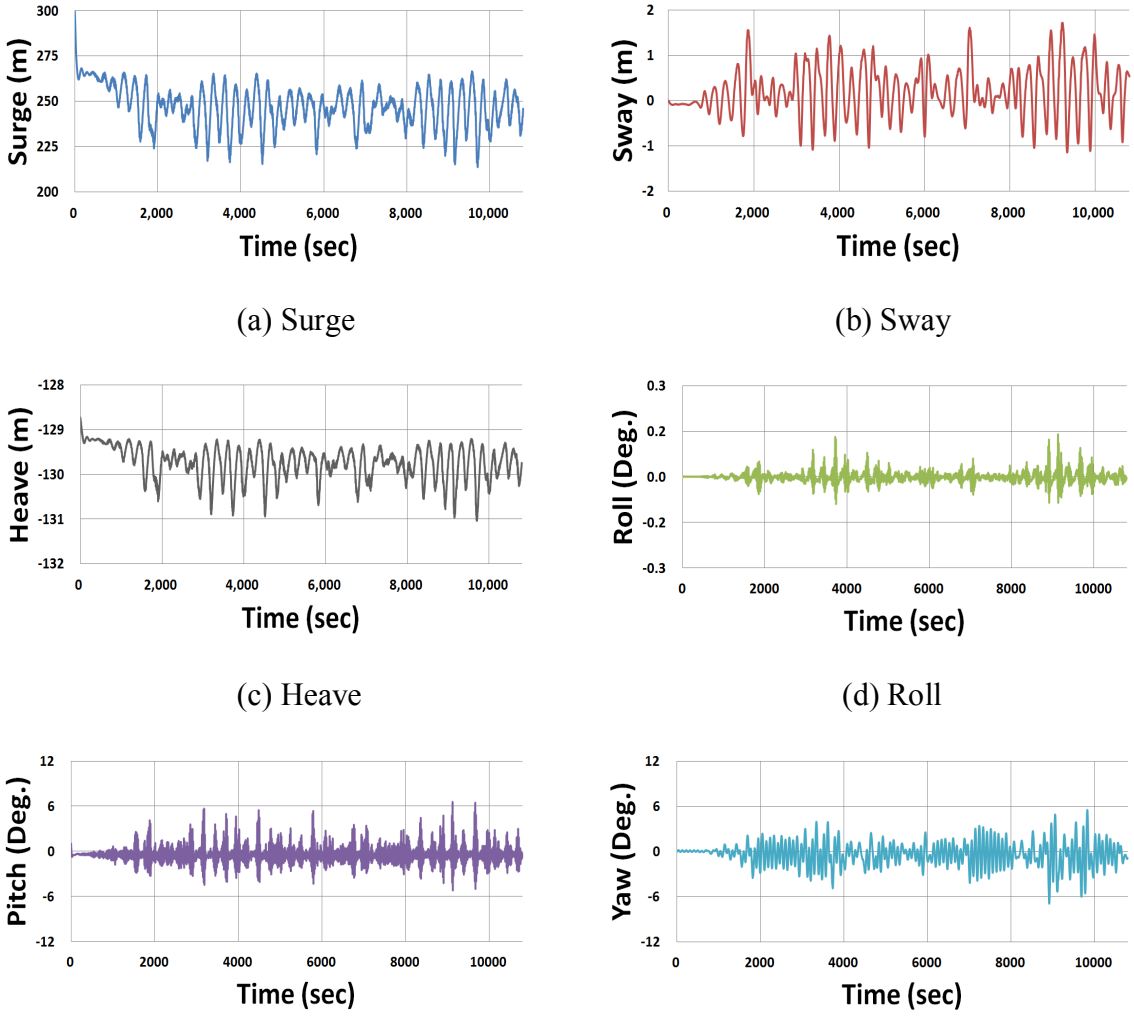

(a) Surge (b) Sway

(c) Heave (d) Roll

(e) Pitch (f) Yaw

Fig. 4.12 6DOF motions of BC & URA in 100-yr hurricane condition

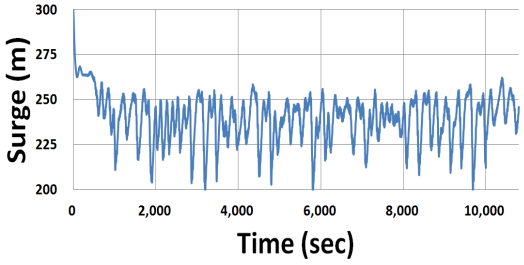

(a) Surge

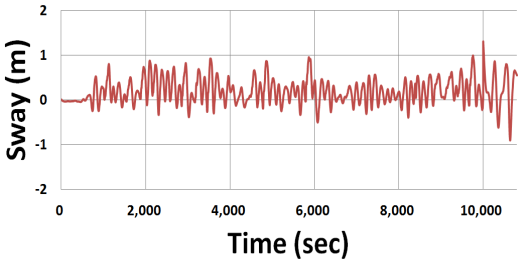

(b) Sway

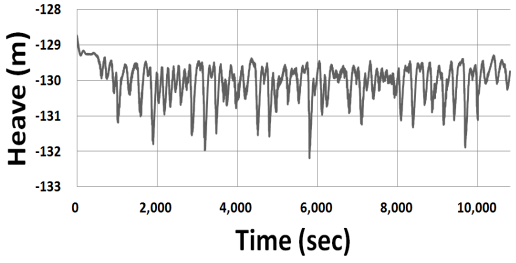

(c) Heave

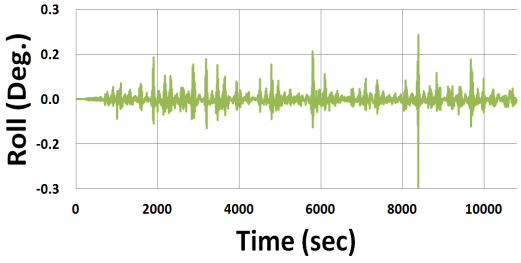

(d) Roll

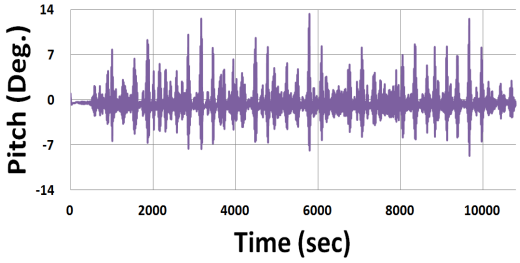

(e) Pitch

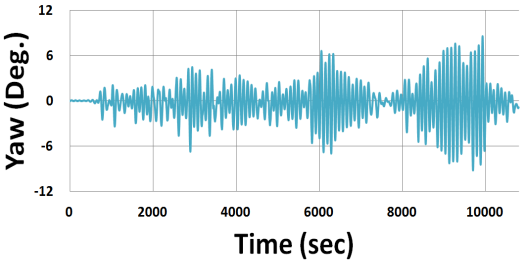

(f) Yaw

Fig. 4.13 6DOF motions of BC & URA in 500-yr hurricane condition

Based on the standard deviation of 6DOF motions, Fig. 4.12 and Fig. 4.13 show that the surge is the most significant both in 100 and 500-yr hurricane conditions. As the direction of the environmental loads is heading from east to west, the submerged structures are significantly affected from the loads. Also, apart from sway in 500-yr, the amplitude of the rest motions are magnified in 500-yr hurricane conditions. The reduced

sway is caused by stronger environmental loads in 500-yr which constrain the lateral motion of the structures. Apart from the surge, the rest motions are relatively stable because of the deep installation depth of the submerged structures and decoupling effect by the flexible jumper. In terms of the motion amplitude, the 6DOF motions are magnified compared with the results of the fixed-fairlead analysis.

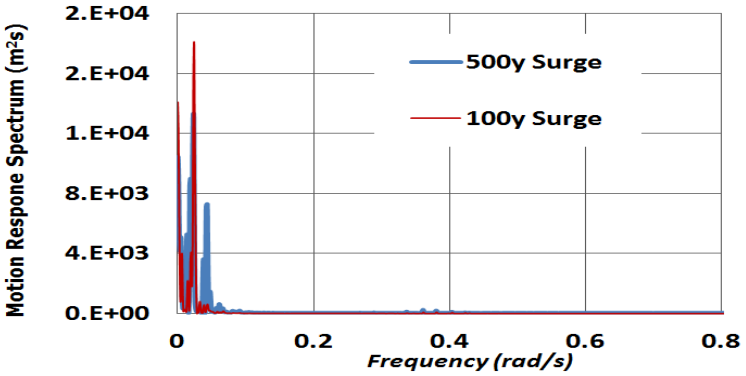

(a) Surge

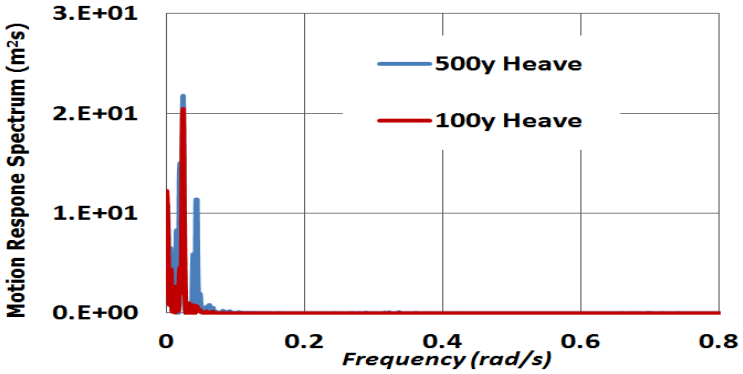

(b) Heave

Fig. 4.14 Response spectra of the surge, heave and pitch of BC & URA

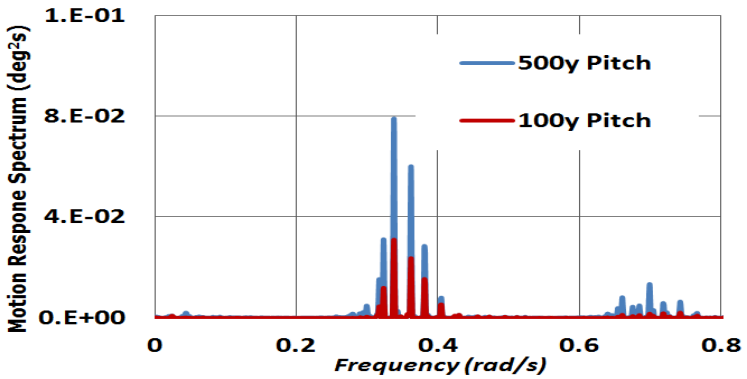

(c) Pitch

Fig. 4.14 Continued

Fig. 4.14 shows the results of the motion response spectra with respect to surge, pitch and yaw. Although, the magnitude of each motion is amplified compared with the fixed-fairlead analysis, the difference of the results between 100 and 500-yr hurricanes is inconspicuous.

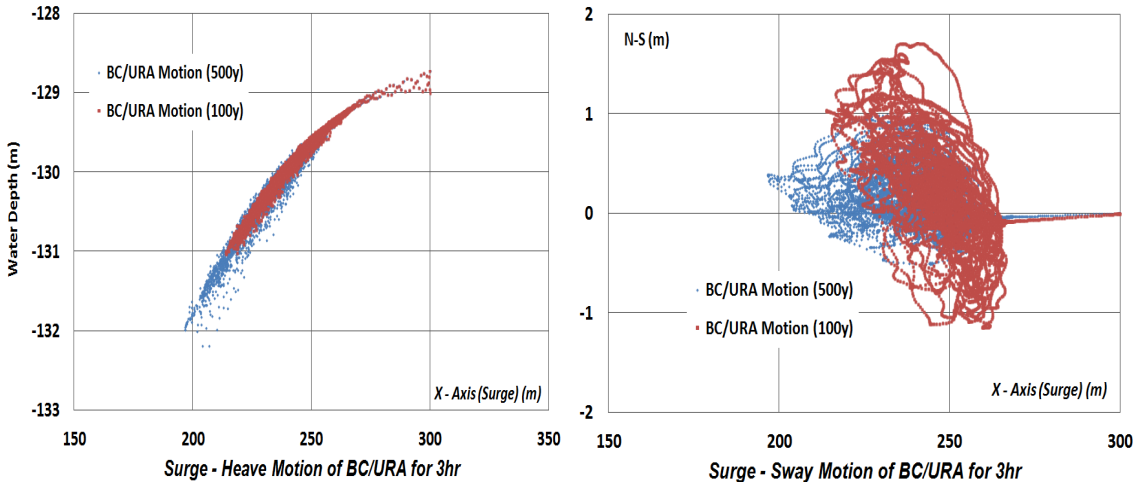

(a) BC/URA surge - heave motion for 3hr (b) BC/URA surge - sway motion for 3hr

Fig. 4.15 Motion tracking of the submerged structures (Top) and FPSO (Down) for 3hr under 100 and 500-yr hurricane conditions

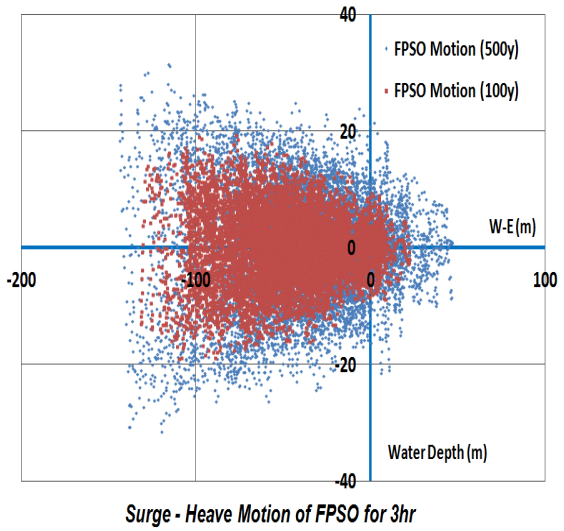

(c) FPSO surge - heave motion for 3hr

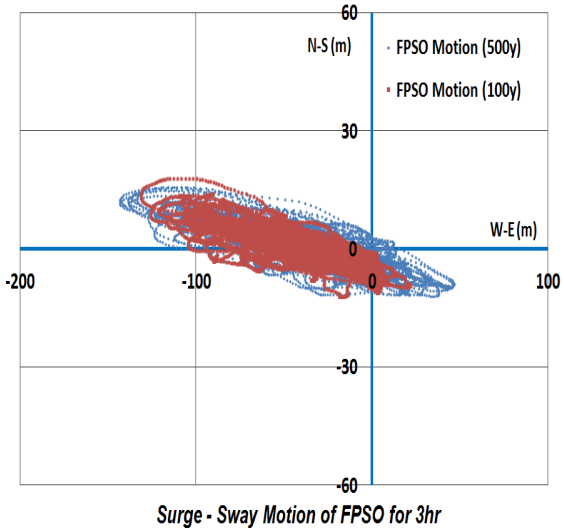

(d) FPSO surge - sway motion for 3hr

Fig. 4.15 Continued

Fig. 4.15 shows the motion traces of the FPSO and the submerged structures in 100 and 500-yr hurricanes for 3hours. From the comparison graphs, the BC and URA have relatively stable motions than the FPSO.

Table 4.4 Statistics of the submerged structures

Motion	***Surge (m)*** (Horizontal Offset from FPSO Turret)		***Sway (m)***		***Heave (m)***	
	100-yr	***500-yr***	***100-yr***	***500-yr***	***100-yr***	***500-yr***
Max.	266.55	258.53	1.71	0.99	-129.21	-129.37
Mean	246.45	240.06	0.23	0.18	-129.72	-129.94
Min.	213.91	196.51	-1.14	-0.51	-131.03	-132.19
STD Dev.	10.15	11.80	0.55	0.27	0.35	0.48

Table 4.4 Continued

Motion	*Roll (deg.)*		*Pitch (deg.)*		*Yaw (deg.)*	
	100-yr	*500-yr*	*100-yr*	*500-yr*	*100-yr*	*500-yr*
Max.	0.15	0.21	9.73	13.32	5.54	8.58
Mean	0.00	0.00	-0.72	-0.92	-0.36	0.00
Min.	-0.09	-0.29	-6.84	-8.63	-6.88	-9.18
STD Dev.	0.02	0.02	1.47	1.72	1.64	2.56

Table 4.5 Statistics of the FPSO

Motion	*Surge (m)*		*Sway (m)*		*Heave (m)*	
	100-yr	*500-yr*	*100-yr*	*500-yr*	*100-yr*	*500-yr*
Max.	22.06	46.71	18.04	15.93	19.31	31.45
Mean	-48.63	-35.79	1.38	0.70	0.01	-0.02
Min.	-131.47	-143.61	-12.17	-11.86	-19.04	-31.52
STD Dev.	28.83	37.46	4.94	5.74	6.18	9.84
Motion	*Roll (deg.)*		*Pitch (deg.)*		*Yaw (deg.)*	
	100-yr	*500-yr*	*100-yr*	*500-yr*	*100-yr*	*500-yr*
Max.	1.39	2.17	7.97	13.37	5.89	6.64
Mean	0.00	0.04	0.01	0.05	0.02	-0.27
Min.	-1.42	-1.91	-7.96	-12.90	-6.74	-6.40
STD Dev.	0.41	0.61	2.49	4.01	2.07	2.40

4.2.2 Inertial and Viscous Forces on Submerged Structures

The same way as shown in the fixed-fairlead analysis, the environmental loads of waves and currents are obtained by using Morison's formula, and the results are shown in the Fig. 4.16 and Fig. 4.17

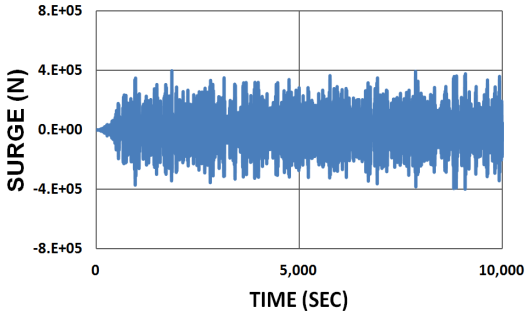

(a) Inertial Force – Surge

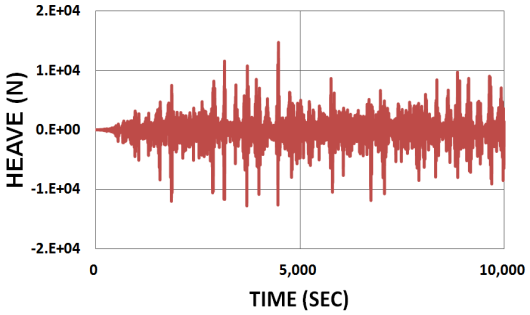

(b) Inertial Force – Heave

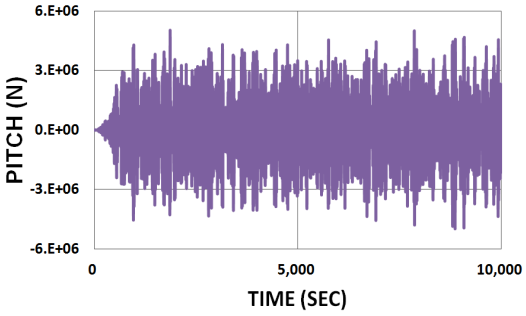

(c) Inertial Force – Pitch

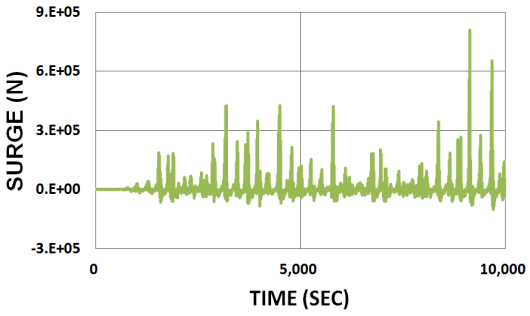

(d) Viscous Force – Surge

Fig. 4.16 Inertial and viscous forces acting on BC& URA under 100-yr hurricane condition

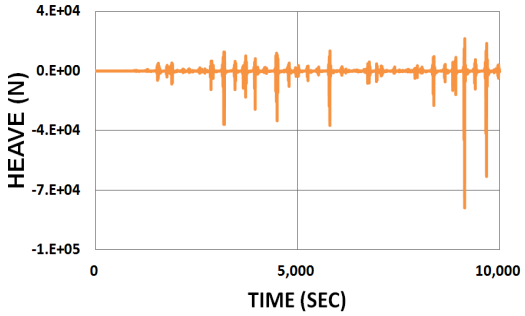

(e) Viscous Force – Heave

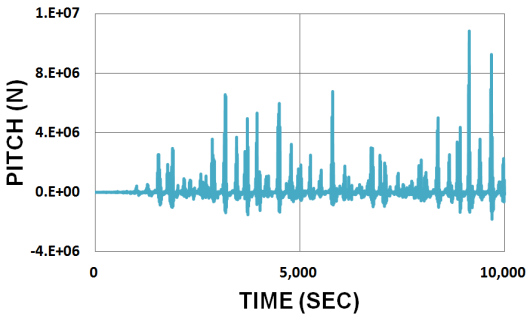

(f) Viscous Force - Pitch

Fig. 4.16 Continued

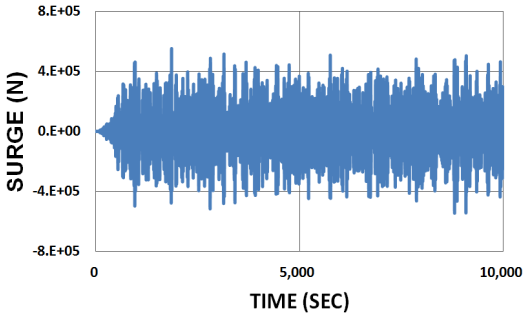

(a) Inertial Force – Surge

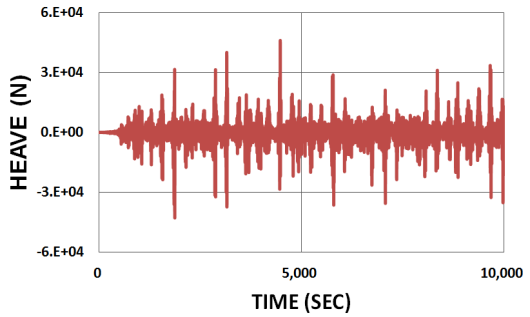

(b) Inertial Force - Heave

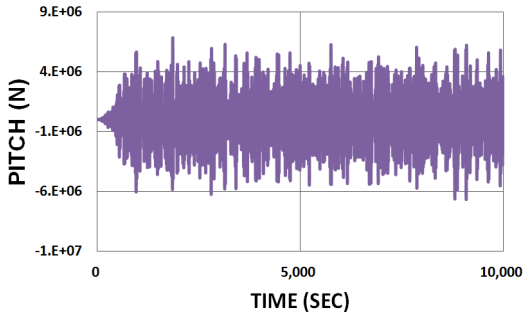

(c) Inertial Force – Pitch

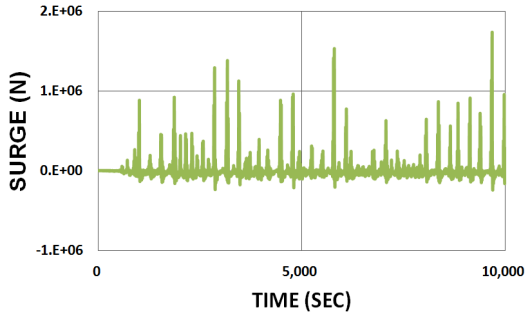

(d) Viscous Force – Surge

Fig. 4.17 Inertial and viscous forces acting on BC&URA under 500-yr hurricane condition

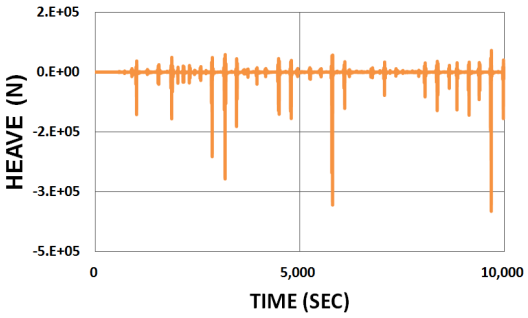

(e) Viscous Force – Heave

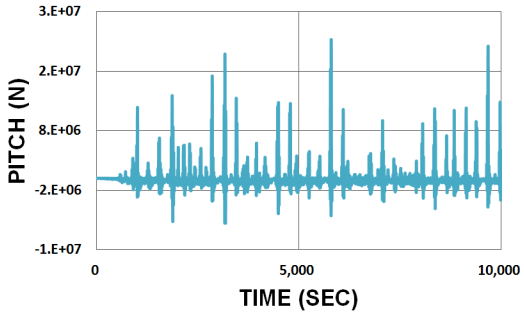

(f) Viscous Force - Pitch

Fig. 4.17 Continued

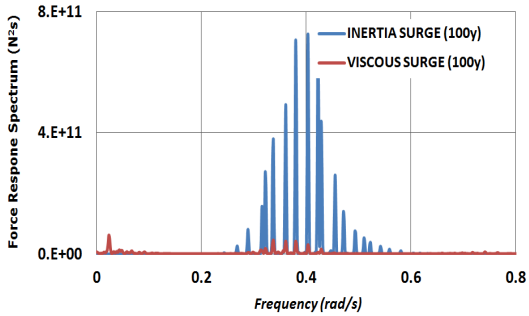

(a) Surge – 100-yr

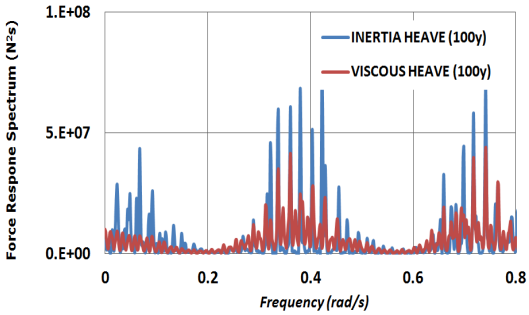

(b) Heave – 100-yr

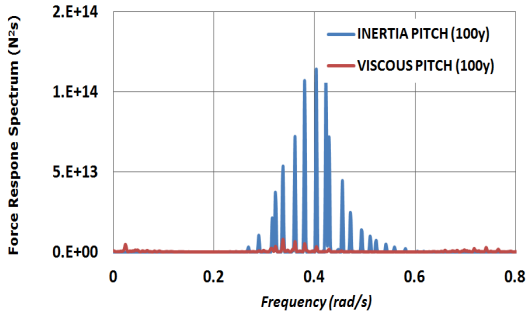

(c) Pitch – 100-yr

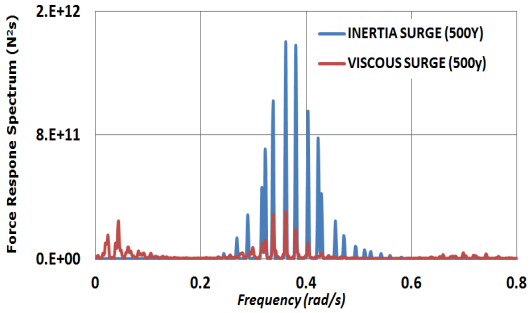

(d) Surge – 500-yr

Fig. 4.18 Inertial and viscous response spectra under 100 and 500-yr hurricane conditions.

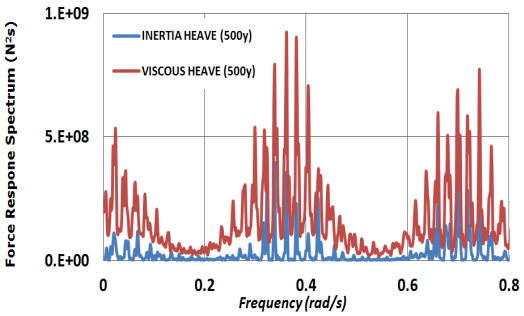

(e) Heave – 500-yr

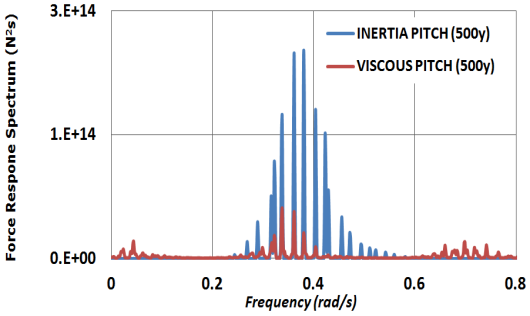

(f) Pitch – 500-yr

Fig. 4.18 Continued

Fig. 4.18 shows the inertial forces are dominant in surge and pitch both in 100 and 500-yr hurricane conditions same as in the fixed-fairlead analysis. However, in case of heave, the viscous force in 100-yr is almost equal to the inertial force. Moreover, the viscous force in 500-yr is greater than the inertial force. As discussed in the theoretical background chapter, the assumption in this research is the characteristic dimension of the buoyancy can and the upper riser assembly is far smaller than wavelength, so there is a limitation to calculate exact the inertial and the viscous forces by employing Morison's equation.

Table 4.6 Statistics of the inertial and viscous forces

Motion	***Inertial Surge (N)***		***Inertial Heave (N)***		***Inertial Pitch (N)***	
	100-yr	***500-yr***	***100-yr***	***500-yr***	***100-yr***	***500-yr***
Max.	3.96E+05	5.51E+05	1.76E+04	4.60E+04	5.01E+06	6.83E+06
Mean	-1.21E+03	-2.65E+03	4.88E+01	1.25E+02	-1.41E+04	-3.70E+04
Min.	-3.96E+05	-5.45E+05	-1.54E+04	-4.29E+04	-4.96E+06	-6.70E+06
STD Dev.	1.26E+05	1.70E+05	2.46E+03	5.41E+03	1.58E+06	2.09E+06
Motion	***Viscous Surge (N)***		***Viscous Heave (N)***		***Viscous Pitch (N)***	
	100-yr	***500-yr***	***100-yr***	***500-yr***	***100-yr***	***500-yr***
Max.	8.08E+05	1.74E+06	1.92E+04	5.33E+04	1.08E+07	2.32E+07
Mean	-9.05E+02	-1.52E+04	-8.27E+00	-2.34E+02	-1.30E+04	-3.40E+05
Min.	-1.01E+05	-2.44E+05	-8.27E+04	-3.48E+05	-1.78E+06	-7.51E+06
STD Dev.	4.67E+04	1.18E+05	2.61E+03	1.30E+04	6.08E+05	1.52E+06

4.2.3 Dynamic Response of Flexible Jumper

In this chapter, the dynamic motion responses of the flexible jumper are investigated under 100-yr and 500-yr hurricanes. As described in the design baseline chapter, the jumper connects the submerged structures with the FPSO, and the flexible jumper plays an important role in reducing significant FPSO induced dynamic motions in this research. The following figure shows the vertical velocity and acceleration along the flexible jumper from the FPSO fairlead point to the upper riser assembly.

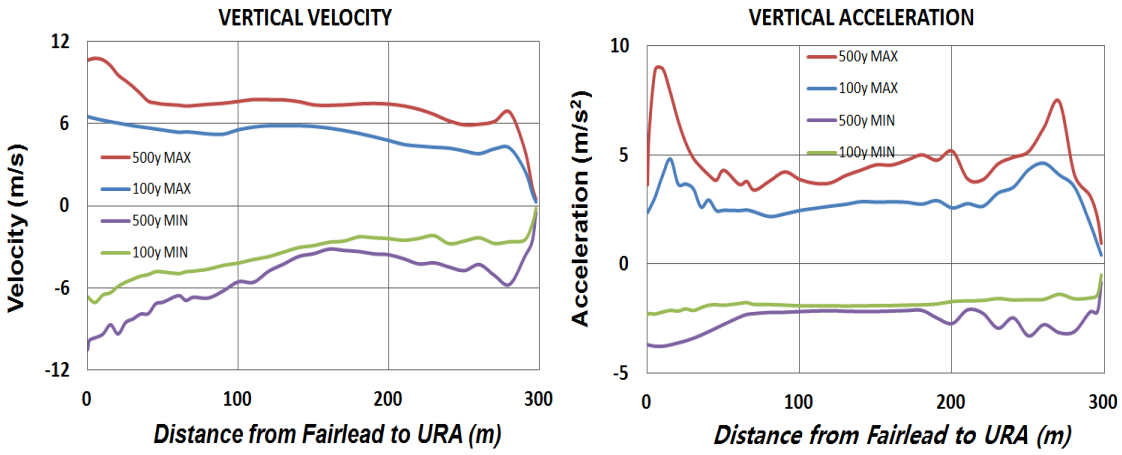

(a) Vertical velocity (b) Vertical acceleration

Fig. 4.19 Vertical velocity and acceleration under 100 and 500-yr hurricane conditions of the flexible jumper

Fig. 4.19 shows that the vertical velocity at fairlead point is most significant and the dynamic motions are smoothly decreased along the flexible jumper. The phenomenon can be explained as the decoupling effect of the hybrid riser by the flexible jumper, and the decoupled effect is very important characteristic in terms of the structure strength and the long fatigue service life.

In order to additionally confirm regarding the variations of vertical displacement and velocity along the flexible jumper, response spectrum is employed with respect to the following three points: (a) fairlead point, (b) mid (sag part) point, and (c) URA touch point.

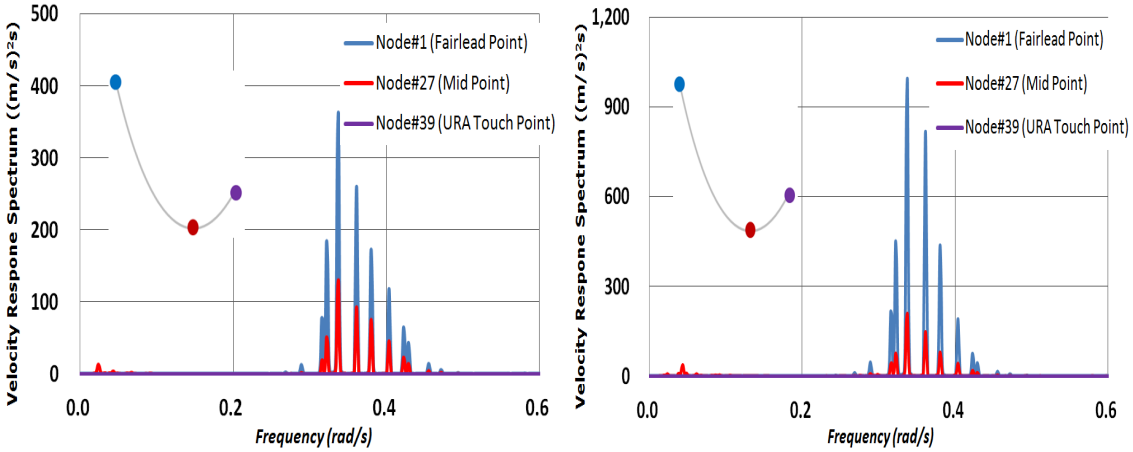

(a) Response spectrum under100-yr (b) Response spectrum 500-yr

Fig. 4.20 Vertical velocity response spectra of the flexible jumper under 100 and 500-yr hurricane conditions

Figs. 4.20 clearly shows that the energy of the vertical velocity is rapidly decreased along the flexible jumper from fairlead point to the upper riser assembly in both 100-yr and 500-yr hurricanes, so the FPSO induced forces cannot directly be transmitted to the submerged structures and the vertical riser by the decoupling effect of the flexible jumper.

Table 4.7 Three points' vertical velocities of the flexible jumper

Designation	***Vertical Velocity (m/s)***					
	100-yr Hurricane			***500-yr Hurricane***		
	Fairlead	***Mid Point***	***URA Touch***	***Fairlead***	***Mid Point***	***URA Touch***
Max.	6.54	5.0	0.29	10.64	7.48	0.49
Min.	-6.67	-2.37	-0.22	-10.51	-3.54	-0.49

As a flexible riser is generally made of several layers of composite materials, calculating yield point and fatigue damage is quite difficult to employing von-Mises yield criterion. In this regard, Minimum Bend Radius (MBR) is important check point for the strength of the flexible jumper.

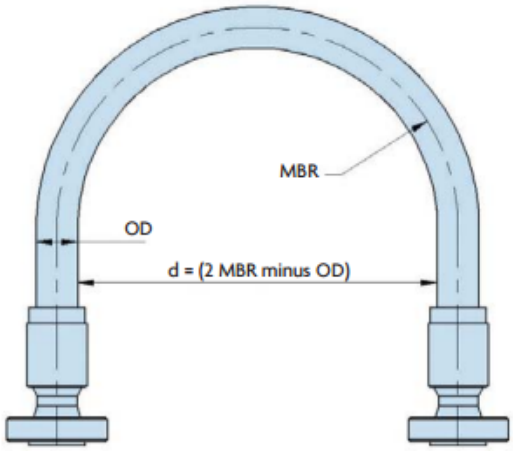

Fig. 4.21 Minimum Bend Radius (MBR) of flexible riser *(Image source: User's Guide of Coflexip Flexible Steel Pipes for Drilling and Service Application of Technip)*

The MBR is generally calculated from the 12 times of inner diameter of the flexible riser as a rule of thumb, so in this study the MBR of the flexible jumper is 4.877 m. In order to obtain the radius of curvature of each node, the bending stiffness Formula ($M\rho = EI$) is employed.

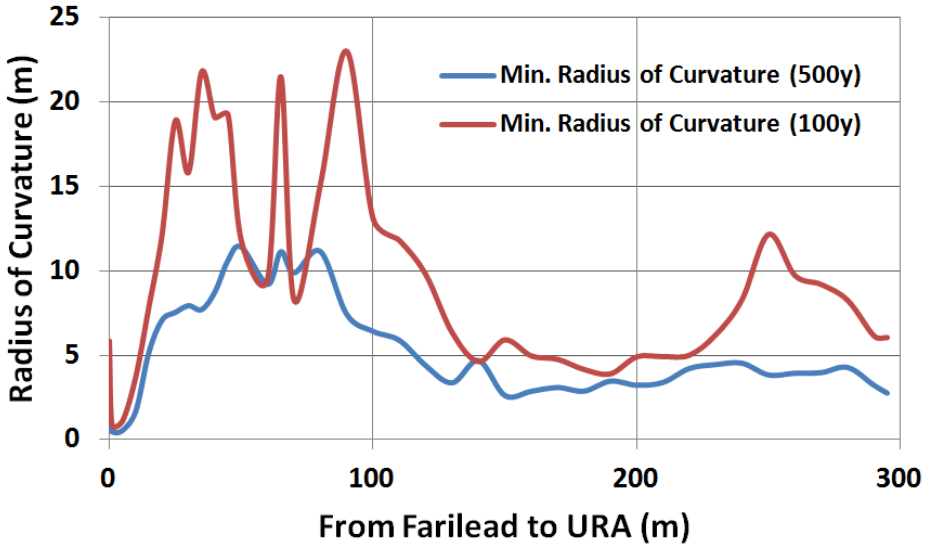

Fig. 4.22 Minimum radius of curvature of the flexible jumper under 100 and 500-yr hurricane conditions

Fig. 4.22 shows that the minimum radius of curvature near hang off location, sag and URA touch points are approaching to the MBR both under 100 and 500-yr hurricane conditions. In addition, as bend stiffeners at hang-off and gooseneck points are not considered in this study, the radii of curvature near two end points of the flexible jumper are exaggerated. Accordingly, it is assumed that the bend stiffener length attached to the hang-off point and gooseneck is 10m, so the results of the two points are excluded in the counting.

Table 4.8 MBR Occurrence time

MBR Occurrence Time (sec.)	
100-yr Hurricane	***500-yr Hurricane***
7	247

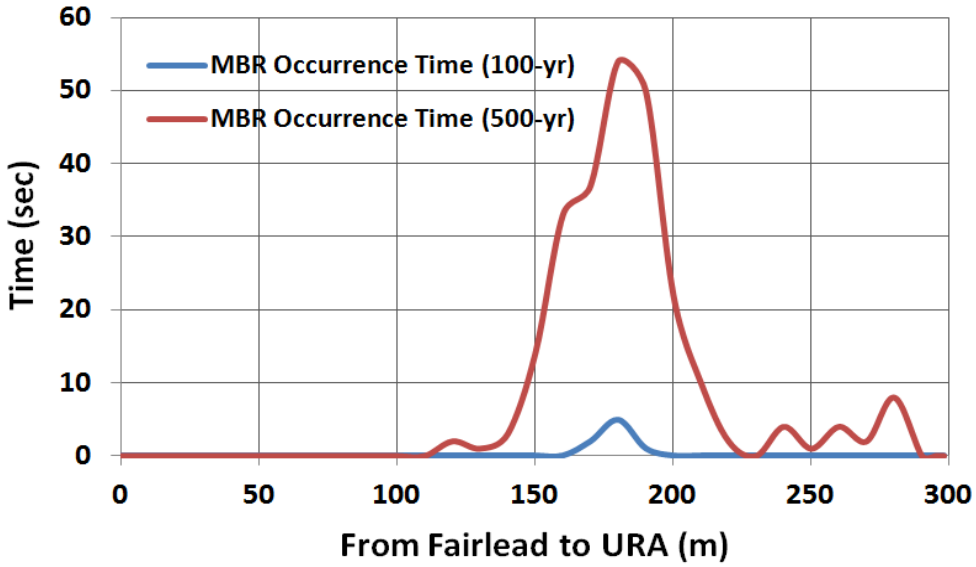

Fig. 4.23 MBR occurrence time of the flexible jumper under 100 and 500-yr hurricane conditions

Table 4.8 and Fig. 4.23 show that the MBR intensively occurs under 500-yr near sag area of the flexible jumper. The extreme bending is occurred corresponding to the significant downward FPSO heave.

4.2.4 Stress Evaluation on Riser

In this chapter, axial and bending normal stresses of the flexible jumper and the vertical riser are investigated. In addition, the variations of the two stresses in terms of the maximum and minimum horizontal offsets between the FPSO and the submerged structures are discussed. The axial and bending normal stresses can be calculated by employing axial force and axis bending moment from moving-fairlead analysis program CHARM3D.

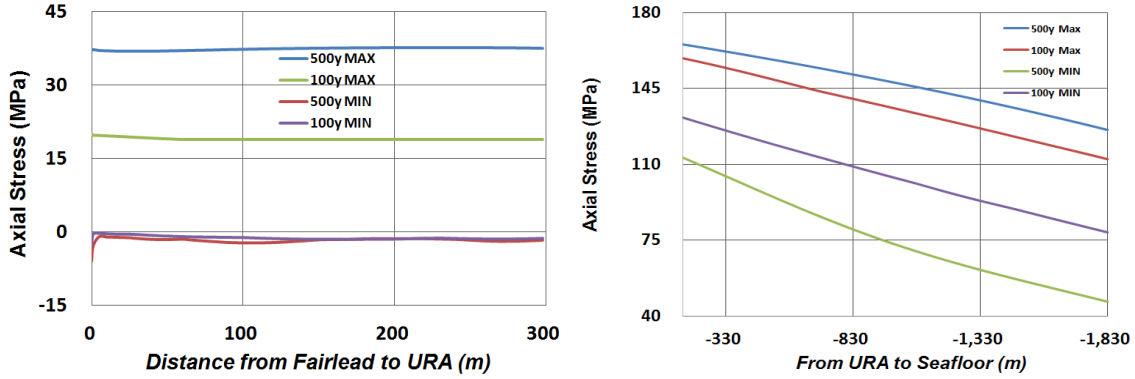

(a) Axial stress of the flexible jumper (b) Axial stress of the vertical riser

Fig. 4.24 Axial stress distributions of the flexible jumper and vertical riser under 100 and 500-yr hurricane conditions

Table 4.9 Axial stresses of the flexible jumper and the vertical riser

Designation	***AXIAL STRESS (MPa)***			
	100-yr Hurricane		***500-yr Hurricane***	
	Max.	***Min.***	***Max.***	***Min.***
Flexible Jumper	20.06	-2.62	37.64	-5.93
Vertical Riser	158.80	112.34	165.46	46.60

Fig.4.24 shows the distribution of maximum and minimum axial stress of the flexible jumper and the vertical riser. Firstly, the distribution pattern of the maximum axial stress of the jumper is constant from fairlead to the URA due to the tension force caused by the FPSO surge. In other words, the environmental loads heading to west make the FPSO move to negative surge direction, so the vessel with significant surge tautens the flexible jumper. The tautened flexible jumper results in showing the constant values of the maximum and minimum axial stresses from the fairlead to the URA touch

point. On the other hand, the distribution pattern of the axial stress with respect to the vertical riser shows different with the jumper. As the axial stress to the vertical riser is induced by the buoyancy can, the maximum and minimum stresses of the vertical riser are linearly decreased from the bottom of the URA to the seafloor along the vertical riser. For 100-yr hurricane case, the distribution pattern of the axial stress with respect to the vertical riser is linear. In other words, the submerged structures are not significantly affected by the FPSO and the environmental loads. Under 500-yr hurricane, however, the distribution pattern of the maximum and the minimum axial stresses shaped curve line that can be explained as the submerged structures are significantly affected by under the 500-yr hurricane condition.

Fig. 4.25 shows the bending normal stress distributions of the flexible jumper and vertical riser in 100 and 500-yr return period of hurricanes.

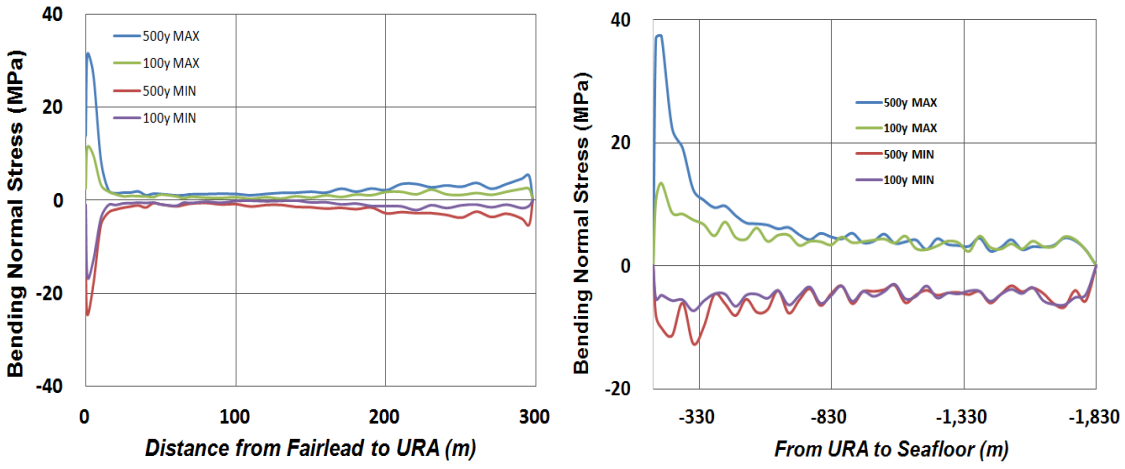

(a) Flexible Jumper (b) Vertical riser

Fig. 4.25 Bending normal stress distributions of the flexible jumper and the vertical riser under 100 and 500-yr hurricane conditions

Firstly, the bending normal stress of the flexible jumper near hang-off area is considerably significant by the impact of the dynamic motions of FPSO. The significant maximum bending normal stress near hang off point is rapidly reduced along the flexible jumper, and the stress is increased again around the sag area due to the occurrence of horizontal (on x - y plane) curvature.

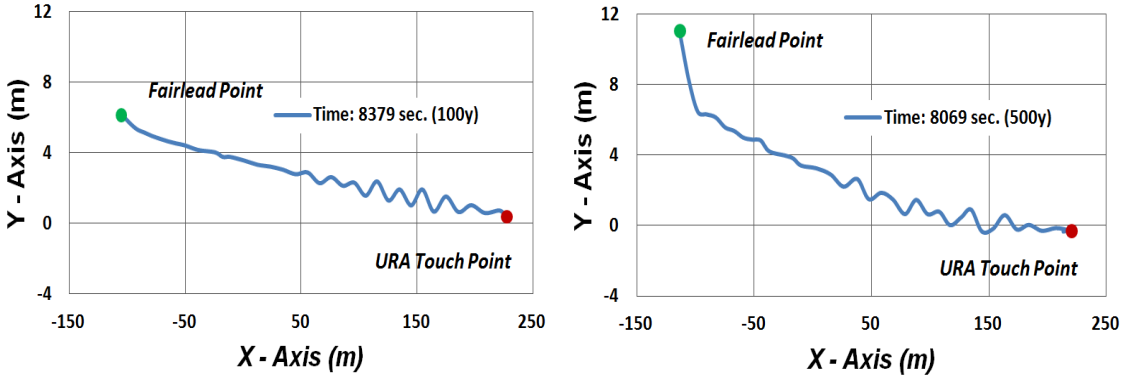

(a) Horizontal curvature under 100-yr (b) Horizontal curvature under 500-yr

Fig. 4.26 Horizontal curvature of the flexible jumper under 100 and 500-yr hurricane conditions

Table 4.10 Bending normal stresses of flexible jumper and the vertical riser

Designation	***BENDING N. STRESS (MPa)***			
	100-yr Hurricane		***500-yr Hurricane***	
	Max.	***Min.***	***Max.***	***Min.***
Flexible Jumper	11.35	-16.34	31.30	-24.64
Vertical Riser	13.43	-7.23	37.33	-12.58

In addition, the relation between the horizontal offset and stress distribution of the flexible jumper is investigated. The check points are the nearest and the farthest horizontal offsets between the FPSO and the submerged structures.

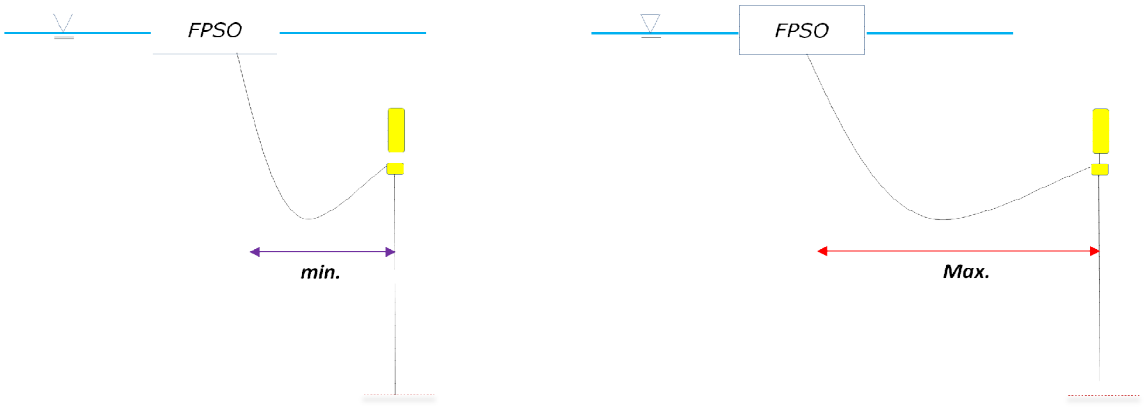

(a) Nearest horizontal offset (b) Farthest horizontal offset

Fig. 4.27 Nearest and farthest horizontal offsets between FPSO and the submerged structures

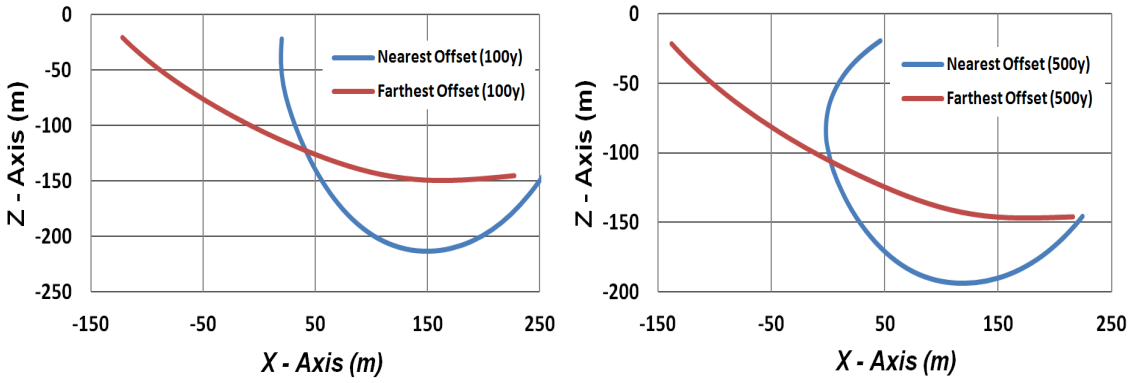

(a) Farthest/Nearest offsets under 100-yr (b) Farthest/Nearest offsets under 500-yr

Fig. 4.28 Configuration of the flexible jumper at nearest and farthest offsets under 100 and 500-yr hurricane conditions

Table 4.11 Horizontal offsets between the FPSO and the Submerged Structures

Designation	*100-yr Hurricane*		*500-yr Hurricane*	
	Farthest	*Nearest*	*Farthest*	*Nearest*
Value (m)	352.98	235.00	358.72	180.52

Fig. 4.28 and Table 4.11 show that maximum horizontal offsets under 100-yr and 500-yr are similar due to the limitation of the flexible jumper length. On the other hand, the minimum horizontal offset of the flexible jumper under 500-yr is around 77% of the flexible jumper length under 100-yr.

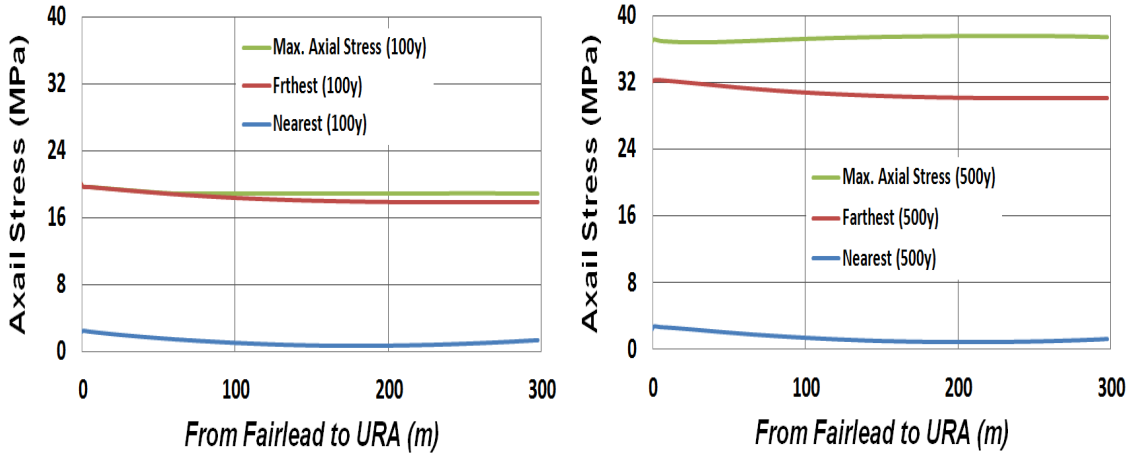

(a) Axial stress under 100-yr (b) Axial stress under 500-yr

Fig. 4.29 Axial stress distribution of the flexible jumper at nearest and farthest offsets under 100 and 500-yr hurricane conditions

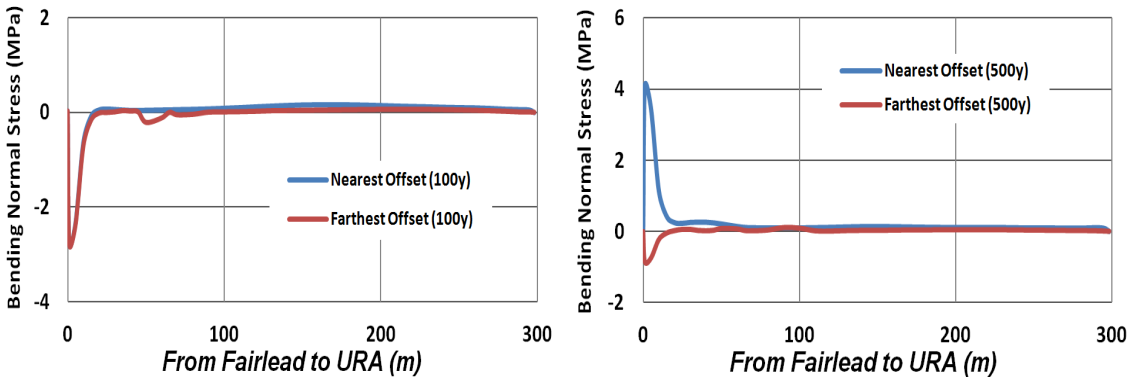

(a) Bending normal stress under 100-yr (b) Bending normal stress under 500-yr

Fig. 4.30 Bending normal stress distributions of the flexible jumper at nearest and farthest offsets under 100 and 500-yr hurricane conditions

Fig. 4.29 shows that the peak value of the axial stresses at farthest offsets under both 100 and 500-yr hurricane conditions approach to the maximum axial stresses during 3hr hurricanes. The maximum axial stress occurs when the submerged structures have maximum pitch both under 100 and 500-yr hurricanes.

Fig. 4.30 shows the bending normal stresses under 100 and 500-yr hurricanes, and the maximum and minimum values at farthest horizontal offset are quite difference with the maximum and minimum bending normal stresses of the flexible jumper during 3hr time-series simulation. As the FPSO induced tension force is dominant at farthest horizontal offset, the bending normal stress does not have relation with environmental conditions at this moment.

Table 4.12 Axial stress of the flexible jumper at farthest offset of FPSO

Designation	*100-yr Hurricane*		*500-yr Hurricane*	
	Farthest ***Max. Axial Stress***	***Max.*** ***Axial Stress***	***Farthest*** ***Max. Axial Stress***	***Max.*** ***Axial Stress***
Value (MPa)	17.76	20.06	32.33	37.64

4.2.5 von-Mises Stress Evaluation on Riser

In this chapter, the limit state of the riser structure strength is checked by employing von-Mises yield criterion of API RP 2RD. As discussed in the theoretical background chapter, three principal stresses, normal stress, hoop and radial stresses, are required to calculate von-Mises stress. As the hoop and radial stresses are calculated by using the internal and external pressures of the riser with the riser thickness and outer diameter, the two stress values are linearly varied by the seawater depth change.

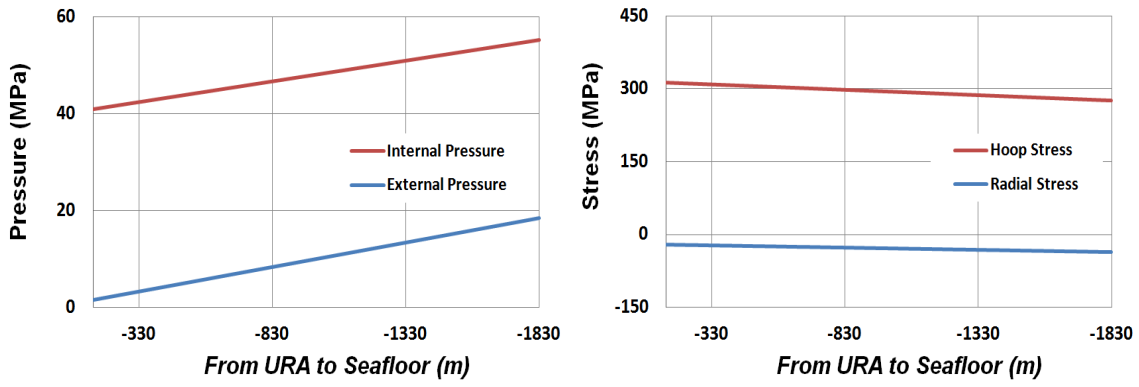

(a) Internal & External Pressures (b) Hoop & Radial Stresses

Fig. 4.31 Internal/External pressures and Radial/Hoop stresses of the vertical riser

Fig. 4.31 shows the linear variation of the hoop and radial stresses that are manly affected by the internal and external pressures of the riser.

Precedence check points should be performed with respect to whether the riser will be burst and hoop buckled before confirming the von-Mises yield criterion. In this research, it is assumed that three types of material, X65, X70 and X80 are used for the vertical riser.

Table 4.13 Bursting confirmation with respect to the vertical riser

X65		***X70***		***X80***	
$P_{li} - P_e$	$\frac{P_b(t)}{\gamma_m \cdot \gamma_{sc}}$	$P_{li} - P_e$	$\frac{P_b(t)}{\gamma_m \cdot \gamma_{sc}}$	$P_{li} - P_e$	$\frac{P_b(t)}{\gamma_m \cdot \gamma_{sc}}$
39.5	***42.0***	*39.5*	***45.2***	*39.5*	***51.7***
Pass		*Pass*		*Pass*	

Table 4.14 Hoop buckling confirmation with respect to the vertical riser

X65		***X70***		***X80***	
$p_e - p_{\min}$	$\frac{p_e(t)}{\gamma_{sc} \cdot \gamma_m}$	$p_e - p_{\min}$	$\frac{p_e(t)}{\gamma_{sc} \cdot \gamma_m}$	$p_e - p_{\min}$	$\frac{p_e(t)}{\gamma_{sc} \cdot \gamma_m}$
18.39	***26.70***	*18.39*	***28.54***	*18.39*	***32.12***
Pass		*Pass*		*Pass*	

Table 4.13 and 4.14 show the confirmation results with respect to the grades X65, X70 and X80 risers from the bursting and the hoop criteria of DNV OS F201

Fig. 4.32 shows the results of the normalized von-Mises stresses ($\sigma_v / c_f c_a \sigma_y$) with respect to X65, X70 and X80 risers in 100-yrr and 200yr return period of hurricanes, respectively.

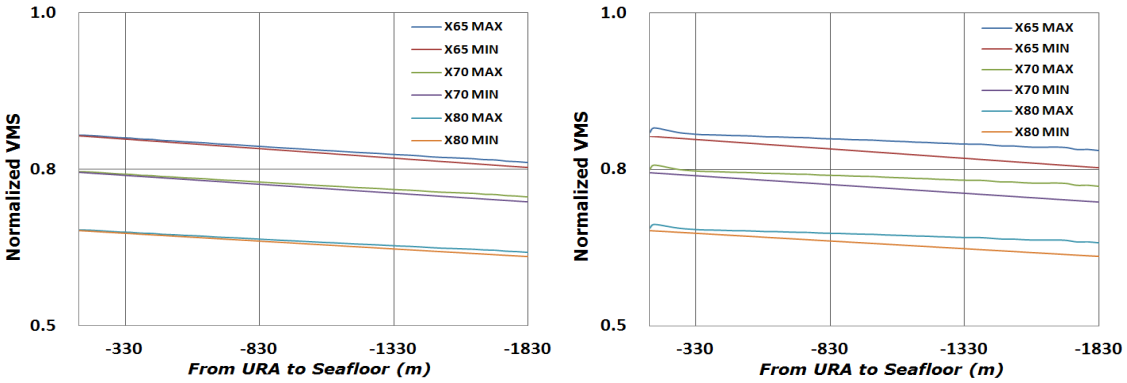

(a) 100-yr Hurricane Condition (b) 500-yr Hurricane Condition

Fig. 4.32 Normalized von-Mises Stress of the Vertical Riser

The overall distribution patterns of the normalized von-Mises stresses are quite similar between 100 and 500-yr hurricane conditions. To specific analyze the normalized von-Mises stresses, the risers are separately analyzed based on the pipe grades.

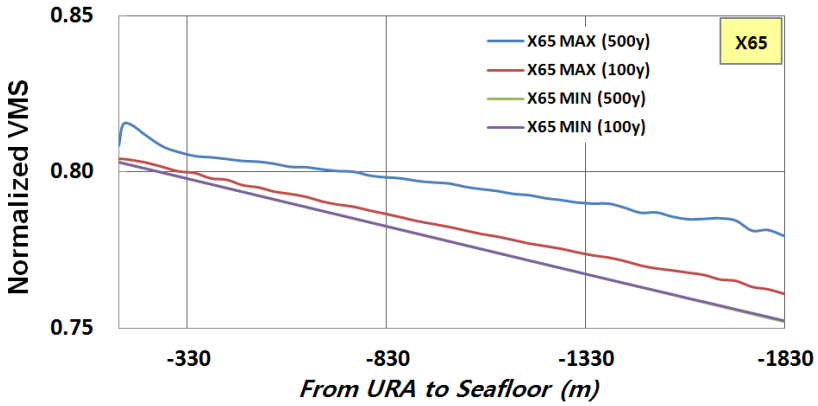

(a) Normalized VMS of Grade X65

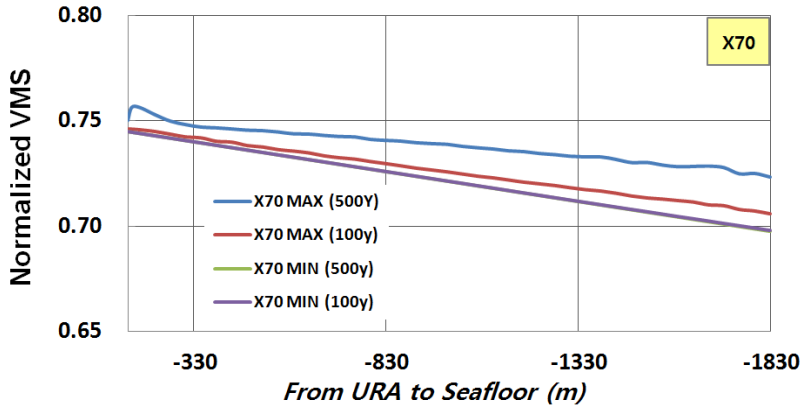

(b) Normalized VMS of Grade X70

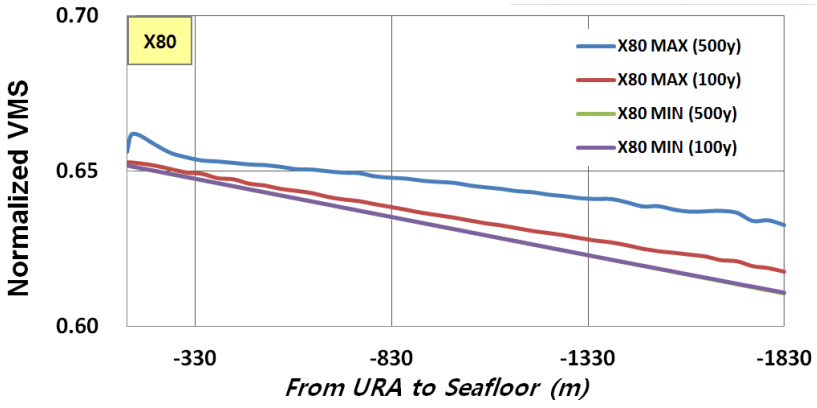

(c) Normalized VMS of Grade X80

Fig. 4.33 Normalized von-Mises Stress of X60, X70 and X80 Vertical Riser

Fig. 4.33 shows the normalized von-Mises stress distributions of each three grades under 100 and 500-yr hurricane conditions, respectively. Under 100-yr hurricane, the overall normalized von-Mises stresses of each grade along the vertical riser are linearly decreased along the vertical riser from the URA to the seafloor. The result quite matches with the axial stress distribution of the vertical riser in the stress evaluation chapter. From the results of the von-Mises yield criterion, it can be reconfirmed that the submerged structures are hardly affected by the environmental loads. On the other hand, under 500-yr the normalized von-Mises stress shows curved shapes with larger values than the 100-yr results near the seafloor and the bottom of the URA which results also well match with the axial stress result of the vertical riser in the stress evaluation chapter.

Table 4.15 Normalized VMS of the vertical riser under 100 and 500-yr hurricane conditions

Designation	***Normalized von-Mises Stress***					
	100-yr Hurricane			***500-yr Hurricane***		
	X65	***X70***	***X80***	***X65***	***X70***	***X80***
Maximum	0.804	0.746	0.653	0.815	0.756	0.662
Minimum	0.753	0.698	0.611	0.752	0.698	0.611

4.2.6 Combined Load Evaluation on Riser

In this chapter, the vertical riser strength is investigated by employing new yield criterion, Method1 of API STD 2RD published September, 2013. Especially, the Method 1 is especially employed to check the limitation on combined membrane load of the riser.

- Method 1: $\left|\frac{M}{M_y}\right| + \left|\frac{T}{T_y}\right| \le \sqrt{F_D^2 - \left(\frac{p_i - p_e}{p_b}\right)^2}$ (4.1)

where ,

M, T : maximum bending moment, effective tension

M_y, T_y : yield moment, yield tension

F_D : design factor (SLS/ULS:0.8)

P_e, P_i : external pressure, internal pressure

P_b : burst pressure

Method 1 can be modified to new terms as below (Brian S. Royer et al., 2014)

- Combined Membrane Load: $\sqrt{\left|\frac{M}{M_y}\right| + \left|\frac{T}{T_y}\right| + \left(\frac{p_i - p_e}{p_b}\right)^2}$ (4.2)

- Design Membrane Load Utilization: Combined Membrane Load/ F_D (4.3)

Firstly, the vertical riser strength is investigated by employing equation 4.2 (combined membrane load) in 100 and 500-yr hurricane conditions, respectively.

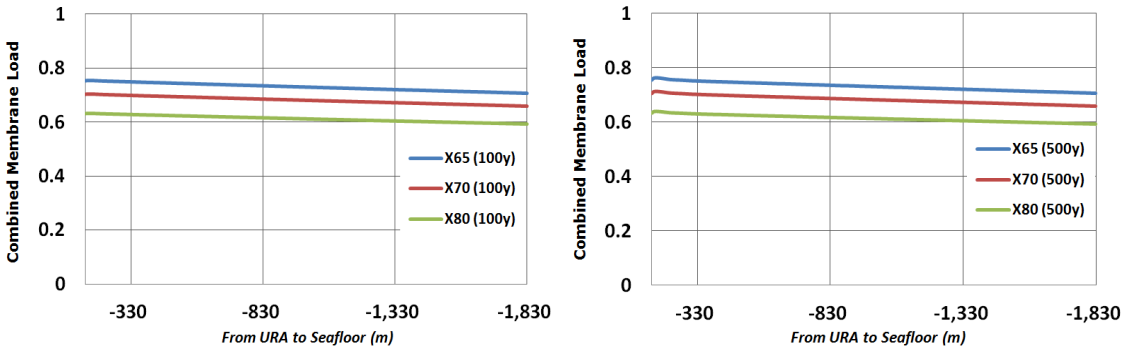

(a) 100-yr hurricane (b) 500-yr hurricane

Fig. 4.34 Combined membrane loads of X65, X70 and X80

Fig. 4.34 shows the results of the combined membrane loads, and the distribution patterns under 100 and 500-yr hurricanes are quite similar except for the vertical riser and the URA connection part. Near upper end area of the vertical riser show the sharp change due to the bending normal stress has significant variation near the upper riser under 500-yr hurricane condition.

Table 4.16 Combined membrane loads of the X60, X70 and X80

Designation	***Combined Membrane Load***					
	100-yr Hurricane			***500-yr Hurricane***		
	X65	***X70***	***X80***	***X65***	***X70***	***X80***
Maximum	0.755	0.704	0.633	0.763	0.712	0.639
Minimum	0.706	0.659	0.592	0.706	0.659	0.592

In order to check the riser strength in an extreme load case, design factor (F_D =0.8 for ULS) is applied in the equation 4.3 to calculate design member load utilization.

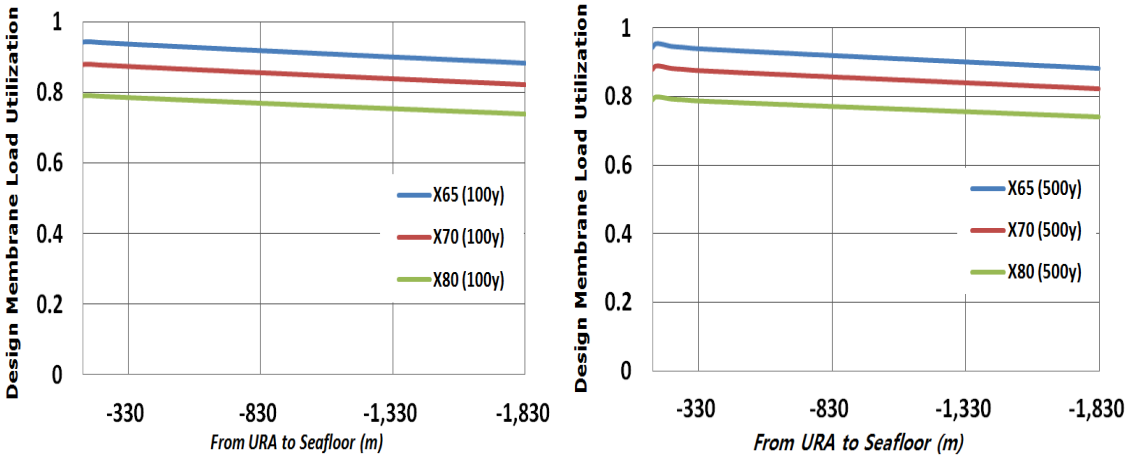

(a) DMLU under100-yr (b) DMLU under 500-yr

Fig. 4.35 Design Membrane Load Utilization of X65, X70 and X80 under 100 and 500-yr hurricane conditions

Fig 4.35 shows the results of the design membrane load utilizations under 100-yr and 500-yr hurricanes, and the overall outcomes are slightly shifting to the limit state of the strength acceptance criterion, 1.0 compared with the results of the combined membrane load due to the design factor, 0.8. Especially, the grades X70 and X65 are nearly approaching the limit state, 1.0 so X80 is recommended in the extreme load case. The DMLUs of the grades X65, X70 and X80 are summarized in the below Table 4.16.

Table 4.17 Design Membrane Load Utilization of the X65, X70 and X80

Designation	*Design Membrane Load Utilization*					
	100-yr Hurricane			*500-yr Hurricane*		
	X65	*X70*	*X80*	*X65*	*X70*	*X80*
Maximum	0.943	0.881	0.791	0.953	0.890	0.799
Minimum	0.882	0.823	0.740	0.882	0.823	0.740

4.2.7 Short-term Fatigue Damage Analysis

In this chapter, the fatigue service life of the vertical riser is investigated under 100 and 500-yr hurricanes. The detail steps of calculating short-term fatigue damage are described in the theoretical background chapter. DNV F1 S-N curve is employed in this research to calculate fatigue damage.

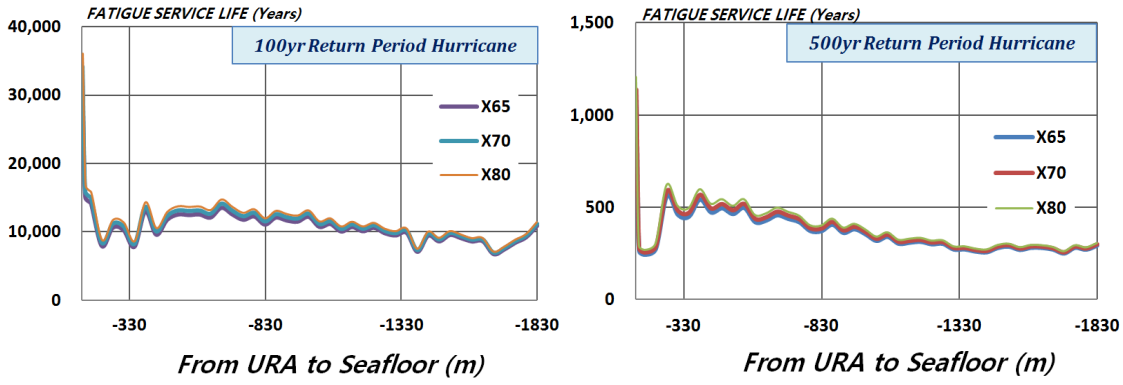

(a) 100-yr Hurricane (b) 500-yr Hurricane

Fig. 4.36 Fatigue service life of the X65, X70 and X80 under 100 and 500-yr hurricane conditions

Table 4.18 Fatigue service life under 100 and 500-yr hurricanes

Designation	***Fatigue Service Life (years)***					
	100-yr Hurricane			***500-yr Hurricane***		
	X65	***X70***	***X80***	***X65***	***X70***	***X80***
Maximum	32450	34121	36119	1083	1138	1205
Minimum	6798	6966	7162	243	255	263

Fig. 4.36 shows the fatigue service lives of grades X65, X70 and X80 risers under 100-yr and 500-yr hurricanes. In terms of the fatigue service life difference, under the 100-yr hurricane, the grades between X65 and X70 or X70 and X80 present within 5% differences. Under 500-yr hurricane, the difference fatigue service life of the grades show similar to 100-yr difference of around 5%. However, the change with respect to the hurricane conditions significantly affects to the fatigue service life of the vertical riser. To directly compare the fatigue service life under 100-yr and 500-yr hurricanes, Fig. 4.37 is presented in next page.

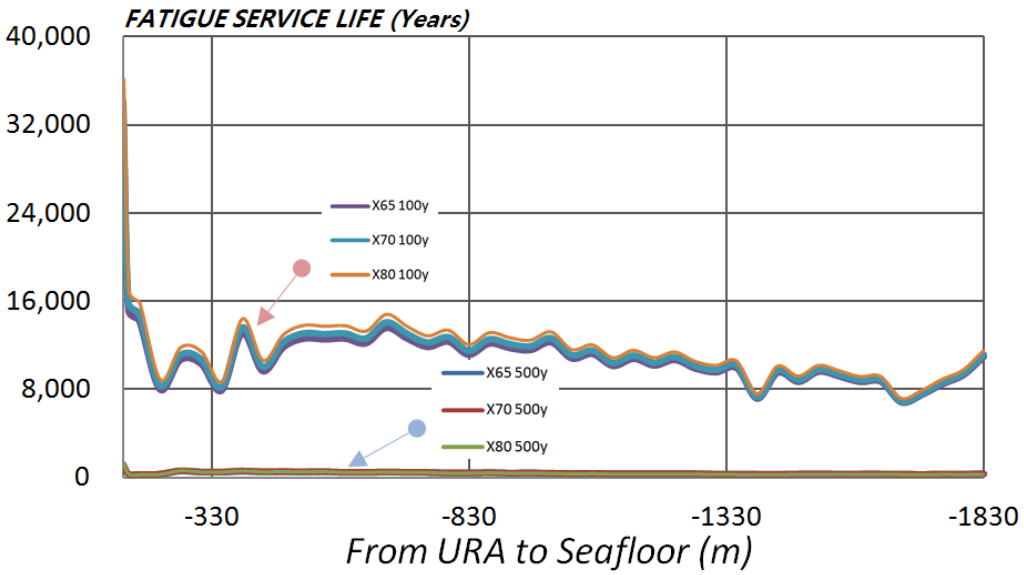

Fig. 4.37 Comparison of the fatigue service life between 100 and 500-yr hurricane conditions with respect to X65, X70 and X80

As shown in the Fig. 4.37, under 500-yr hurricane, the fatigue service life of the all three grades are only around 3% of the calculated fatigue service life of grades X65, X70 and X80 under 100-yr hurricane. With respect to the strength check of the vertical riser, the change of the environmental condition is not significant factor. However, in short-term fatigue damage analysis, the change of the environmental condition from 100-yr to 500-yr makes significant difference to the fatigue service life.

As discussed in the theoretical background chapter, the DNV-RP-F204 requires that the design fatigue factors (DFF) among high, normal and low safety classes should be taken into accounted to calculate the fatigue damage. The outcome from multiplying accumulated damage index by design fatigue factor should be equal to or less than 1.0. The fatigue service life with applied DFF of the X65, X70 and X80 vertical riser is presented following figures.

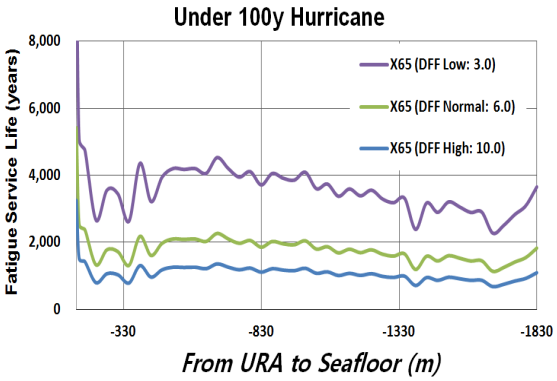

(a) X65 under 100-yr

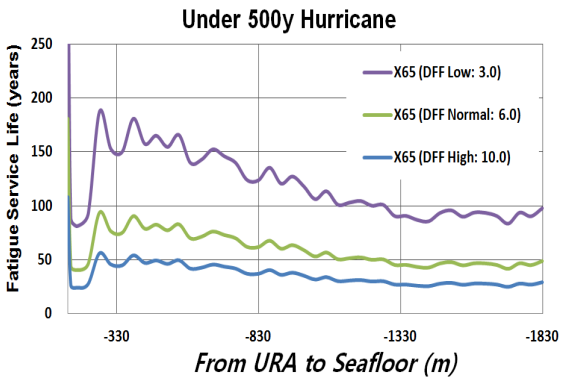

(a) X65 under 500-yr

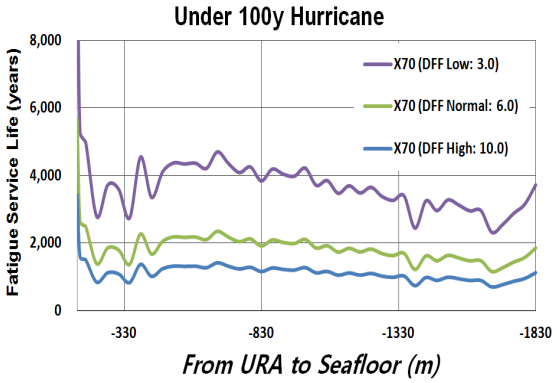

(a) X70 under 100-yr

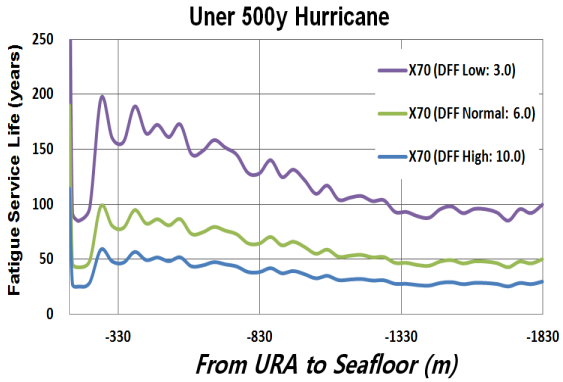

(a) X70 under 500-yr

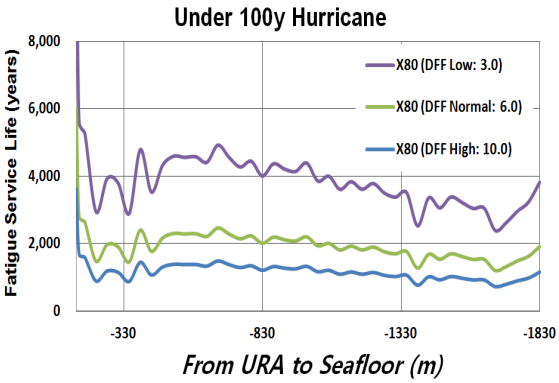

(a) X80 under 100-yr

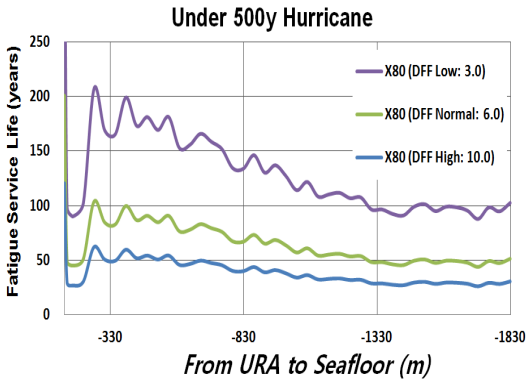

(a) X80 under 500-yr

Fig. 4.38 Fatigue service life of X65 under 100 and 500-yr hurricane conditions

Fig. 4.38 shows the results of the DFF applied fatigue service life under 100-yr and 500-yr hurricanes. The minimum fatigue service life of the vertical riser is around 24 years under 500-yr hurricane when applying the high safety class 10.0 to grade X65. In design baseline chapter, the targeted product service life set as 25 years, and the minimum fatigue service life should be over the product service life. Accordingly, X65 is unallowable to be used as riser material.

Table 4.19 Fatigue service life with applied DFF of the vertical riser

Fatigue Service Life of the Vertical Riser (Years)						
Material	***X65***					
Condition	***100-yrr Hurricane***			***500-yrr Hurricane***		
DFF	***Low*** *(3.0)*	***Normal*** *(6.0)*	***High*** *(10.0)*	***Low*** *(3.0)*	***Normal*** *(6.0)*	***High*** *(10.0)*
Maximum	10817	5408	3245	361	180	108
Minimum	2266	1133	680	81	40	24.3
Material	***X70***					
Condition	***100-yrr Hurricane***			***500-yrr Hurricane***		
DFF	***Low*** *(3.0)*	***Normal*** *(6.0)*	***High*** *(10.0)*	***Low*** *(3.0)*	***Normal*** *(6.0)*	***High*** *(10.0)*
Maximum	11374	5687	3412	379	190	114
Minimum	2322	1161	697	85	43	25.5
Material	***X80***					
Condition	***100-yrr Hurricane***			***500-yrr Hurricane***		
DFF	***Low*** *(3.0)*	***Normal*** *(6.0)*	***High*** *(10.0)*	***Low*** *(3.0)*	***Normal*** *(6.0)*	***High*** *(10.0)*
Maximum	12040	6020	3612	402	201	120
Minimum	2387	1194	716	88	44	26.3

Finally, the outstanding structure performance of the FSHR can be compared with different types of risers such as steel catenary riser (SCR) and lazy-wave steel catenary riser (LWSCR) regarding short-term fatigue estimation. For the SCR and LWSCR, Kim and Kim (2014) presented the maximum damage indices of SCR and LWSCR. The study was conducted under the same environmental conditions in this study. Therefore, it is meaningful to compare the short-term fatigue damages and the fatigue service life given same conditions.

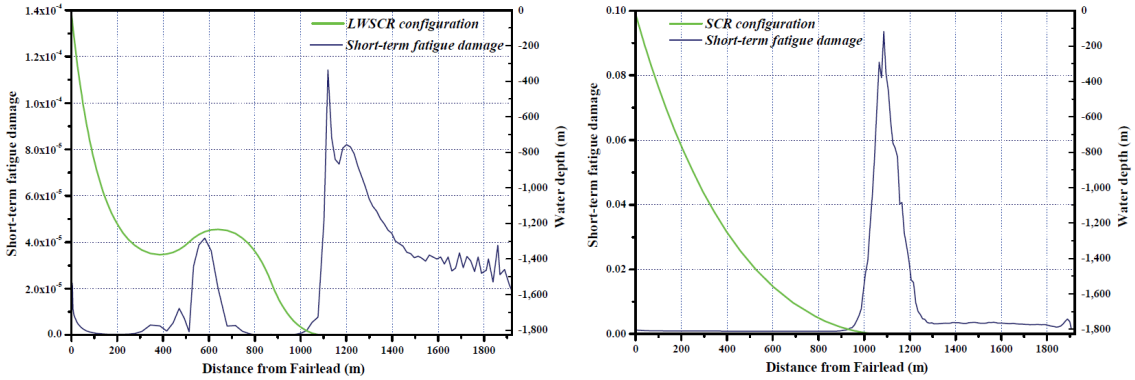

Fig. 4.39 Short-term fatigue damages of LWSCRs (left) and SCRs (right)
(Reference: Kim et al., 2014 Structural Performance of Deepwater Lazy-Wave Steel Catenary Risers for FPSOs)

Table 4.20 Comparison of short-term fatigue damage without applying DFF

Riser Type	***SCR***	***LWSCR***	***FSHR***
Max. Damage Index	0.091	1.14E-4	4.78E-08

* Environmental condition is 100-yr return period of hurricane for 3 hour

** Riser material is grade X65

Table 4.20 shows that the Free Standing Hybrid Riser shows superior advantages of fatigue service life over the SCR and LWSCR under same environmental conditions.

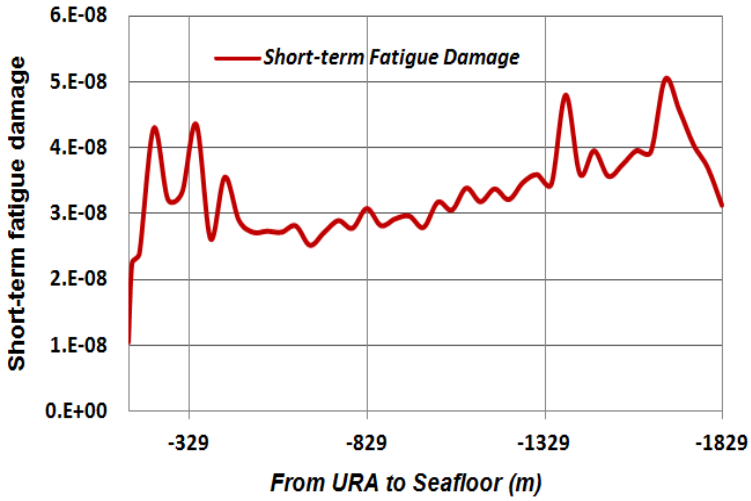

Fig. 4.40 Short-term fatigue damage distribution of free standing hybrid riser

Fig.4.40 shows the short-term fatigue damage distribution along the vertical riser. the overall values in the graph are extremely lower than those of SCRs and LWSCRs.

CHAPTER V

SUMMARY AND CONCLUSION

This study was examined FPSO coupled Free Standing Hybrid Riser for 100- and 500-yr hurricane conditions in the time domain using hull/mooring/riser moving-fairlead analysis program, CHARM3D. The analysis proceeded in three steps. Firstly, global motion analysis was performed for the submerged structures and flexible jumper. Secondly, stress evaluation was conducted for the flexible jumper and the vertical riser, and then the structure strength was checked. Finally, the short-term fatigue damage and fatigue service life were estimated for the vertical riser, and then compared with SCRs and LWSCRs. In addition, fixed-fairlead analysis was carried out separately with the FPSO uncoupled Free Standing Hybrid Riser in order to confirm the motion and structure responses to environmental loads.

The fixed-fairlead analysis of the FPSO uncoupled FSHR was investigated for 100- and 500-yr hurricane conditions with parallel waves and currents. The results of global motion and stress evaluation analyses showed that the effect of the environmental loads on the riser system was insignificant in 100- and 500-yr hurricane conditions.

The moving-fairlead analysis of FPSO coupled FSHR was conducted under parallel winds, waves and currents environment. Regarding the 6DOF motions of the submerged structures, there were clear differences between 100- and 500-yr hurricane conditions. Apart from the sway, the remaining 5DOF motions in 500-yr were larger than those in 100-yr hurricane conditions. The reduced sway phenomenon was caused by the surge direction of the stronger environmental loads. In case of the forces acting on

the submerged structures, except for the viscous heave force in the 500-yr, the inertial forces were dominant in both 100 and 500-yr. The dynamic motion responses of the flexible jumper exhibited two behavioral characteristics. Firstly, the FPSO induced significant dynamic motions were gradually dissipating along the jumper due to the decoupling effect. Secondly, the flexible jumper bent beyond the minimum bend radius when the FPSO had significant downward heave motion.

In the stress evaluation, the maximum axial stress of the flexible jumper occurred when the submerged structures had the largest pitch both in 100 and 500-yr hurricane conditions. Also, the structure strength results on the vertical riser showed that the given three grades X65/X70/X80 were suitable for the vertical riser material in 100- and 500-yr hurricane conditions based on the von-Mises yield criterion. However, the X65 riser approached close to fail limitation based on the Design Membrane Load Utilization with the design factor of 0.8 for ultimate limit state in 500-yr hurricane conditions.

In short-term fatigue damage estimation, rainflow counting method and Miner's rule were used to estimate the damage for the given three grades. The results indicated that all the given grades were suitable for vertical riser material. However, grade X65 did not meet the targeted product service life of 25 years when considering the design fatigue factor of 10 for the high safety class in 500-yr hurricane conditions. In this regards, X70 and X80 are recommendable material for the vertical riser.

Although the Free Standing Hybrid Riser exhibited exceptional global motions and structural performances under the extreme and semi-survival conditions, the high

capital expenditure, the complex engineering and some long lead items are regarded as the draw backs of the hybrid riser. In order to improve the analysis of the accuracy, more varied case studies or model tests are needed.

REFERENCES

API BULLETIN 2INT-MET., 2007. Interim guidance on hurricane conditions in the Gulf of Mexico, Washington, USA. (ftp://law.resource.org/pub/us/cfr/ibr/002/api.2int-met.2007.pdf)

API RP 2RD., 2009. Design of risers for floating production systems (FPSs) and tension-leg platforms (TLPs), Washington, USA. (http://www.techstreet.com/products/47839)

API STD 2RD., 2013. Dynamic Risers for Floating Production Systems, second edition, Washington, USA. (http://www.americanpetroleuminstitute.com/publications-standards-and-statistics/standards/whatsnew/publication-updates/new-exploration-and-production-publications/api_standard_2rd)

Bai, Y., Bai, Q., 2005. Subsea pipelines and risers, Elsevier Science; 2nd edition (December 19, 2005), ISBN-10: 0080445667.

Bob-Manuel, J., 2013. Risers for Deep Water FPSO's, 2013 FPSO Vessel Conference.

Brian S. Royer.,Thomas L. Power., Daniel O. Ayewah., William Head., 2014. Assessment of Ultra Deepwater Riser Concepts for High-Motion Vessels, OTC-25297-MS, Houston, Texas.

Chaudhuri, J., McNamara, J.F., O'Brien, P.J., 1987. Nonlinear Dynamic Analysis of Hybrid Riser System for Deepwater Application, OTC 5466, Houston, Texas.

DNV OS F201, 2010. Dynamic Risers, DNV Services, Research and Publications, Hovik, Norway.

DNV RP C203, 2010. Fatigue design of offshore steel structures, DNV Services, Research and Publications, Hovik, Norway.

DNV RP F204, 2010. Riser fatigue, DNV Services, Research and Publications, Hovik, Norway.

Fisher, E.A., Berner, P.C., 1988. Non-Integral Production Riser for Green Canyon Block 29 Development, OTC 5846, Houston, Texas.

Hatton, S., Lim, F., 1999. Third Generation Hybrid Risers.

Iob, F., Mecozzi, E., Vito, L.D., Darcis, P., Marines-Garcia, I., Quintanilla-Carmona, H.M., 2014. Hybrid Riser Resistance to In-Service Fatigue Loading, OMAE2014-24023, San Francisco, California.

Kim, Y.B., Kim, M.H., 2002. Hull/Mooring/Riser Coupled Dynamic Analysis of a Tanker-Based Turret-moored FPSO in Deep Water, ISOPE 2002, Kitakyushu, Japan.

Kim, M.H., Tahar, A., Kim, Y.B., 2001. Variability of TLP motion analysis against various design methodologies/parameters, ISOPE 2001, Stavanger, Norway.

Kim, S.J., Kim, M.H., Shim, S.H., Im, S.W.,2014. Structural Performance of Deepwater Lazy-Wave Steel Catenary Risers for FPSOs, ISOPE 2014, Busan, Korea.

Luppi, A., Cousin, G., O'Sullivan, R., 2014. Deep Water Hybrid Riser System, OTC 24802, Kuala Lumpur, Malaysia.

Mercier, R., 2014. OCEN 676: Dynamics of Offshore Structures. Course Material, Texas A&M University, College Station, Texas.

Petruska, D.J., Zimmermann, C.A., Krafft, K.M., Thurmond, B.F., Duggal, A., 2002. Riser System Selection and Design for a Deepwater FSO in the Gulf of Mexico, OTC 14154, Houston, Texas.

Roveri, F.E., Filho, A.G.V., Mello, V.C., Marques, L.F., 2008. The Roncador P52 Oil Export System - Hybrid Riser at a 1800m Water Depth, OTC 19336, Houston, Texas.

Roveri, F.E., Pessoa, P.R., 2005. FREE STANDING HYBRID RISER 1800 M WATER DEPTH, OMAE2005-67178, Halkidiki, Greece.

Sertã, O.B, Longo, C.E.V., Roveri, F.E., 2001. Riser Systems for Deep and Ultra-Deepwaters, OTC 13185., Houston, Texas.

Tahar, A., Ran, Z., Kim, M.H., 2002. Hull/mooring/riser coupled spar motion analysis with buoyancy-can effect. ISOPE 2002, Kitakyushu, Japan.

Tahar, A., Kim, M.H., 2003. Hull/Mooring/riser coupled dynamic analysis and sensitivity study of a tanker-based FPSO. Applied Ocean Research Volume 25, ISSUE 6, 367-382.